Doctoral Dissertation
博士論文

Modulation of Wnt Signaling through Macrocyclic Peptide Wnt3a Ligands

（Wnt3a結合大環状ペプチドを用いたWntシグナル伝達制御）

A Dissertation Submitted for the Degree of Doctor of Philosophy
March 2020

令和２年3月博士（理学）申請

Department of Chemistry, Graduate School of Science,
The University of Tokyo

東京大学大学院理学系研究科化学専攻

OTERO RAMIREZ, Manuel Emilio
オテロ　ラミレス　マヌエル　エミリオ

Abstract

The Wnt pathway, both in its canonical and non-canonical signaling cascades, represents one of the best-studied mechanisms underpinning embryonic development and adult homeostasis. Although able to occur through diverse mechanisms, in its most-studied form, canonical Wnt signaling, Wnt protein ligands engage cell-surface Frizzled receptors initiating a signal transduction cascade that ultimately increases intracellular β-catenin concentration and thereby alters the expression of diverse genes. This mechanism involves a variety of proteins and their complexes, many of which have been targeted for therapeutic development due to their involvement in disease states such as colorectal cancer. However, such approaches have generally avoided direct Wnt ligand targeting due to the relative instability and hydrophobicity of Wnt proteins that can cause them to readily aggregate and lose their biological activity, although such direct Wnt inhibitors have the potential for advantageous specificity profiles compared to other agents.

In the present thesis work, we applied the Random, non-standard Peptides Integrated Discovery (RaPID) System with novel selection schemes and comparative sequence analysis in order to identify and develop *de novo* cyclic peptide ligands to a Wnt ligand, Wnt3a. In Chapter 2, through the use of a mouse Wnt3a (mWnt3a) protein in complex with a stabilizing protein partner, human Afamin (hAFM), we were able to identify several cyclic peptides capable of binding the target Wnt ligand with no considerable simultaneous binding to its partner, among which a rare peptide hit exhibited potent Wnt signaling inhibition through direct binding to the mWnt3a protein ligand. Further optimization of this molecule through the design of an inhibitor-based library for block mutagenesis and re-selection with the mWnt3a-hAFM complex allowed the development of a peptide with greatly improved binding and signaling inhibition traits, the first of its kind to exhibit such properties by direct binding an extracellular Wnt protein.

In Chapter 3, taking into consideration the results obtained while targeting a Wnt ligand within a protein-stabilized complex, we targeted the mWnt3a ligand in another form, bound to its natural Frizzled (Fz) receptor, mFz8. Although the presence of a natural binding partner (with therefore highly enhanced binding kinetics) in such a complex was not expected to favor the recovery of peptides that could outcompete the receptor for binding to mWnt3a's active site, we envisioned the process would still allow the identification of peptides with an allosteric effect on signaling activity. Through a similar selection scheme as with the mWnt3a-hAFM complex, we were able to find several peptide binders that showed a higher degree of structural variability than seen before, from which a single lariat peptide was able to considerably inhibit the signaling pathway. Surprisingly, we also identified a different peptide that appeared to strengthen Wnt signaling instead of inhibiting it, an effect that we were able to confirm through independent biological assays. Furthermore, these two novel peptide binders to mWnt3a showed structures notably different from the one found by targeting the mWnt3a-hAFM complex, while binding sites and bioactivity effects are expected to occur through different mechanisms.

The results found through this work represent the first report of non-natural, mid-sized binding molecules to mWnt3a exerting a strong signaling modulation effect (both inhibition and stimulation) by directly binding a Wnt ligand. Moreover, the results also highlight the potential for using stabilizing protein partners such as hAFM used in this work as a strategy for targeting insoluble and/or unstable proteins through affinity-based selection schemes, as well as increasing the range of protein targets that can be screened with RaPID approaches.

Table of Contents

Chapter 1: General introduction

1.1. The Wnt (Wingless) signal transduction chain

The Wnt pathway comprises a complex signaling cascade regulating the transcription of a variety of genes pivotal for differentiation, proliferation and overall cell fate, representing one of the best-studied mechanisms underlying the embryonic development and adult homeostasis of an organism[1]. The first findings regarding the pathway's involvement in development were originally reported more than 40 years ago by Sharma *et al.* while studying the *wingless* (hence the name) mutant phenotype within the *Drosophila* genome, which in combination with later studies allowed the identification of a gene with an activity critical for attaining the organism's adequate final morphology and physiology[2,3]. Subsequent studies were also able to recognize this gene's homology with an oncogenic viral integration site called *int-1* and a remarkably high conservation among different species, which in turn supported a change of the denomination of this gene and its encoded proteins to *Wnt*, finding from very early on a connection between this gene and oncological processes[4,5]. Further in-depth studies focusing on the structure, function and interactions of these proteins have allowed the current description of an intricate mechanism involving Wnt proteins and a wide variety of their complexes, receptors and both extra- and intracellular signals. Such processes incur in an overall functional scheme that manages to regulate growth and development mainly through cellular proliferation, consequently controlling the resulting morphology of a tissue and maintaining its architecture even after developmental stages[6]. Furthermore, the mechanism's role in disease, particularly in cancer, and its advantageous stabilization of stem cell phenotypes has also brought great attention to both its components and target genes[7].

Though a complex mixture of co-dependent components, overall Wnt signaling affects the transcription of specific genes in order to promote morphology definition during development. One of the most common processes through which this occurs is by using β-catenin, a multifunctional protein, and for which the most studied form of the mechanism is denominated as β-catenin-dependent, or "canonical". Notably, the

mechanism can also involve processes of planar cell polarity (PCP) or Ca^{2+} flux modulation in order to carry out the phenotypic changes in a β-catenin-independent manner, additional pathways that are defined as "non-canonical". Nonetheless, all Wnt signaling processes have a starting point in common: the binding of Wnt ligands to their corresponding Frizzled (Fz) receptors, which promotes and starts several stages of complex formation, phosphorylation, ubiquitination, and overall signal transduction for transcription and cellular fate modulation.

1.1.1. Canonical Wnt signaling

Canonical Wnt signaling is the most studied form of the mechanism, where signaling that is initiated by the binding of secreted Wnt ligands to specific, seven-pass transmembrane Fz receptors, ultimately increases the cytoplasmic concentration of β-catenin and thereby alters the expression of diverse target genes (Figure 1.1). This form of the signaling cascade has been reviewed extensively[6,7], is highly complex in itself and further intricate by the presence of numerous Wnt and Fz isoforms (19 Wnts and 10 Fz in mammals) and their phenotype-specific, individual responses. This form of the pathway is, however, mainly controlled through the function of a large multi-unit complex targeting β-catenin for proteasome degradation: the destruction complex (DC). This complex is, for the most part, maintained by the presence of axin, a largely unstructured protein that serves a scaffolding role. Although flexible, this scaffold contains some structured domains that serve as binding regions for other components of the DC: β-catenin, the Ser/Thr phosphorylases casein kinase 1 (CK1) and glycogen synthase kinase 3 (GSK3) and the adenomatous polyposis coli (APC) protein[8]. The scaffolding activity of axin is well exemplified in the close proximity it binds the CK1 and GSK3 phosphorylases and β-catenin, facilitating the reaction for the latter's phosphorylation, while it is also able to accommodate several equivalents of its target β-catenin, and further oligomerize with other axin proteins through its DIX domain to create large, multi-unit complexes.

When Wnt signaling is in an off state (Figure 1.1), the phosphorylation of β-catenin happens sequentially, starting by phosphorylation of its (human) Ser45 mainly by CK1's α isoform, making the necessary motif that in turn promotes phosphorylation of (human) Thr41, Ser37 and Ser33 by GSK-3 α or β isoforms. Once phosphorylated, these residues interact with the propeller region of the beta-transducin repeats-containing protein (βTrCP) E3 ubiquitin ligase, which in turn has been proposed to be recruited with assistance of the Hippo pathway's elements YAP/TAZ[9]. βTrCP's interaction with β-catenin ubiquitinates the latter, targeting it for proteasome degradation and ultimately regulating intracellular β-catenin concentration levels[10]. Additionally, Fz membrane population is also controlled with the help of another agonist, R-spondin, and its interaction with Leucine-rich repeat-containing G-protein-coupled receptors (LGR) 4 to 6, which when in absence of the former is able to interact with Zinc/RING finger protein 3 (ZNRF3) and RING finger protein 43 (RNF43), two transmembrane E3 ubiquitin ligases able to tag Fz's intracellular domain for endocytosis and lysosomal degradation with the help of Dishevelled (Dvl) proteins[11-13]. Furthermore, inside the nucleus, T-cell and lymphoid enhancer-binding transcription factors (TCF/LEF) directly bind DNA, commonly in the sequence 5'-AGATCAAAGG-3', but are normally found to interact with Groucho/transducing-like enhancer of split (TLE) transcription repressor proteins, silencing genes controlled by this pathway[14,15].

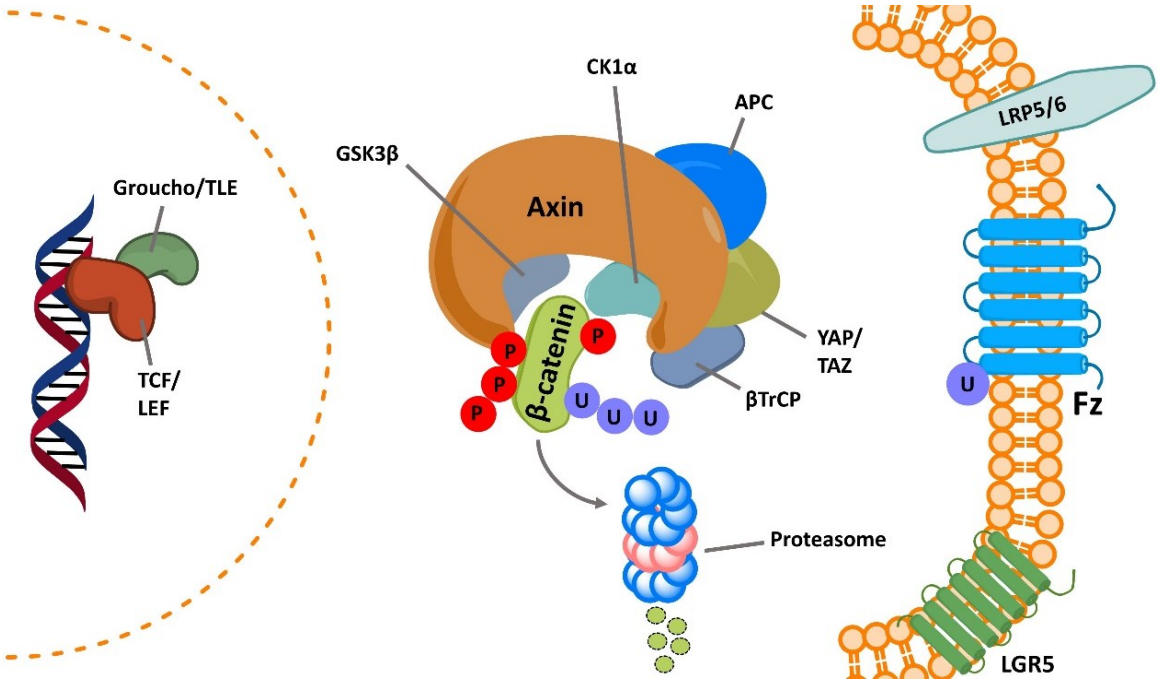

Figure 1.1 Scheme of interacting components of canonical Wnt signaling when in an "off" state. Lacking any Wnt ligand binding, β-catenin is tagged for proteasome degradation through the DC machinery, while target genes' expression is silenced by Groucho/TLE components' interaction with TCF\LEF transcription factors.

Upon Wnt ligand binding to Fz receptors, however, the whole scheme of aforementioned interactions changes, turning Wnt signaling on (Figure 1.2). Conspicuously, Wnt ligands interact not just with Fz, but with low-density lipoprotein receptor-related protein (LRP), which act as a co-receptor, cooperating with Fz in such a way that receptor dimerization and formation a Wnt-Fz-LRP oligomer is thought to occur, although the full identification of the latter complex is still currently under debate[16]. The cytoplasmic tail of LRP is then phosphorylated, recruiting Dvl proteins that can bind internal domains of Fz and polymerize, and due to the presence of DIX domains in their structure, call for axin, effectively sequestering the DC[17]. During this process, YAP/TAZ and βTrCP are displaced, and due to a hindered activity of the DC, cytoplasmic β-catenin levels increase, consequently translocating to the nucleus. After internalization, β-catenin displaces Groucho/TLE elements, binding TCF/LEF factors and recruiting histone-modifying,

promoter and enhancing elements, turning on a transcriptional switch to activate the expression of the regulated genes[18,19].

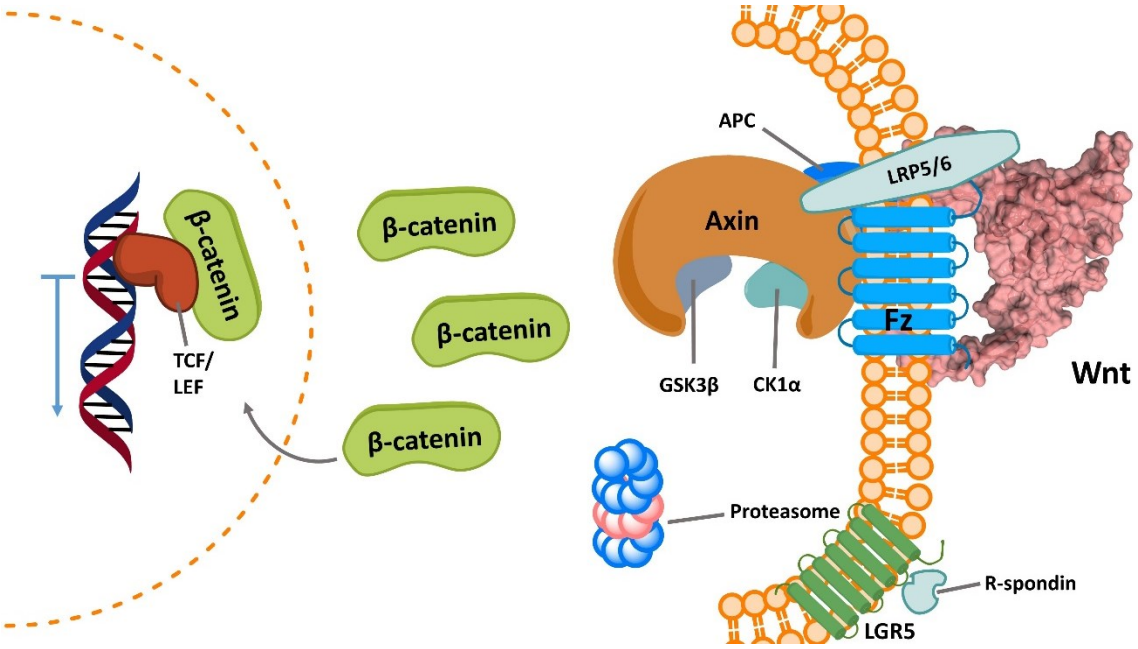

Figure 1.2 Scheme of interacting components of Wnt signaling when in an "on" state. Upon Wnt ligand binding (shown here as PDB 6AHY), DC machinery is sequestered and consequently inactivated, thereby facilitating the accumulation of cytoplasmic, β-catenin, which translocates to the nucleus, displaces Groucho/TLE repressors and binds TCF\LEF factors, recruiting other transcription promoters as well to allow target gene expression.

As shown, even the most-studied canonical form of Wnt signaling is highly complex and retains uncertainty on several levels and steps during the signaling cascade that regulates gene expression. Consequently, development of therapeutics targeting members of the Wnt pathway face additional challenges when trying to have a specific effect on a symptom or disease being treated. This lack of control represents one of the reasons many of them are not designed to be selective against one component of the pathway, instead working as non-specific inhibitors or activators of Wnt signaling, a trait that, however, can hinder their advance through clinical stages.

1.1.2. Non-canonical Wnt signaling

Direct transcription regulation through β-catenin, however, is not the only mechanism through which Wnt-Fz interactions can affect cell morphology and functionality. These additional mechanisms are known as β-catenin-independent or "non-canonical", and involve a wide array of components, including ones thought to be involved in canonical Wnt signaling up to some level as well. Nonetheless, some Wnt-Fz combinations have been found to favor non-canonical rather than canonical responses, as in the case of Wnt 5, 7 and 11 and Fz 2, 6 and 7, although their specific responses and classification as canonical or non-canonical are continuously discussed[20,21]. These responses are found to work in two main pathways derived from Wnt interactions: Planar Cell Polarity (Wnt/PCP) and Ca^{2+} (Wnt/Ca^{2+}), although other β-catenin-independent processes are plausible, possibly interacting with its canonical form.

Although much less is known about non-canonical Wnt signaling processes than their canonical counterparts, the Wnt/PCP pathway is particularly recognized for being deeply involved in oncogenic processes, controlling tumor initiation, cancer proliferation and migration, and even cell death, mainly by affecting the PCP developmental network (Figure 1.3). PCP constitutes a polarization mechanism through which cells are able to coordinate and apply directional information (*e.g.* apical-basal polarities in epithelial cell lining or trailing edges in fibroblasts), crucial for breaking cellular symmetry and to localize structures to perform functions in one direction, generating complex shapes and the architecture required for tissues and organs to form and function adequately[20,22,23]. The machinery in charge of this functionality is largely conserved among species, and includes both inter- and intracellular interactions, but mainly with receptors Fz, Flamingo (Fmg) and Van Gogh-like (Vgl), as well as cytoplasmic adaptors Dvl, Prickle (Pk) and Diego (Dgo). Intercellularly, the necessary cell-to-cell communication for PCP transmission is carried out by the interaction of Fz and Vgl, which are thought to interact directly or facilitated by the bridging Fmg, which independently interacts with both of them, as Fz and Vgl complex are localized on opposite membrane locations[24,25]. On the other side, at an intracellular level, Pk can directly bind Dvl and, through

the binding-support and membrane-recruitment by Vgl, efficiently hinder Fz-Dvl interactions and their issuing downstream signaling[26]. Countering this, Dgo can antagonize the flow by competing with Pk for binding to Dvl, ensuring the latter's Fz-mediated recruitment to the membrane[27]. This particular interaction is essential for the pathway, and begins with the binding of Wnt ligands, in particular Wnt5a, to Fz in complex with co-receptors such as Receptor Tyrosine kinase-like Orphan Receptor 2 (ROR2), upon which recruitment of Dvl promotes the activation of G-proteins of the Rho family (namely Rac1 and Rho, with the latter after interaction with Disheveled-associated activator of morphogenesis 1, DAAM1), triggering Rho kinases (ROCK) and c-Jun N-terminal kinases (JNK) that modulate cell polarization for protrusion and elongation, actin polymerization, actin-myosin contractibility and cell-to-cell contacts[28].

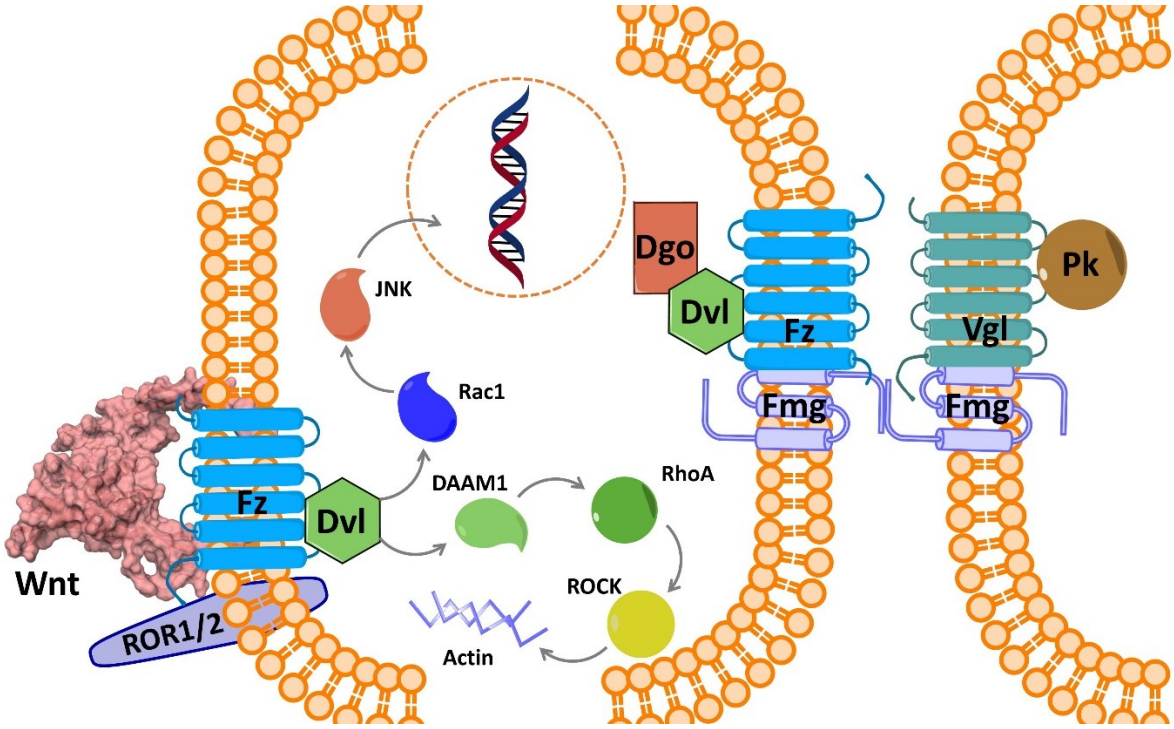

Figure 1.3 Scheme of interacting components of an activated non-canonical Wnt/PCP signaling pathway. Intracellularly, upon Wnt ligand binding (shown here as PDB 6AHY), complex formation with neighbor ROR1/2 promotes Dvl recruitment, which in turns activates Rho proteins RhoA and Rac1 (the latter after interaction with DAAM1). RhoA activates ROCK, which can promote actin polymerization and its consequent morphological effects, while Rac1 can go to activate JNK, which in turn can regulate selected genes' expression. Additionally, antagonizing Dgo-Pk couple, controlling regulating intracellular signaling is also shown in a state favored to Dgo, allowing Dvl recruitment to the cell membrane. Finally, intercellular interactions promoting PCP expansion through Fz-Vgl interaction is also shown with a neighboring cell, mediated by a Fmg bridge.

1.2. Wnt proteins: Structure and interactions

Whether the mechanism following Wnt signaling is based on β-catenin transcription modulation, PCP-based morphology changes or Ca^{2+} level variations, all processes are dependent on the same initial step: Wnt ligand binding of Fz receptors. Due to the nature of Wnt protein structures mentioned above, and particularly because of their high hydrophobic character, for many years no precise structural information had been obtained for these ligands, while their study was commonly based on sequence identification or using collected cell-culture media, which has been used for analyzing Wnt signaling proliferation and differentiation effects[29,30]. Consequently, however, experiments requiring purified forms of the ligands, including structural analysis and therapeutics development, have been traditionally hindered. In turn, studies focusing on how these structurally-frail proteins are biologically synthesized and maintained throughout their activity lifetime have given a current scheme of their formation, basic properties and characteristics, although many of the steps involved have not yet been fully elucidated.

1.2.1. Wnt maturation and secretion

The challenging structural traits of Wnt ligands have been long attributed to their characteristic lipidated moiety, known to be critical for the protein's secretion, as well as its adequate binding and activity with Fz[31]. Initial reports at the beginning of the decade confirmed the hydrophobicity of Wnt ligands through partition to detergent phases, while metabolic labeling and mass analysis indicated that the lipidation of Wnt corresponded to a monounsaturated palmitoyl moiety (16:1)[30]. Further studies were able to pinpoint its location to a protein's Ser (*e.g.* Ser209 for hWnt3a), while also disproving a previously thought potential lipidation on Cys[32]. Moreover, recent studies have been also performed using click chemistry and *in situ* proximity ligation in order to visualize acylated Wnts in cells, allowing a better understanding of the enzymes required for their maturation and secretion and Wnt localization within a cellular environment[33].

Ligation of the palmitoleoyl group to Wnt's Ser residue and its following transport are crucial steps that allow the protein's controlled modification and secretion (Figure 1.4). The palmitoyl lipid moiety, as well as many other ones for lipid modifications, has been found to be initially ligated to Coenzyme A (CoA), a fatty acid synthase, and sequentially modified regioselectively to a monounsaturated form using an endoplasmic reticulum (ER) steroyl-CoA desaturase (SCD)[34]. Finally, Wnts are modified with this moiety using a Serine O-palmitoleoyltransferase denominated as Porcupine (Porcn), which is also located in the ER membrane, though the reaction has been found to occur within ER lumen[35,36]. This particular enzyme is the only one found to perform the posttranslational lipid modification of Wnts, while this modification has also been shown to be antagonized by Notum, an endogenous extracellular palmitoleoyl carboxylesterase that cleaves the lipidation motif, therefore making an additional natural Wnt activity regulation pair[37]. The modified Wnt is thereafter able to interact with Wntless (Wls), a partner cargo receptor that aids in its transport to the Golgi apparatus, additionally aided by p24 proteins[38,39]. Notably, Wls partners the modified Wnts throughout all their movement to the cell membrane for secretion and can also be recycled afterwards. Extracellularly, however, the exact mechanisms through which Wnts are stabilized and transported are still under debate, though transport has been suggested to be aided by lipoprotein or extracellular partners[40,41].

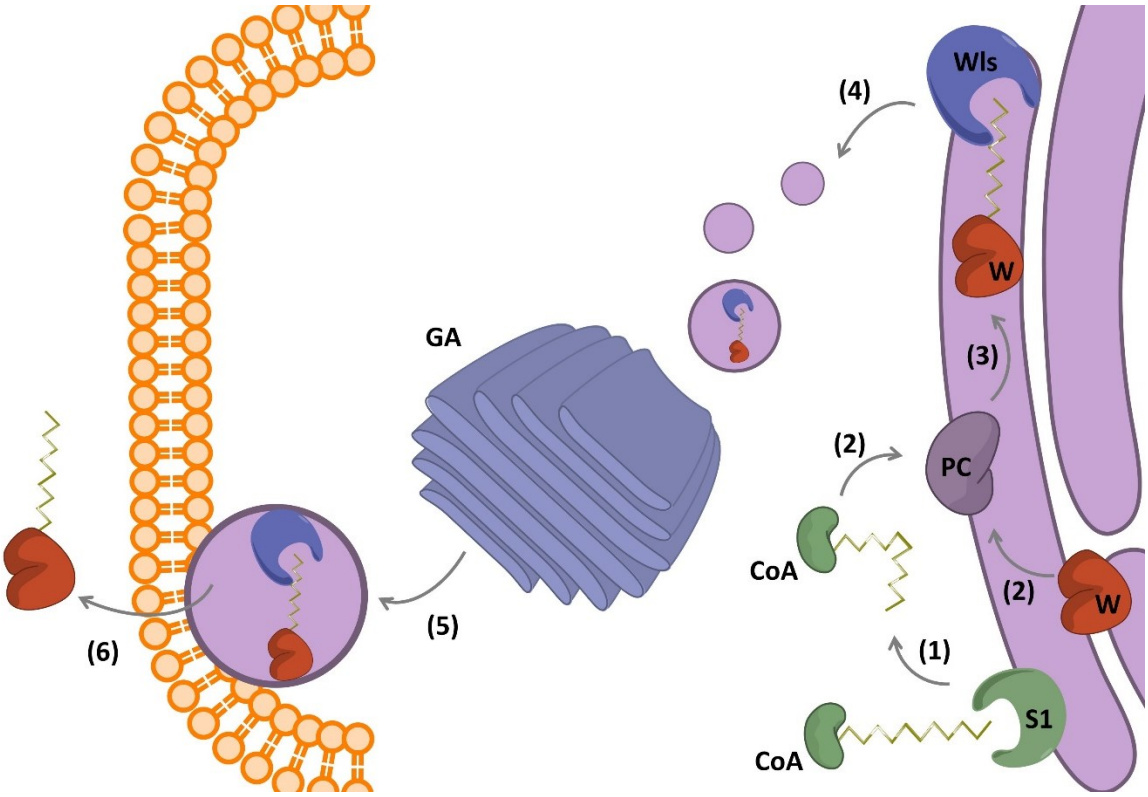

Figure 1.4 Scheme of maturation and secretion of Wnt ligands. The characteristic lipidated moiety of Wnt ligands is generated as a post-translational modification, and its attachment to the protein begins with (1) the modification to a singly unsaturated form of the lipid, performed by the ER desaturase SCD1 (S1) on a CoA-lipid substrate (2) The modified lipid and the immature, ER lumen Wnt (W) react with the ER transferase Porcn (PC) to generate the lipidated form of the Wnt ligand (3) This form of the protein is able to interact with the transporter Wls for extrusion from the ER (4) The Wls-acylated Wnt complex is then transported in vesicular bodies to the Golgi apparatus (GA) for final maturation of the Wnt ligand (5) The mature Wnt is then transported to the cell membrane, where (6) it is freed from Wls and extruded the extracellular space, from which point is is thought to interact with different proteins for its stabilization and transport.

1.2.2. Wnt structure

Notwithstanding such intricate characteristics of Wnt proteins, the structural traits of a Wnt protein in complex with its natural Fz receptor was first resolved by Janda *et al*. in 2012 (Figure 1.5a)[42]. The pivotal study managed to describe in detail the crystal structure of mouse Fz8 (mFz8)'s cysteine-rich domain (CRD) in complex with *X. laevis* Wnt8 (xWnt8), highlighting the elaborate structure of Wnt in its binding to the receptor. More specifically, Fz was shown to be bound by two opposite sides of Wnt "finger" domains, with the first of them burying the lipidated Ser residue deep inside the receptor's groove, while the second makes highly conserved hydrophobic contacts on its opposite surface. The binding mode was not found to resemble any other folding found elsewhere, while it also characteristically presented a "hole", unbound location generated above Fz, and a large surface area without any contact with the receptor, potentially suggesting additional sites for co-receptor interactions. More recently, Hirai *et al* were able to achieve the isolation of lysine-methylated and deglycosylated human Wnt3 in complex with mouse Fz8's CRD (Fig. 1.5b), finding a nearly identical binding mode together with a surprising 2:2 complex formation in the crystal that allocated the two palmitoleoyl chains in-between parallel opposite sides of the Fz-Fz interface[43]. In addition, identification of key components for binding and activity revealed potential binding positions for co-receptor binding, particularly the interaction of the tip of one of the Fz-bound Wnt3's β-hairpin with LRP6.

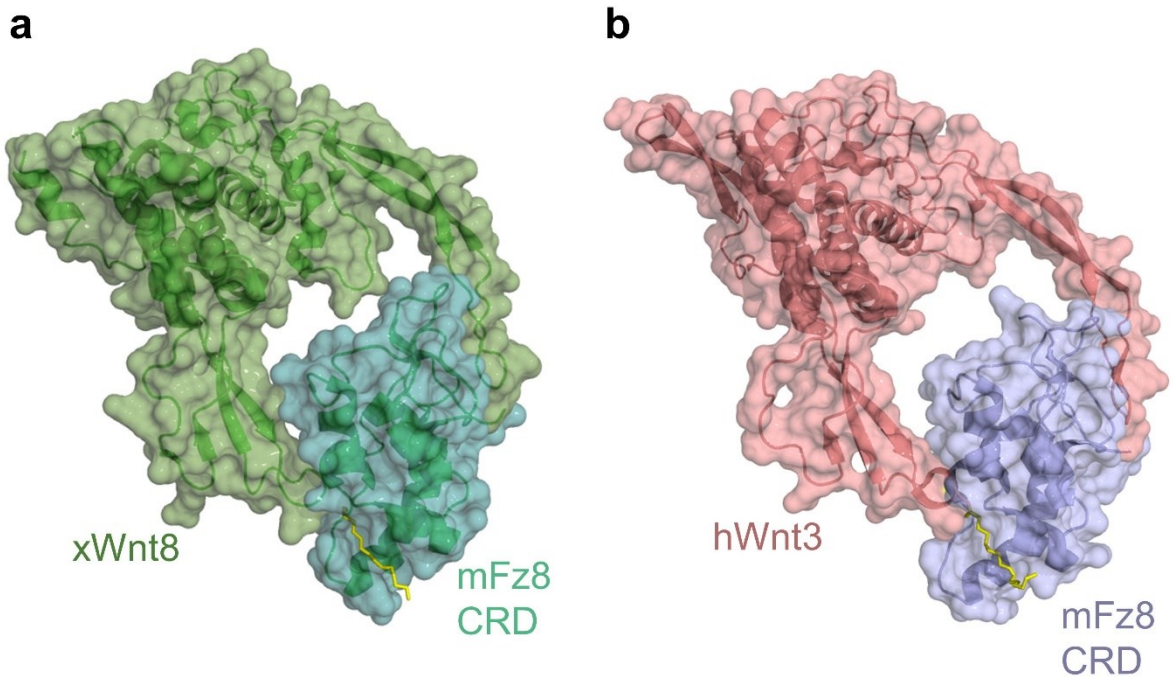

Figure 1.5 Structure and binding modes of Wnt ligands to Fz receptors. (**a**) Crystal structure of xWnt8 (green) in complex with the CRD region of mFz8 (light blue), as found by Janda *et al.* (PDB 4F0A), with the palmitoleoyl moiety (Ser187 in xWnt8) shown in yellow (**b**) Crystal structure of the homodimer formed by hWnt3 (red) and the CRD region of mFz8 (blue), as determined by Hirari *et al*. (PDB 6AHY), with the palmitoleoyl moiety (Ser209 in hWnt3) shown in yellow. Although different Wnt types from different species, the two Wnt proteins show a very similar binding mode, with the palmitoleoylated Ser moiety buried within the Fz receptor's hydrophobic groove.

1.2.1. Wnt and Afamin

In 2016, Mihara *et al*. accomplished the remarkable task of isolating soluble and bioactive mouse Wnt3a (mWnt3a) with exceptional stability, found to exhibit these properties only when in a 1:1 complex with a co-expressed partner Afamin (AFM, Figure 1.6) that stabilizes the Wnt ligand[44]. The authors identified the partner carrier protein while purifying secreted tagged mWnt3a, and observed its benefits to maintain mWnt3a stabilized for the long-term, while retaining its full signaling activity and expressing it in large amounts and in a detergent-free environment, avoiding a well-known hindrance for stem cell studies. The partner however, represents and unnoted plasma glycoprotein of the albumin protein family that characteristically completely lacks Trp, and has been thought to serve as a transporter of hydrophobic small molecules like Vitamin E[45,46]. These particular traits could indicate a possible logic for binding such hydrophobic proteins as are Wnts, but AFM by itself has not been shown to exert any functional roles on Wnt signaling. However, its presence in culture media that has been traditionally used for Wnt activity studies could indicate a role as an endogenous extracellular transporter of Wnts. Furthermore, its actual physiological and structural roles are still currently under discussion, with some studies finding association between AFM levels and diverse disease states, particularly with metabolic syndrome[47,48]. Moreover, even though the heterogeneous glycan distribution can be detrimental in structural studies, simulation trials have also shown that it might possibly bind Wnt lipidated motifs through a hydrophobic groove in a similar manner as Fz receptors do[49,50].

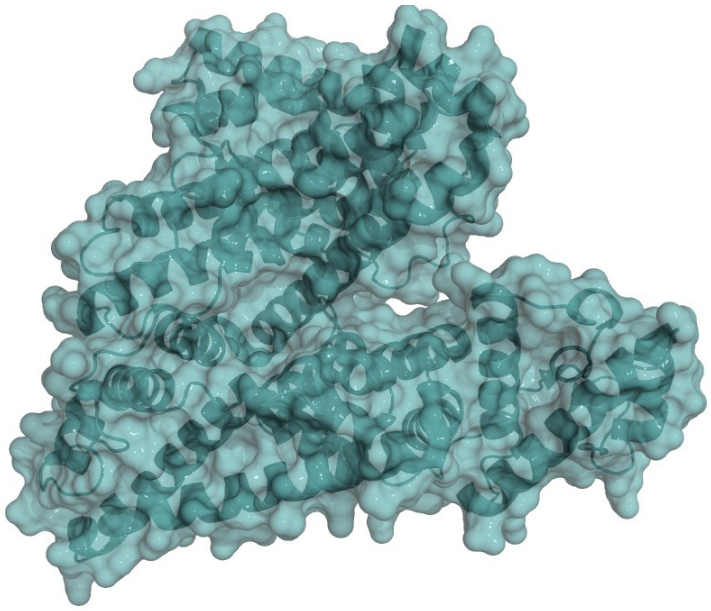

Figure 1.6 Crystal structure of hAFM, as determined by Naschberger *et al.* (PDB 6FAK)[51].

1.3. Wnt signaling relevance in disease

Along with the recent progress towards studying Wnt signaling and its components, great efforts have been devoted to targeting it for drug discovery and development. In particular, the pathway's relationship with cancer has been long discussed[6,7], finding it to be involved in a variety of the disease's states, particularly in gastrointestinal cancer[52]. Furthermore, mutations in different components of the pathway have been found to correlate with low prognosis in different types of cancer. For example, mutations in APC and its function have been found to account largely to alterations in signaling and to be consistently associated with large intestine tumors, while large increase in Wnt signaling has been found to occur in most types of leukemia and activation of the signaling in breast cancer has been linked with low survival rates[7]. Moreover, both canonical and non-canonical Wnt signaling have been found to be related to tumor genesis and promotion of metastasis, as well as expansion through circulating tumor cells[53]. In addition, mutation of components of the pathway has also been found to correlate in degenerative diseases such as bone density defects or progressive vision loss[54,55].

Corresponding to the known relationship with different types of disease, a large range of therapeutics have been developed targeting different components of the Wnt pathway, ranging from small molecules[56] to antibodies[57] to whole lipid systems[58] that can modulate signaling or act as receptor decoys[59]. Notable examples of these include target Porcn for inhibition such as IWPs[60], though other means of signaling alteration like Foxy5[61], a Wnt5 mimetic, or recent staple peptide binders of β-catenin[62] have been discovered recently as well (Figure 1.7).

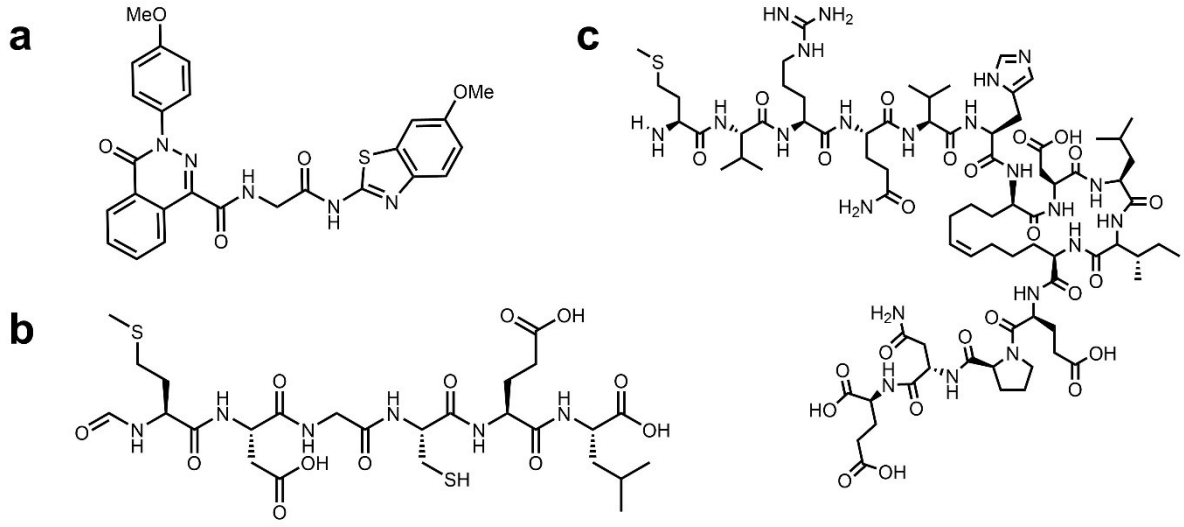

Figure 1.7 Exemplary Wnt pathway inhibitors. Shown are different classes of inhibitor molecules, which in turn target varied components of the pathway: (**a**) the small molecule IWP-1 against Porcn (**b**) the formylated hexapeptide Foxy5 against Wnt5 Fz receptors (**c**) a 15-residue stapled peptide against β-catenin.

Despite the fact that several of these are currently at varying development stages, it is notable that direct targeting of isolated Wnts has not progressed on par with other members of the pathway, despite its potential therapeutic advantages due to target specificity. Besides the aforementioned inherent structural instability, the task is even more challenging considering the general lack of structural information for rational design and the necessity of acquiring pure Wnts in high yield in order to target them with a potential drug.

1.4. The RaPID screening system

Cyclic peptides are an emerging class of potential pharmacological modulators, capable of disrupting the protein-protein interfaces underlying cell-surface receptor-ligand interactions[63,64]. It has been shown that display screening techniques are exceptionally powerful approaches for the discovery of bioactive cyclic peptides, and that the identified molecules generally exhibit high binding affinity, selectivity and bioactivity[65-68]. However, such approaches commonly require purified protein targets to act as "bait" during the screening process, making their application to unstable targets (such as Wnt proteins, for example) highly challenging.

Within the different screening systems available for developing therapeutics, the Random, non-standard peptides Integrated Discovery (RaPID) platform represents one of the most versatile tools for the generation and simultaneous screening of potentially bioactive cyclic peptide libraries (Figure 1.8a). The system itself is based on the use of a flexizyme-assisted flexible *in vitro* translation system (FIT), facilitating the formation of peptides that can include both natural and non-proteinogenic amino acids with diverse structures, coupled with mRNA display to allow the recovery and identification of selective, strong-binding members within originally large libraries ($>10^{12}$ members) through affinity-based selection schemes[65,66,69]. Furthermore, the platform is compatible with a wide variety of both synthetic and enzymatic reactions for posttranslational modifications or the ribosomal expression of complex large blocks of natural product-like structures, allowing remarkably large possibilities in library design (Figure 1.8b).

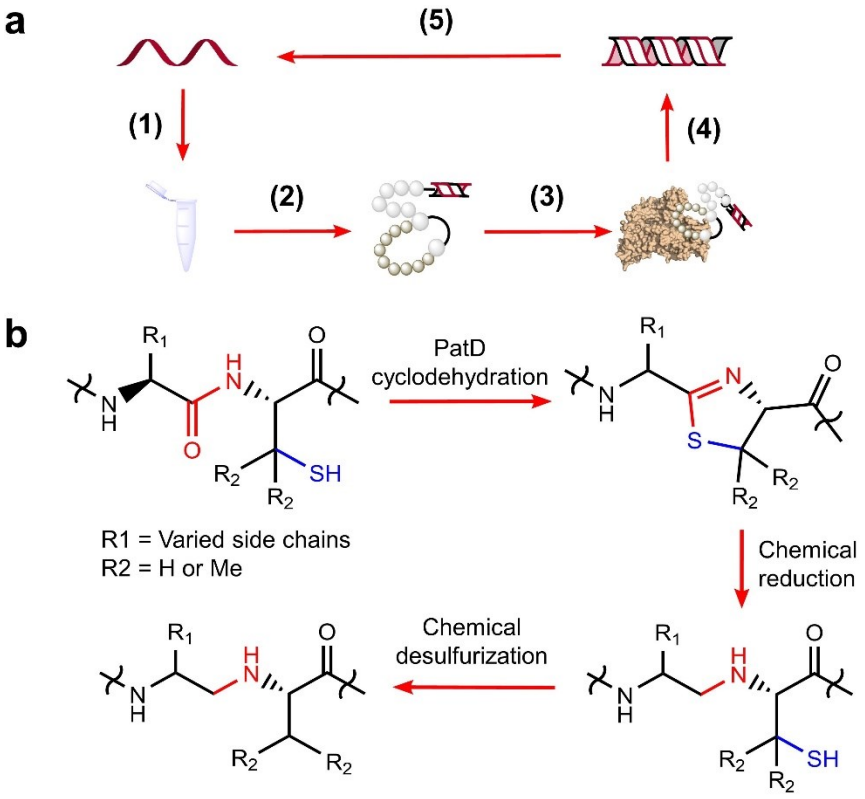

Figure 1.8 Simplified scheme of RaPID system screening and exemplary compatible posttranslational modification. (**a**) System is applied sequentially beginning with (1) designing an mRNA library containing all the necessary motifs for (2) customized FIT, which includes the cell-free translation machinery to generate the desired peptide library, in turned used for (3) mRNA-based affinity screening and (4) the recovery of binding sequences, which are amplified and transcribed to generate the initial library of a new round (**b**) An example of one of many chemical or enzymatic compatible reactions with the translation system component of RaPID, the chemoenzymatic generation of ψ[CH_2NH]-containing peptides as developed by Katoh *et al.*[70]

Though the mRNA display technique coupled in the system allows screening a wide diversity of libraries, one of the most versatile and pivotal aspects of the system lies in the use of flexizymes to design them. These enzymes are artificially evolved ribozymes, capable of selectively aminoacylating bioorthogonal tRNA, which allows for the translation of peptides with tailored characteristics, including cyclization through a thioether or the inclusion of non-proteinogenic amino acids at specific locations along the peptide chain. Through this activity, they perform in a similar manner to a highly promiscuous aminoacyl-tRNA synthetase, recognizing different leaving groups (depending on flexizyme variant) attached to the

carboxy terminus of the required amino acid to be ligated to the 3' of tRNA[71] (Figure 1.9). Pairing of this technology with a reconstituted *E. coli* cell-free translation system containing these pre-charged bioorthogonal tRNA complexes and specific amino acids eliminates any potential competition with natural counterparts and enables the *in vitro* translation of peptides with the desired characteristics, constituting the FIT component of the system and overall bringing large advantages for vast libraries and their design.

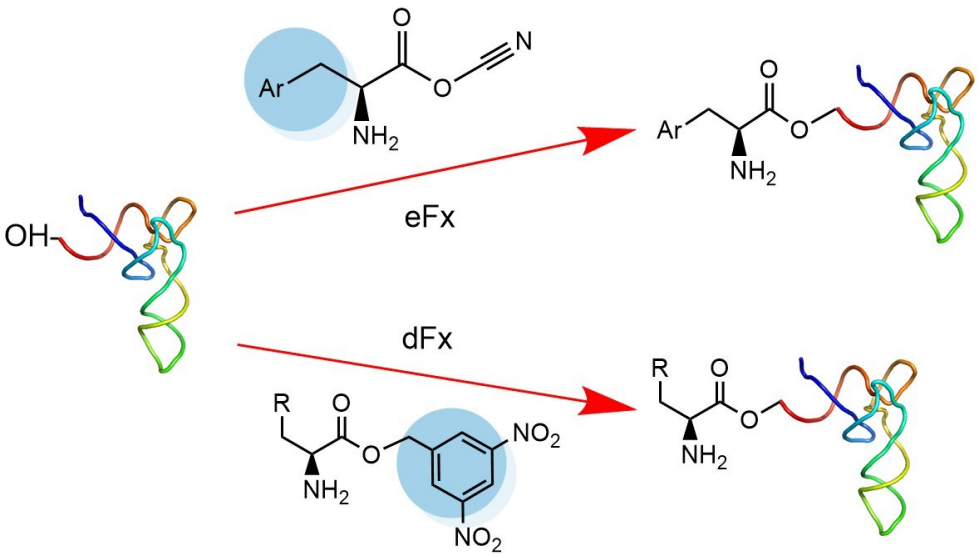

Figure 1.9 Scheme of flexizyme-assisted aminoacylation of tRNA. The free 3' end of tRNA can be charged with activated amino acids containing a recognition group (light blue) specific for the flexizyme being used and an adequate leaving group.

Chapter 2: Screening of Peptide Ligands against an Afamin-stabilized Wnt3a complex

Results from this chapter have been submitted for publication as "Macrocyclic Peptides that Inhibit Wnt Signaling via interaction with Wnt3a" Otero-Ramirez, M.E.; Matoba, K.; Mihara, E.; Passioura, T.; Takagi, J. and Suga, H. ***2020****, , while bioactivity measurements were performed in collaboration with Ms. Kyoko Matoba, Dr. Emiko Mihara and Prof. Jun Takagi at the Laboratory of Protein Synthesis and Expression at The University of Osaka, Osaka, Japan.*

Introduction

As aforementioned, Wnt proteins present several inherent characteristics pertaining to their structure and activity that make them challenging to isolate, study and target for therapeutics development, even though their involvement in several disease states has been known for decades. These traits also highlight the current need for more versatile platforms that can allow the study of unstable protein ligands, and ideally, their screening for bioactive binding molecules as well.

Though it has been well-known that the lack of stability of Wnt proteins can hinder their biological studies, breakthroughs described above by Janda *et al.*[42] and Mihara *et al.*[44] have brought into the field new possibilities for understanding the repercussions of Wnt-Fz interactions, as well as the currently poorly understood knowledge of other binding partners.

In particular, the discovery of a bioactive form of a Wnt ligand in complex with a signaling-inert protein partner prompted us to exploit this feature and approach the challenge of discovering potential peptide therapeutics against Wnt signaling. Though several actives molecules have been discovered and developed in the past few years, many of them generally lack selectivity, hindering their progress through clinical stages, while even approved therapeutics with intracellular targets often face difficulties in assessing disease prognosis due to the involvement of their targets in varied signaling chains. Even more so, the

intricate relationships between active or inactive Wnt signaling in different states of a disease, many of which have not been fully elucidated as of yet, require a delicate effect and dosing balance, and may therefore require the generation of both inhibitors and activators of the pathway.

Though the task of targeting Wnt signaling modulation for developing therapeutics appears largely demanding, we approached the challenge by selectively targeting a Wnt protein not as a single unit, but within a stabilized complex with AFM, using it as a "bait" protein for RaPID screening of randomized cyclic peptide libraries, working with the mWnt3a-hAFM complex throughout the study. Such therapeutics are known for having the potential of binding large areas in varied sites within their protein targets, which greatly increases their chances for interfering protein-protein interactions, a factor that would benefit Wnt signaling modulation due the exclusive effect on the interactions between extracellular Wnt ligands and their membrane receptor partners. Though such a strategy is not commonly used in affinity-based screening schemes, we envisioned the use of the inert partner during different stages of the selection process and a detailed high-throughput sequencing analysis would aid in identifying peptides with high selectivity solely towards the Wnt ligand target, for which we developed an adequate selection, sequence analysis and structure optimization scheme.

Results

Library design and selection

In order to identify direct inhibitors of human Wnt3a signaling, we employed an affinity-based selection by means of the RaPID system (Figure 2.1). Although Wnt3a alone can readily denature upon isolation, the Wnt ligand can be stabilized through the formation of a complex with AFM, which would give us an opportunity to explore the available interaction surface with Fz receptors. Thus, we decided to use the bioactive and biotinylated mWnt3a-hAFM complex as a bait protein and applied our standard mRNA library consisting of AUG, $(NNK)_{6–15}$ (N = A, C, G or U and K = U or G), UGC, followed by $(GGCAGC)_3$-UAG codons to express two independent, thioether-cyclized macrocyclic peptide libraries under a reprogrammed genetic code assisted by flexizymes[71-73]. The AUG initiator codon was assigned to L-*N*-chloroacetyl-Tyr (Y-library) or D-*N*-chloroacetyl-Tyr (y-library) in order to induce subsequent head-to-sidechain thioether cyclization with a downstream Cys residue, which could appear in the random region and/or the designated UGC codon after the random region[74]. A triple repeat of a Gly-Ser peptide linker assigned by $(GGCAGC)_3$ allowed linking to a 3'-puromycin-CC-PEG-5' attached to the 3'-end of the mRNA library.

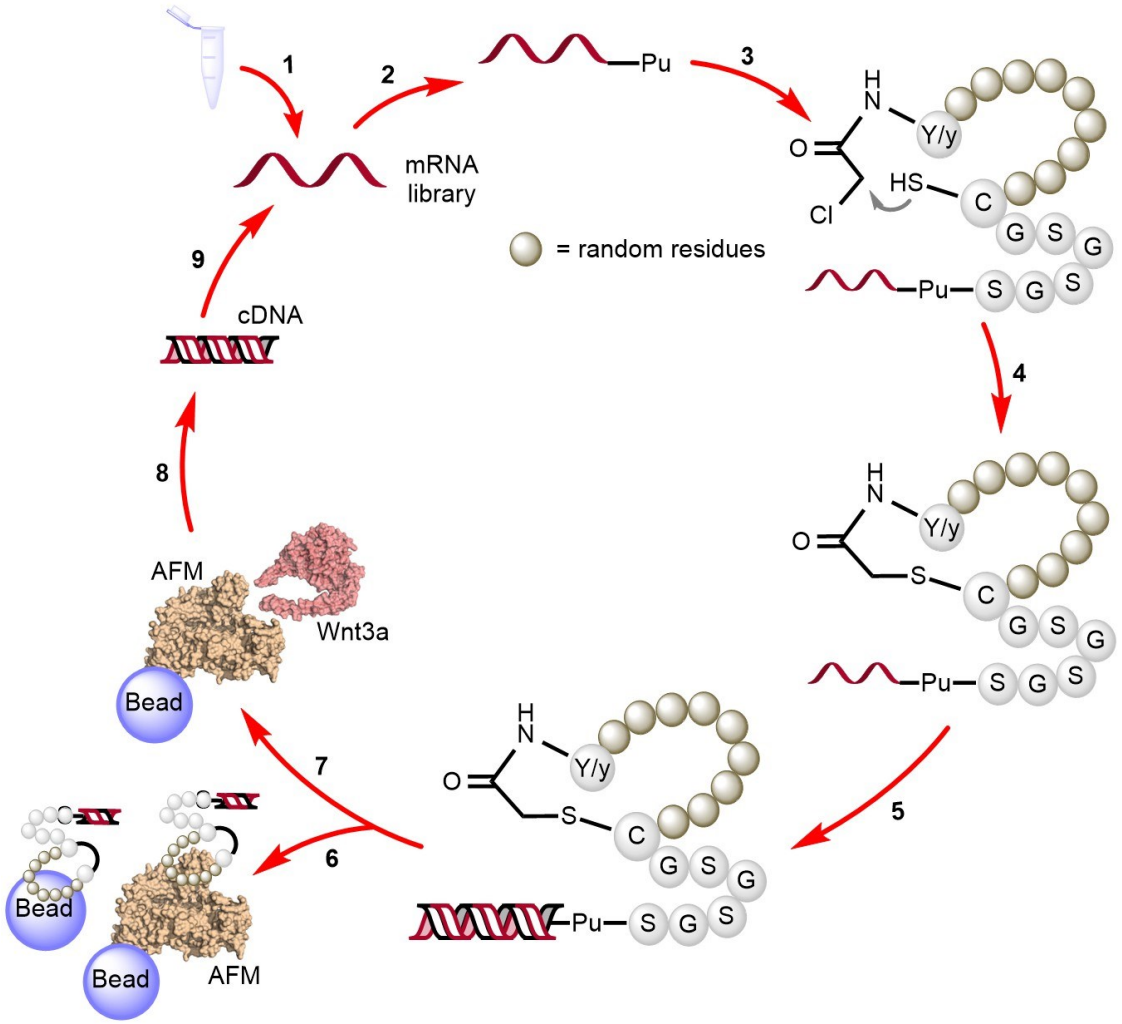

Figure 2.1 RaPID selection scheme for the identification of peptides selective to mWnt3a. On par with a standard scheme, (1) the designed mRNA library is prepared, (2) ligated with Puromycin (Pu) using a T4 RNA ligase (3) and translated into peptides using the FIT system to generate peptide-Pu-mRNA fusions. , after which (4) macrocyclization would occur by reaction of L-Tyr (Y) or D-Tyr (y) with a downstream Cys at the end of the random region (brown spheres) or within the random region itself (5) This macrocyclic peptide library is ligated to each cognate RNA through a $(Gly\text{-}Ser)_3$ and Pu-linker region, and the RNA template is reverse transcribed into its cDNA (6) The library is then exposed several times to a combination of unloaded, biotin-saturated and biotinylated hAFM-loaded magnetic beads in order to lower the likelihood of recovering non-specific binders as much as possible (7) These fractions are discarded and the depleted library is then exposed in a single cycle to the biotinylated mWnt3a-hAFM complex-loaded magnetic beads (8) cDNA bound to the complex is then recovered and amplified by PCR followed by (9) transcription to generate the enriched mRNA library for the next round.

Upon the ribosome-catalyzed specific formation of a peptide linked to its cognate puromycin-mRNA (Pu-mRNA) in the absence of RF-1, the resulting peptide-mRNA fusion was "counter-selected" against immobilized hAFM in order to deplete species that had affinity only for hAFM. Following 10 cycles of counter-selection, the peptide library was then panned against a beads-immobilized mWnt3a-hAFM complex in the presence of free (non-tagged) soluble hAFM to further reduce the binding of peptides unselective for mWnt3a. The cognate cDNAs for peptides that bound the mWnt3a-hAFM complex target were then recovered by PCR amplification and transcribed in vitro to generate an enriched mRNA library for the subsequent round of selection. However, despite our many precautions to deplete hAFM ligands by the negative (counter) selection procedure, qPCR analysis after 5 sequential rounds of selection indicated similar levels of cDNA recovered from both the hAFM-coated counter-selection beads and the mWnt3a/hAFM-coated beads, suggesting that the recovered peptide libraries could indeed be a mixture of species that bind to both hAFM and mWnt3a (Figure 2.2).

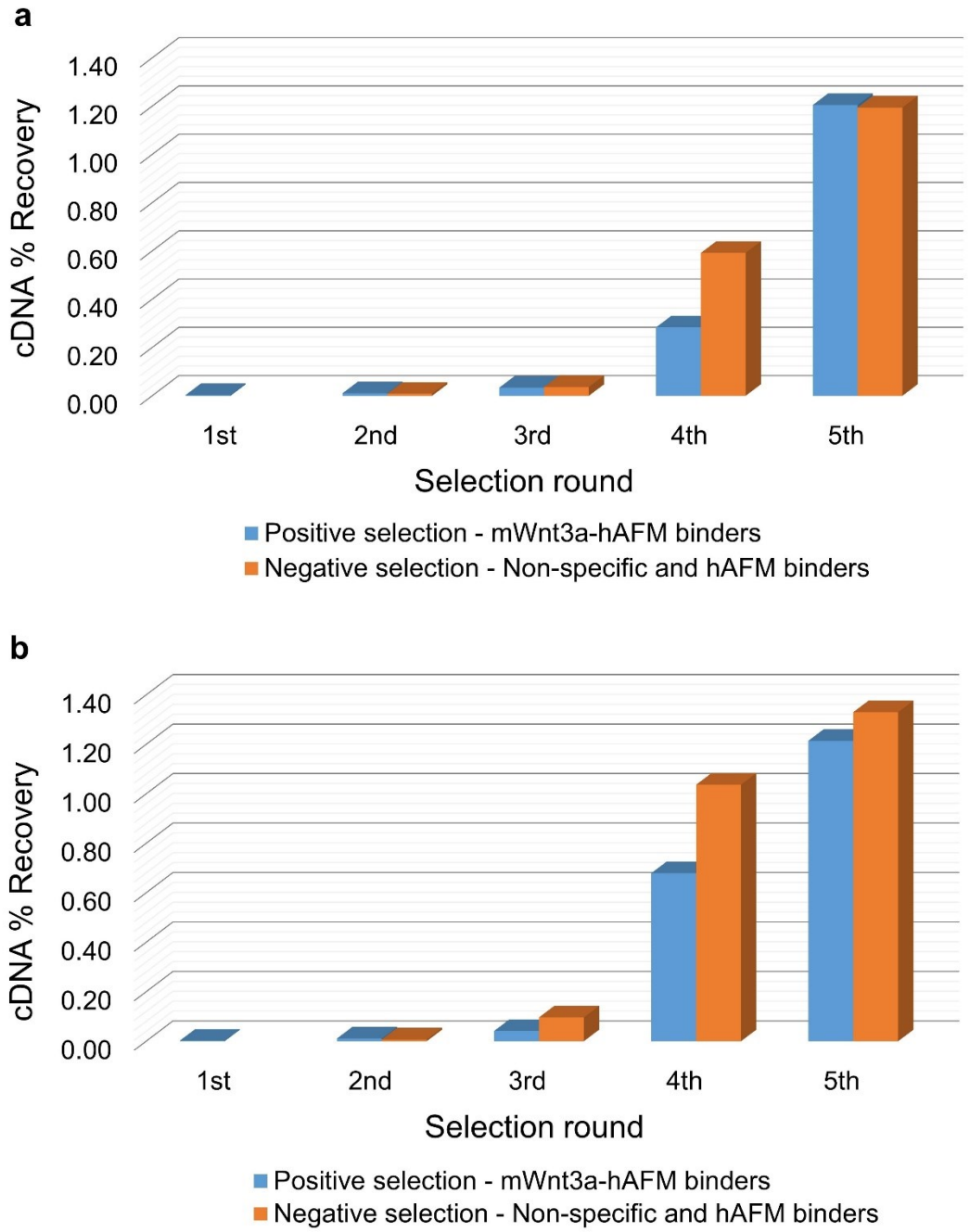

Figure 2.2 qPCR selection results of targeting the mWnt3a-hAFM complex with the RaPID system. (**a**) Graph shows recovered cDNA per round of selection against mWnt3a-hAFM, obtained from the macrocyclic peptide library initiated by D-Tyr (**b**) Similar results corresponding to the library initiated by L-Tyr. Blue bars indicate the fraction corresponding to the cDNA of peptides bound to the complex, while orange bars indicate non-specific binders, including ones binding to only-hAFM-loaded magnetic beads.

Initially, recovered cDNA from each round bound to the complex were sequenced using high-throughput sequencing, in order to analyze the enrichment of the sequences shown to have the highest potential for binding the target Wnt ligand throughout the selection process (Figure 2.3). From this analysis, two sequences from the D-Tyr-initiated and two more from the L-Tyr-initiated one were shown to be the most enriched, with three of them corresponding to 14-16 residues-long macrocycles and one small ring lariat, while their overall secondary structure was not shown to have any particular similarities with each other.

Even though several sequences were shown to have successfully enriched throughout the selection, as aforementioned, the initial qPCR results left unconfirmed whether the peptides in the recovered libraries were indeed binding solely to the Wnt ligand target (in this case, mWnt3a within the mWnt3a-hAFM complex), instead having more probability of exhibiting non-specific binding to hAFM or unloaded beads even after the numerous counter-selection cycles and the presence of the free inert partner in solution. To circumvent this unexpected outcome, a two-dimensional deep-sequencing analysis comparing the most enriched sequences found to bind hAFM alone or the mWnt3a-hAFM complex was performed. For this analysis, the cDNA libraries corresponding to the 5^{th} round of selection targeting either hAFM alone (from the final counter-selection cycle) or the mWnt3a-hAFM were sequenced separately (Figures 2.4 and 2.5), and the individual peptide sequences within each of them were compared with in terms of identity and frequency (*i.e.* those sequences appearing near the x-axis in Figures 2.4 and 2.5). As a result, peptides binding to hAFM, mWnt3a-hAFM or both of them could be segregated, assessing their enrichment within the recovered final libraries and allowing the discrimination of cyclic peptides with specific affinity for Wnt3a out of the background of more prevalent ligands to hAFM.

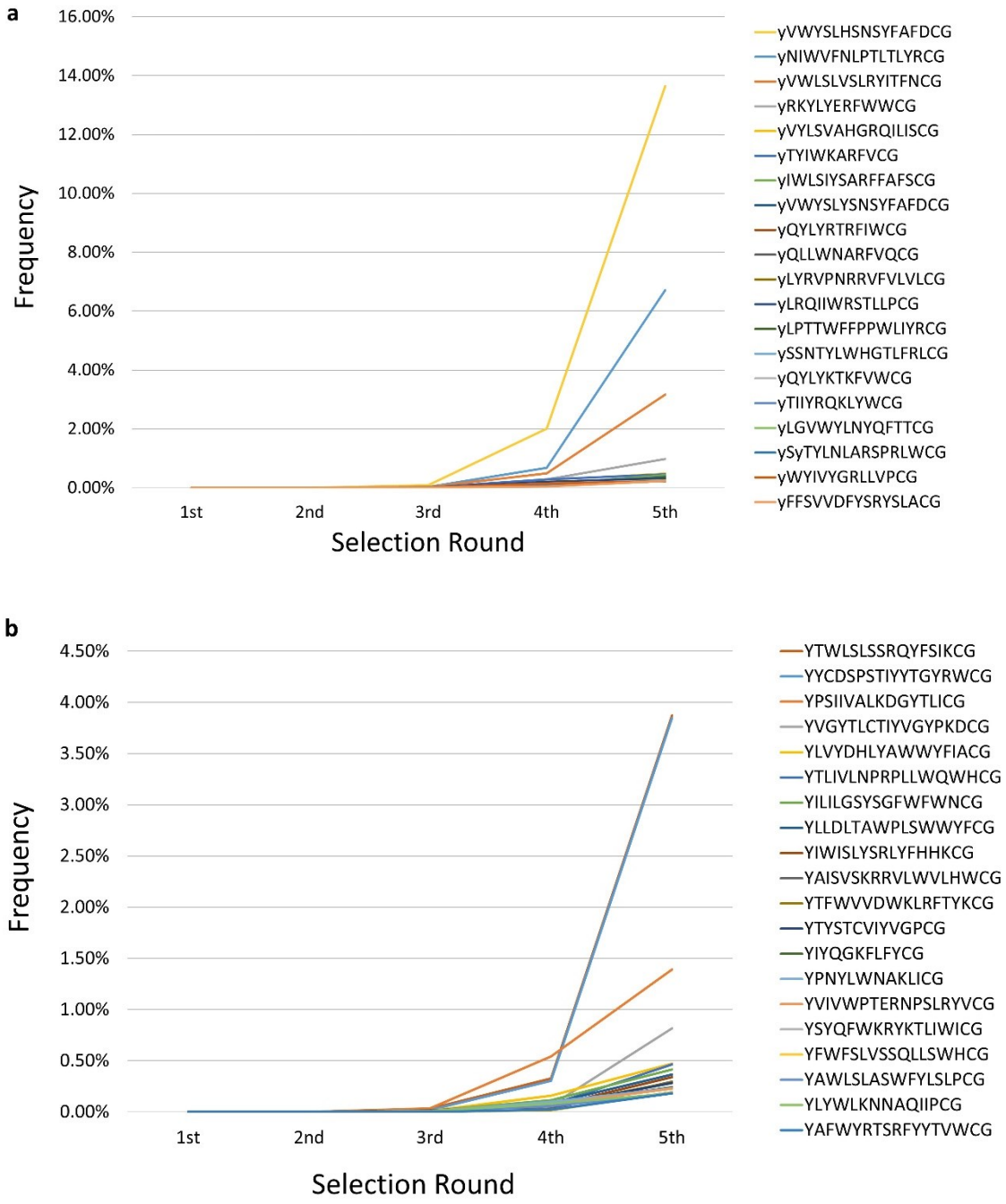

Figure 2.3 High-throughput sequencing of the selected peptide sequences against the mWnt3a-hAFM complex. (**a**) Graph show frequency (enrichment) per round of the 20 most abundant sequences throughout the selection process coming from the recovered libraries initiated by D-Tyr (**b**) Similar results for libraries initiated by L-Tyr. Individual sequences are shown in the right side, where y = D-Tyr and Y = L-Tyr.

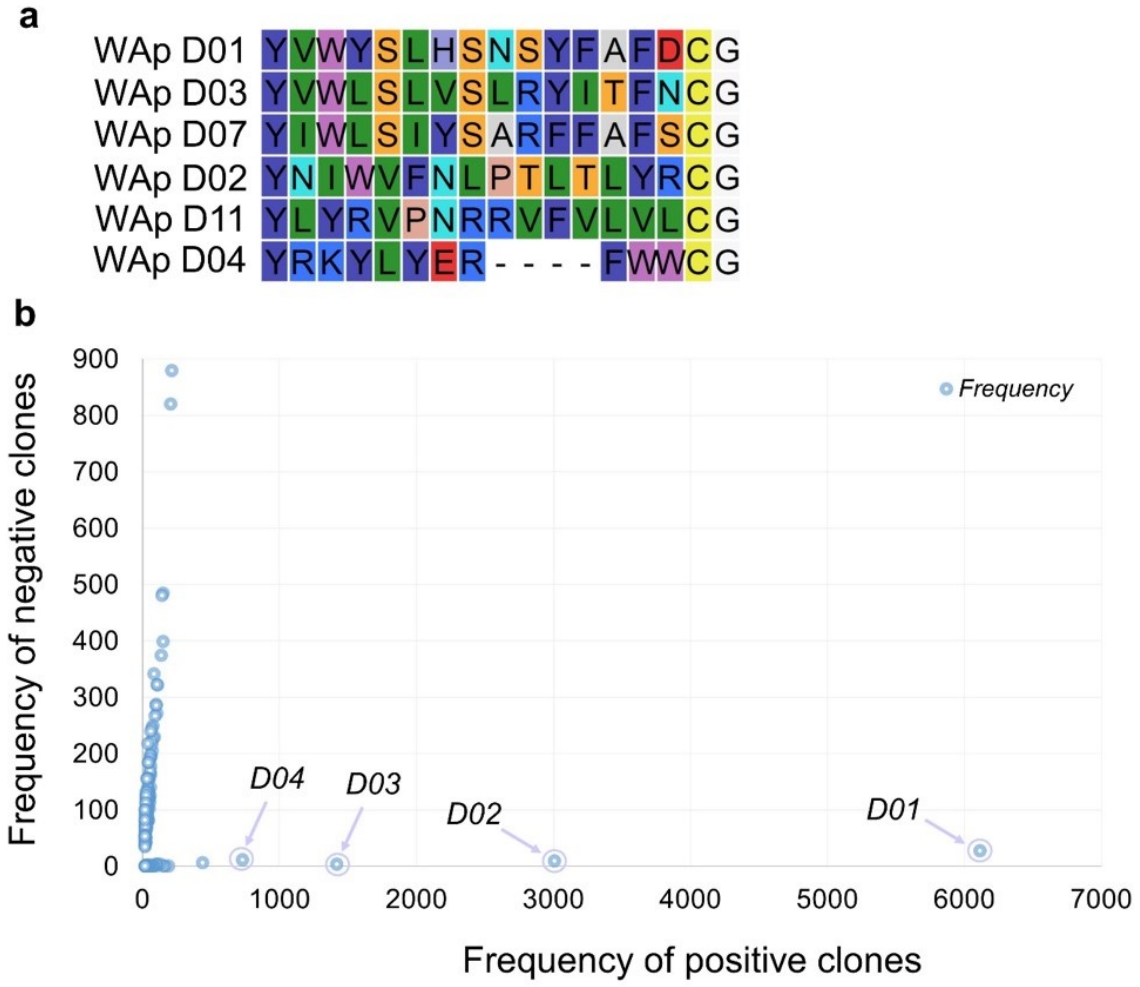

Figure 2.4 Alignment and 2D analysis of sequences in the enriched D-Tyr-initiated library. (**a**) Alignment of a few of the most enriched (frequent) sequences found within the library corresponding to the final round of selection against mWnt3a-hAFM (**b**) 2D analysis of a set of the 80 most frequent sequences from said library, found to bind to hAFM (negative clones) or mWnt3a-hAFM (positive clones). Individual sequences are marked as blue spots, with some highlighted for comparison.

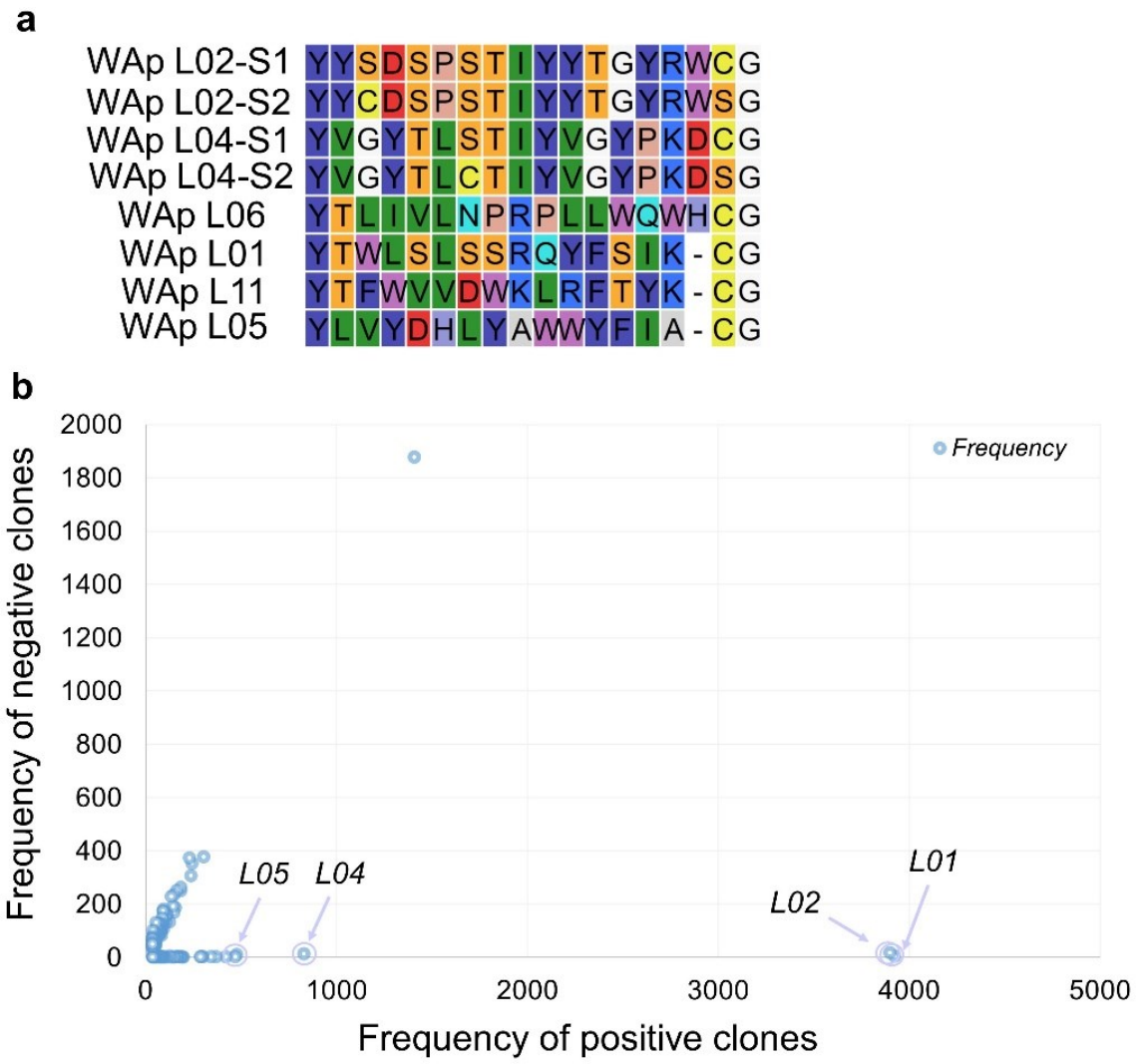

Figure 2.5 Alignment and 2D analysis of sequences in the enriched L-Tyr-initiated library. (**a**) Alignment of a few of the most enriched (frequent) sequences found within the library corresponding to the final round of selection against mWnt3a-hAFM (**b**) 2D analysis of a set of the 80 most frequent sequences from said library, found to bind to hAFM (negative clones) or mWnt3a-hAFM (positive clones). Individual sequences are marked as blue spots, with some highlighted for comparison.

From the group of sequences that appeared to have higher frequencies of isolation toward the mWnt3a-hAFM complex rather than hAFM alone, a total of 14 peptides (Table 2.1) were chosen for a RaPID-based monoclonal display assay. We found that all of these peptides showed favorable binding to the mWnt3a-hAFM complex over hAFM or beads alone (Figure 2.6). These were then chemically synthesized by solid-phase peptide synthetic method, purified by HPLC, and their structure and purity were confirmed through MALDI-TOF-MS (Figures 2.7 and 2.8) and UPLC (Figures 2.9 and 2.10). It is important, however, to note that even with all the cautions taken and analysis performed, our approach does not necessarily ensure all of them could have a biological effect on Wnt signaling, *i.e.* those capable of modulating the interaction between mWnt3a and cognate Fz, which made necessary further characterization of the individual macrocyclic peptides for not only binding affinity but also bioactivity.

Peptide name	Sequence	Read number
WAp-D01	^{Ac}yVWYSLHSNSYFAFDCG	6114
WAp-D02	^{Ac}yNIWVFNLPTLTLYRCG	3010
WAp-D03	^{Ac}yVWLSLVSLRYITFNCG	1420
WAp-D04	^{Ac}yRKYLYERFWWCG	440
WAp-D07	^{Ac}yIWLSIYSARFFAFSCG	191
WAp-D11	^{Ac}yLYRVPNRRVFVLVLCG	150
WAp-L01	^{Ac}YTWLSLSSRQYFSIKCG	3924
WAp-L02-S1	^{Ac}YYSDSPSTIYYTGYRWCG	3899
WAp-L02-S2	^{Ac}YYCDSPSTIYYTGYRWSG	3899
WAp-L04-S1	^{Ac}YVGYTLSTIYVGYPKDCG	829
WAp-L04-S2	^{Ac}YVGYTLCTIYVGYPKDSG	829
WAp-L05	^{Ac}YLVYDHLYAWWYFIACG	477
WAp-L06	^{Ac}YTLIVLNPRPLLWQWHCG	471
WAp-L11	^{Ac}YTFWVVDWKLRFTYKCG	294

Table 2.1 Chosen sequences from libraries selected against mWnt3a-hAFM. Shown is an alignment of the 14 peptides chosen for clone assays and synthesis, originated from D-Tyr (WAp-D) and L-Tyr (WAp-L)-initiated libraries found to bind the mWnt3a-hAFM complex. Sequences are numbered in increasing order of frequency (number of reads) within each recovered library at round 5.

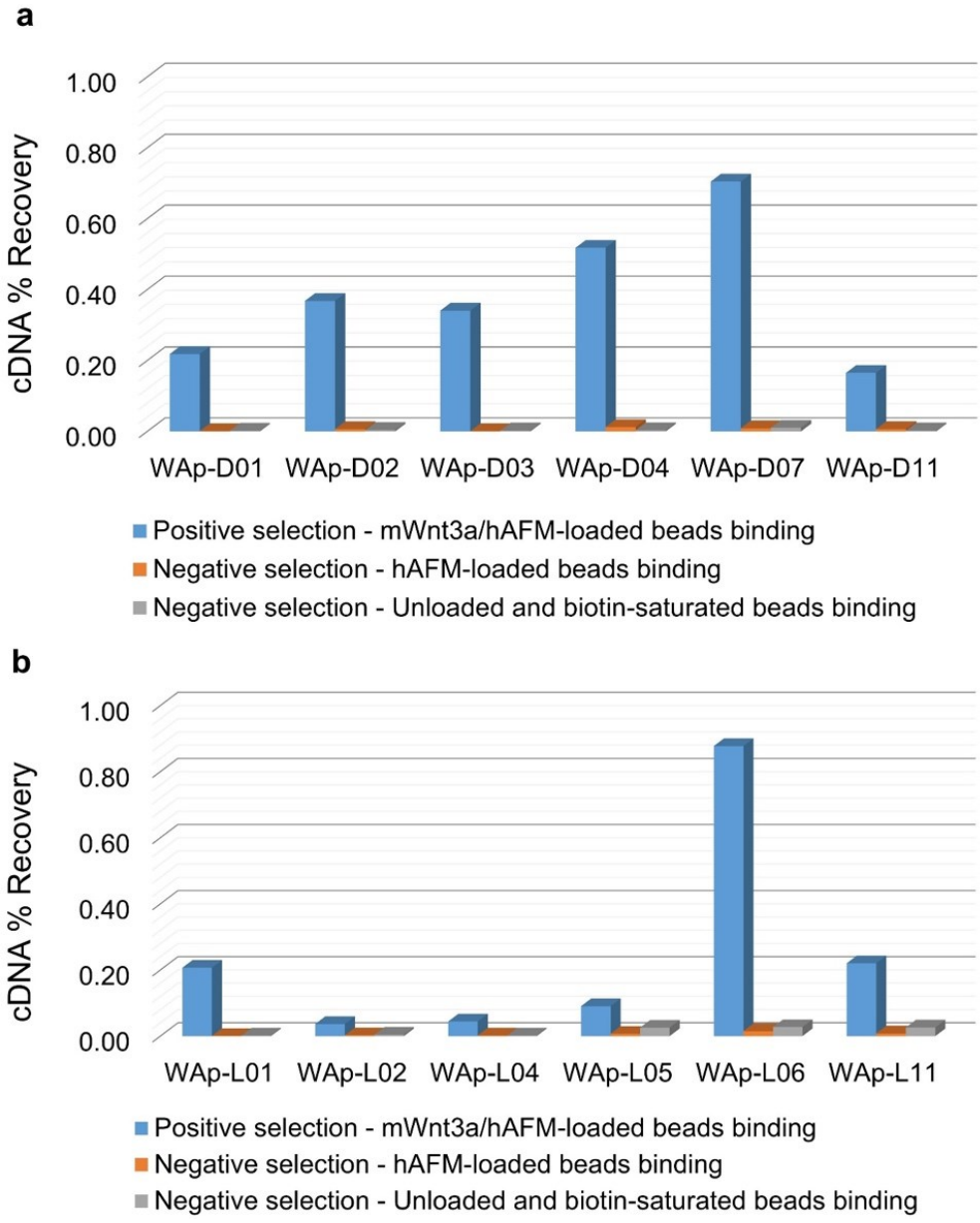

Figure 2.6 qPCR clone assay results of selected peptides against mWnt3a-hAFM. (**a**) Graph shows results obtained from single-clone, single-round selection assays (clone assays) targeting beads loaded with mWnt3a-hAFM (blue bars), hAFM (orange bars), or unloaded and biotin-saturated (gray bars) using individual sequences chosen from the selected libraries, all initiated by D-Tyr. (**b**) Similar results from the remaining sequences initiated by L-Tyr. Note that peptides WAp-L02 and WAp-L04 are shown as single peptides due to the simultaneous ribosomal expression of their S1 and S2 forms in the assay.

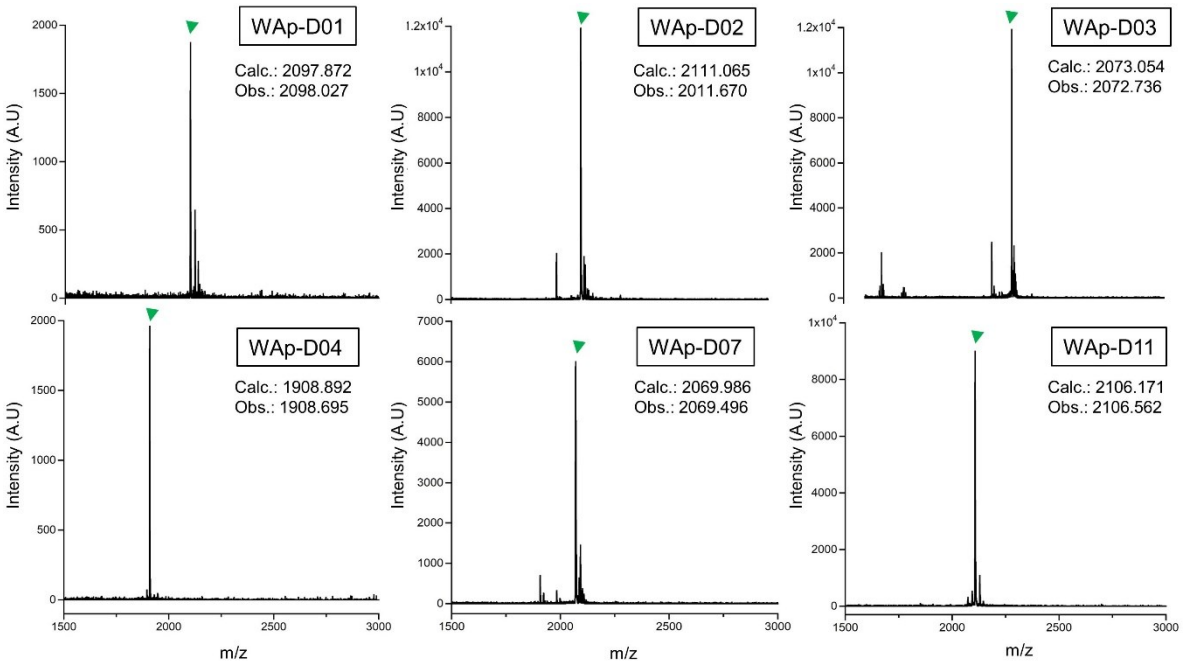

Figure 2.7 MALDI-TOF-MS spectra of selected and synthesized peptides. Shown as MS spectra of peptides shown in Table 2.1, all initiated by D-Tyr. Green triangles indicate the $[M+H]^+$ molecular ion of each peptide, of which calculated (Calc.) and observed (Obs.) masses are also shown.

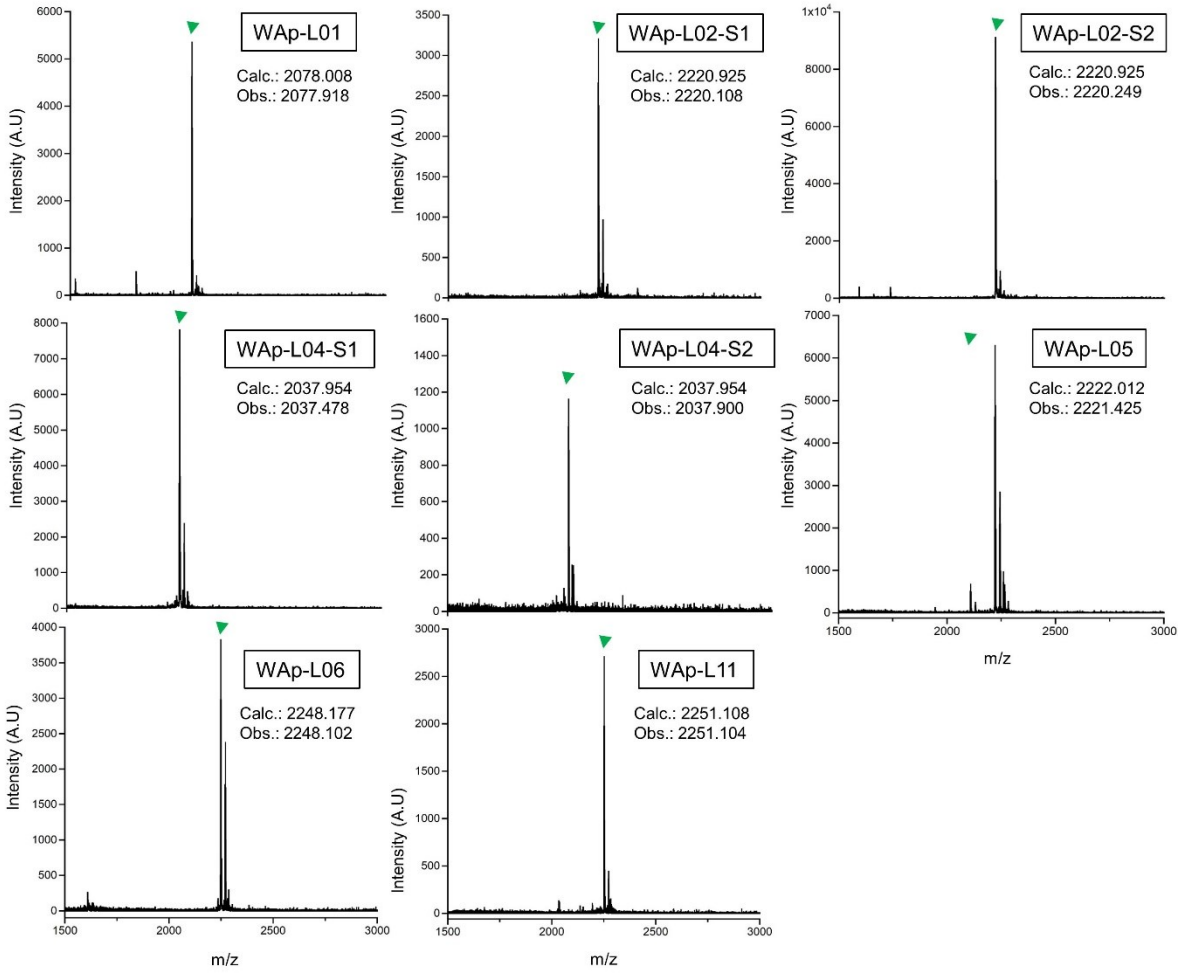

Figure 2.8 MALDI-TOF-MS spectra of selected and synthesized peptides. Shown as MS spectra of peptides shown in Table 2.1, all initiated by L-Tyr. Green triangles indicate the $[M+H]^+$ molecular ion of each peptide, of which calculated (Calc.) and observed (Obs.) masses are also shown.

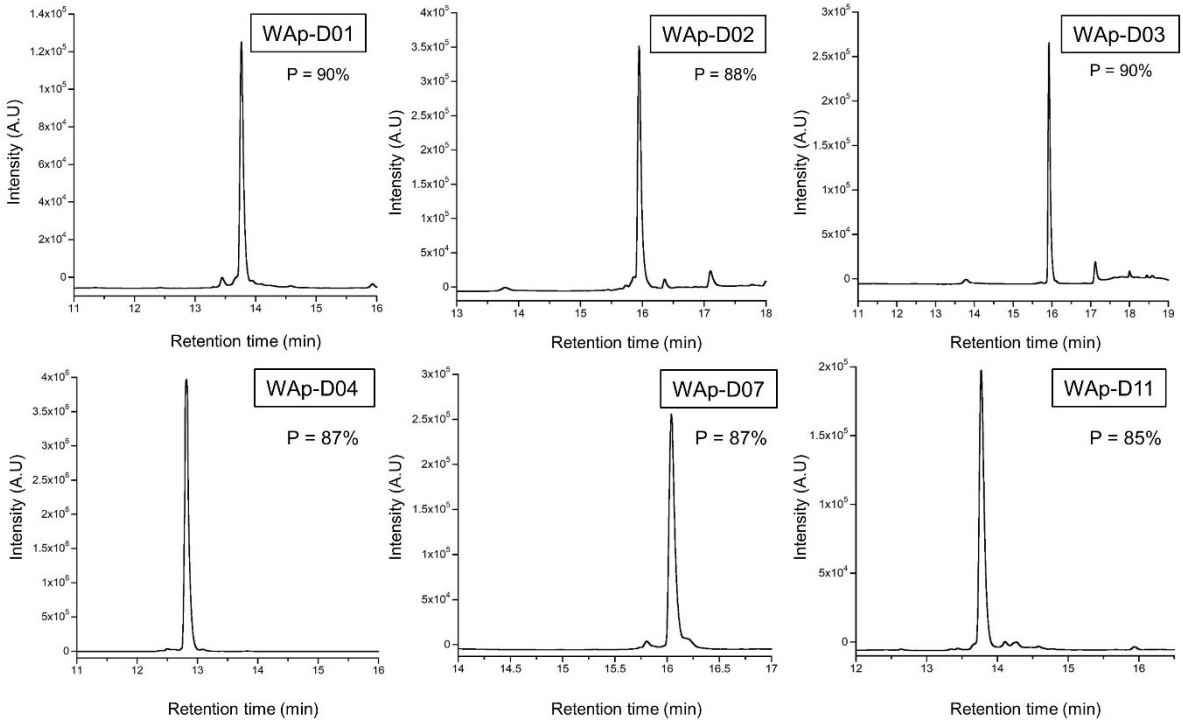

Figure 2.9 RP-UPLC chromatograms of selected and synthesized peptides. Shown are chromatograms of peptides shown in Table 2.1, all initiated by D-Tyr, with their calculated purity (P) also indicated.

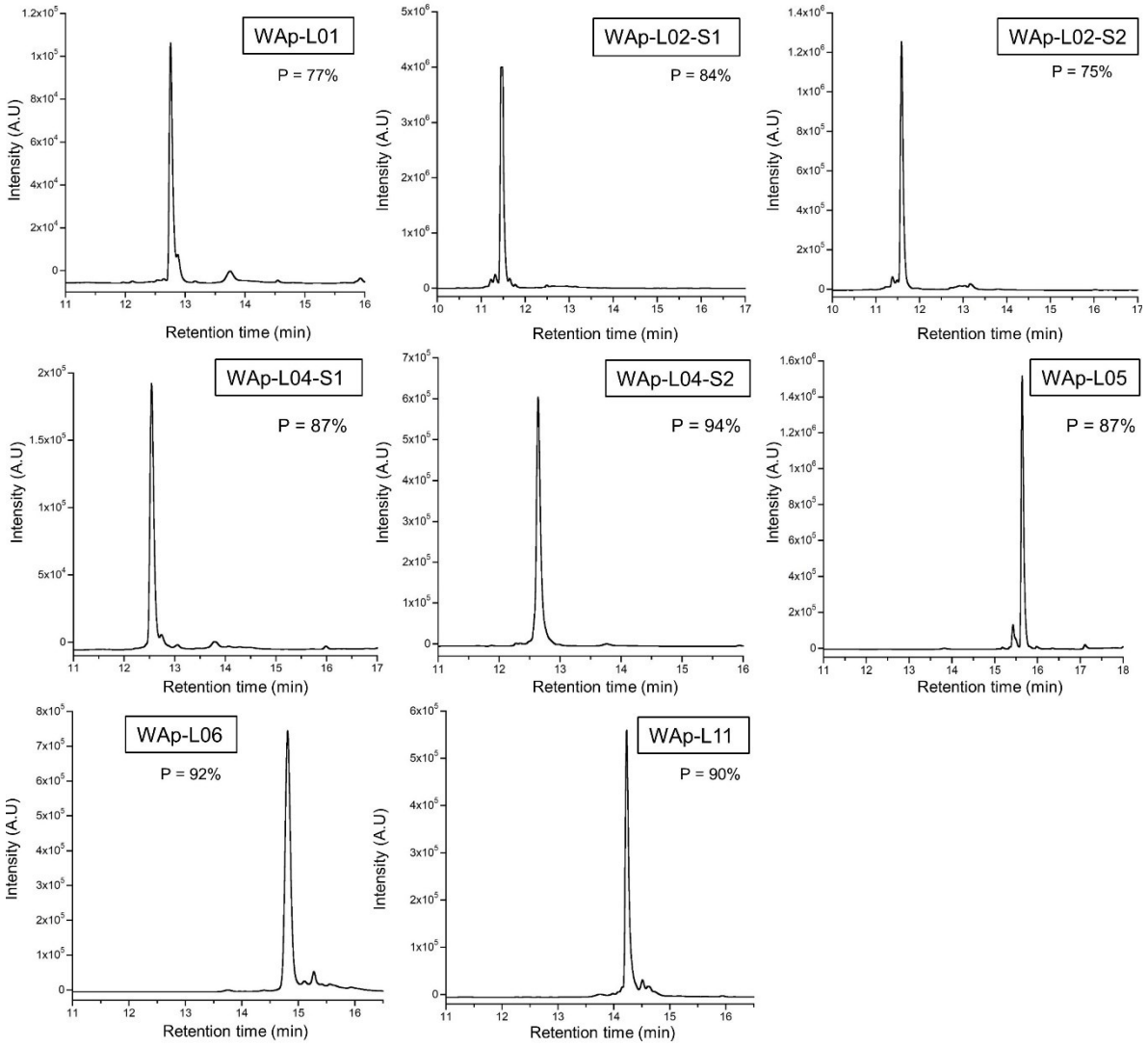

Figure 2.10 RP-UPLC chromatograms of selected and synthesized peptides. Shown are chromatograms of peptides shown in Table 2.1, all initiated by L-Tyr, with their calculated purity (P) also indicated.

Binding profile and activity of selected peptides

The binding profile of each of the 14 synthesized peptides was next assessed using surface plasmon resonance (SPR) against hAFM and mWnt3a-hAFM immobilized through amine coupling, using the former's signal as background subtraction in a 1:1 binding fitting model for a more accurate assessment of the peptides' behavior (Figure 2.11).

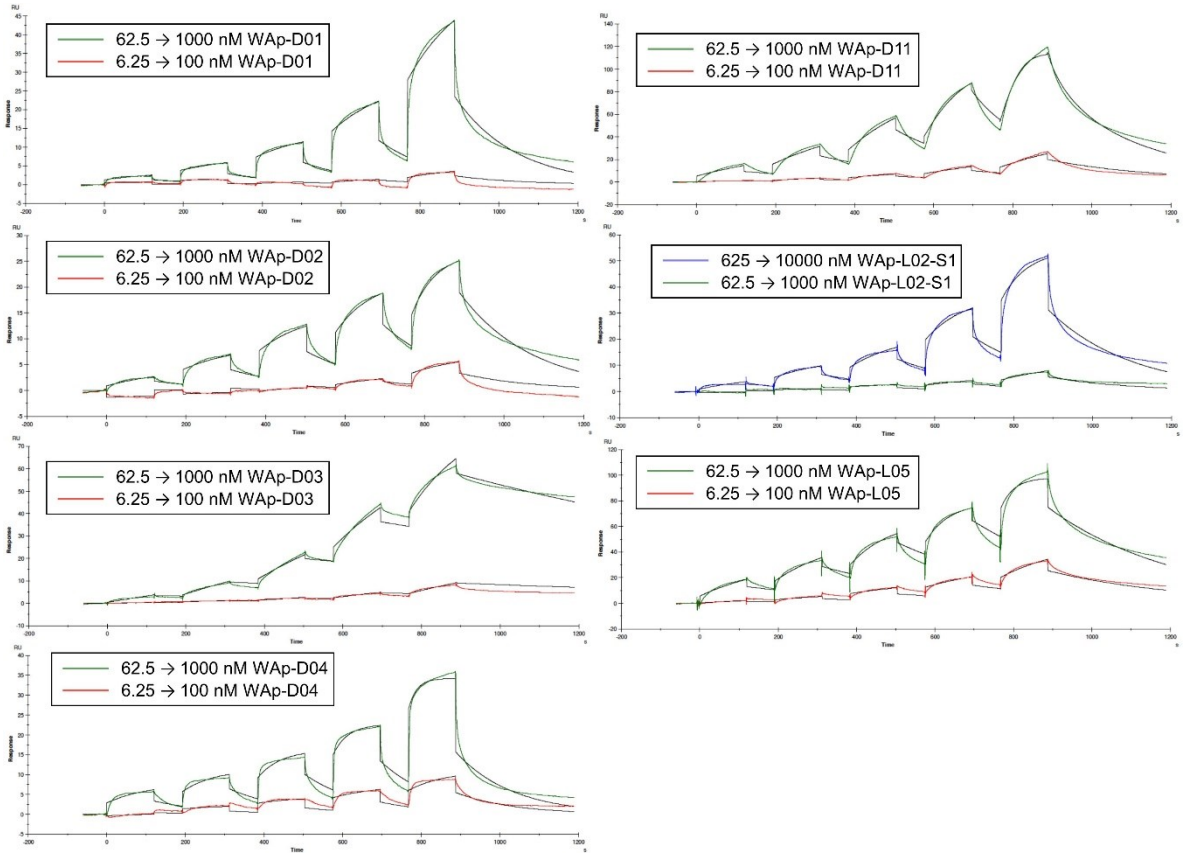

Figure 2.11 Binding profiles (kinetic analysis) of peptides selected against mWnt3a-hAFM. Sensorgrams show results from concentration ranges of 625 to 10,000 nM (blue), 62.5 to 1000 nM (green) and 6.25 to 100 nM (red) of peptides with appreciable binding response. Black lines indicate software fitting for K_D value determination.

However, unambiguous binding affinities could be determined only for four out of the 14 peptides that yielded reliable SPR profiles, while peptides WAp-D07 from the y-library and peptides WAp-L02-S2, WAp-L04-S1, WAp-L02-S2 and WAp-L06 were not found to show appreciable binding to the complex through this analysis. Additionally, even stable profiles were found to lose their fitting accuracy in higher degree binding models, for which we limited the fitting to a 1:1 binding fit. Although model fitting exhibited considerable bulk contribution for all binding measurements even after condition optimizations, four peptides with reliable and more accurate profiles (*i.e.* found to have lowest absolute residuals and Chi^2 values and closest to measurement noise levels as well as minimum standard error), exhibited potencies for mWnt3a with general nanomolar dissociation constants (K_D in Table 2.2).

Peptide name	Sequence	Number of reads	K_D (nM)
WAp-D02	^{Ac}yNIWVFNLPTLTLYRCG (S–S)	3010	490
WAp-D04	^{Ac}yRKYLYERFWWCG (S–S)	440	171
WAp-D11	^{Ac}yLYRVPNRRVFVLVLCG (S–S)	150	318
WAp-L05	^{Ac}YLVYDHLYAWWYFIACG (S–S)	477	110

Table 2.2 Characterization of macrocyclic peptides selected against mWnt3a. Shown are sequence alignments and K_D values of peptides capable of binding to mWnt3a-hAFM. WAp-Dxx peptides originated from y-library, while WAp-L05 from Y-library. Sequences are numbered in increasing order of frequency (number of reads) within each recovered library at round 5.

We next sought to assess Wnt3a signaling inhibition in a cell culture model. To validate this, we made use of a TCF/LEF element-dependent Wnt signaling luciferase reporter[75], and measured reporter response following exposure to hAFM (no signal stimulation) or mWnt3a/hAFM (Wnt signaling stimulation) in combination with each of the selected peptides, for inhibition (Figure 2.12). Notably, this initial bioactivity screening identified a single hit peptide, WAp-D04 (one of the most abundant species in the y-library), which exhibited nearly complete inhibition at a 1 μM concentration. The activity titration of WAp-D04 in a range of concentrations of 7.8–4,000 nM determined an IC_{50} value near 290 nM (Figure 2.21).

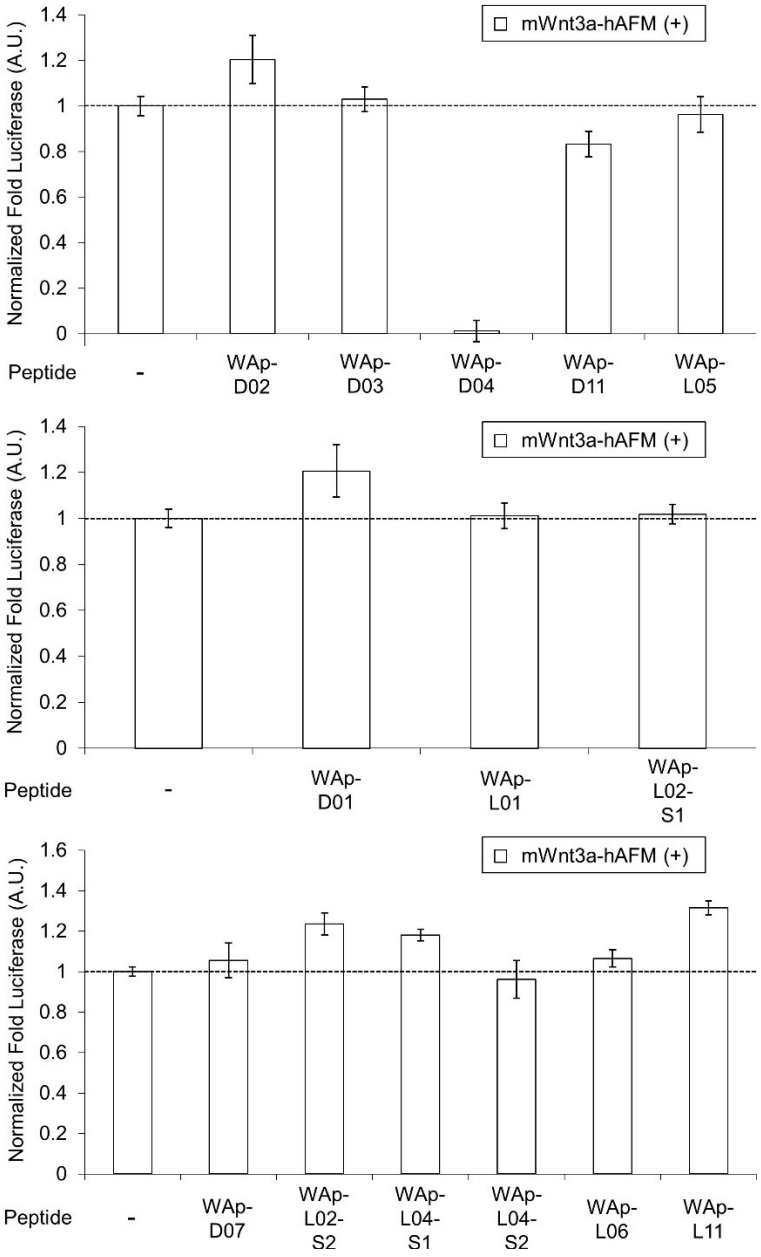

Figure 2.12 Inhibition of Wnt3a signaling by WAp-D04. Luciferase reporter activity was assessed following cell treatment with mWnt3a-hAFM-containing cell culture media, in the presence or absence of 1 μM candidate WAp-peptides. Bars show mean values of a set of four data points, all relative to a reference signal stimulated by mWnt3a-hAFM in the absence of any peptide (of which level is indicated in dotted line), while error bars indicate standard error. Data was normalized to a blank signal generated in the presence of 10 nM AFM and in the absence of any peptide, subtracted from every value.

WAp-D04 constitutes, to our knowledge, the first instance of a non-naturally occurring molecule that inhibits the Wnt signaling pathway by binding directly to a specific Wnt ligand, mWnt3a. Although the finding of such a unique and bioactive peptide with selective binding to mWnt3a constitutes an advance in developing synthetic modulators of Wnt signaling, we considered its binding and activity properties could be further improved. Notably, our unusual approach targeting mWnt3a in complex with a large stabilizing partner, hAFM, allowed us to access a very rare inhibitory species by use of 2D analysis of sequencing data. However, as we could not rule out a possibility that more potent variants of this hit peptide might not have been available in the original library (consisting of $>10^{12}$ members), we were prompted to further investigate on optimizing the initial hit WAp-D04 sequence to one with higher affinity to mWnt3a.

WAp-D04 focused library and re-selection of its active variants

In order to identify more potent analogues of WAp-D04, we next constructed a focused peptide library based on the original WAp-D04 sequence, randomizing five amino acid residues of the pharmacophore's total 10 residues. The positions for randomization were chosen as shown in Figure 2.13, where 0 to 5 (X-1 to X-5) consecutive mutations occurred. We prepared individual synthetic DNA template libraries and transcribed them into mRNA libraries. All of the resulting mRNA libraries were mixed into a focused mRNA library for the expression of macrocyclic peptide libraries. Additionally, a library of the same design initiated by L-Tyr was also prepared and selected, in order to analyze the effects t\of the stereochemistry of the initial Tyr. Five rounds of selection were then performed to enrich the active population (Figure 2.14), and the enriched libraries were finally deep-sequenced to identify improved analogues of WAp-D04 (Figure 2.15).

Figure 2.13 Design of WAp D04-focused libraries. The library was composed of five groups of structural variations, changing consecutive amino acids according to group number and translocating the variation along the chain. X indicates a random amino acid determined by an NNK codon. Additional library initiated by L-Tyr was also prepared following the same design scheme.

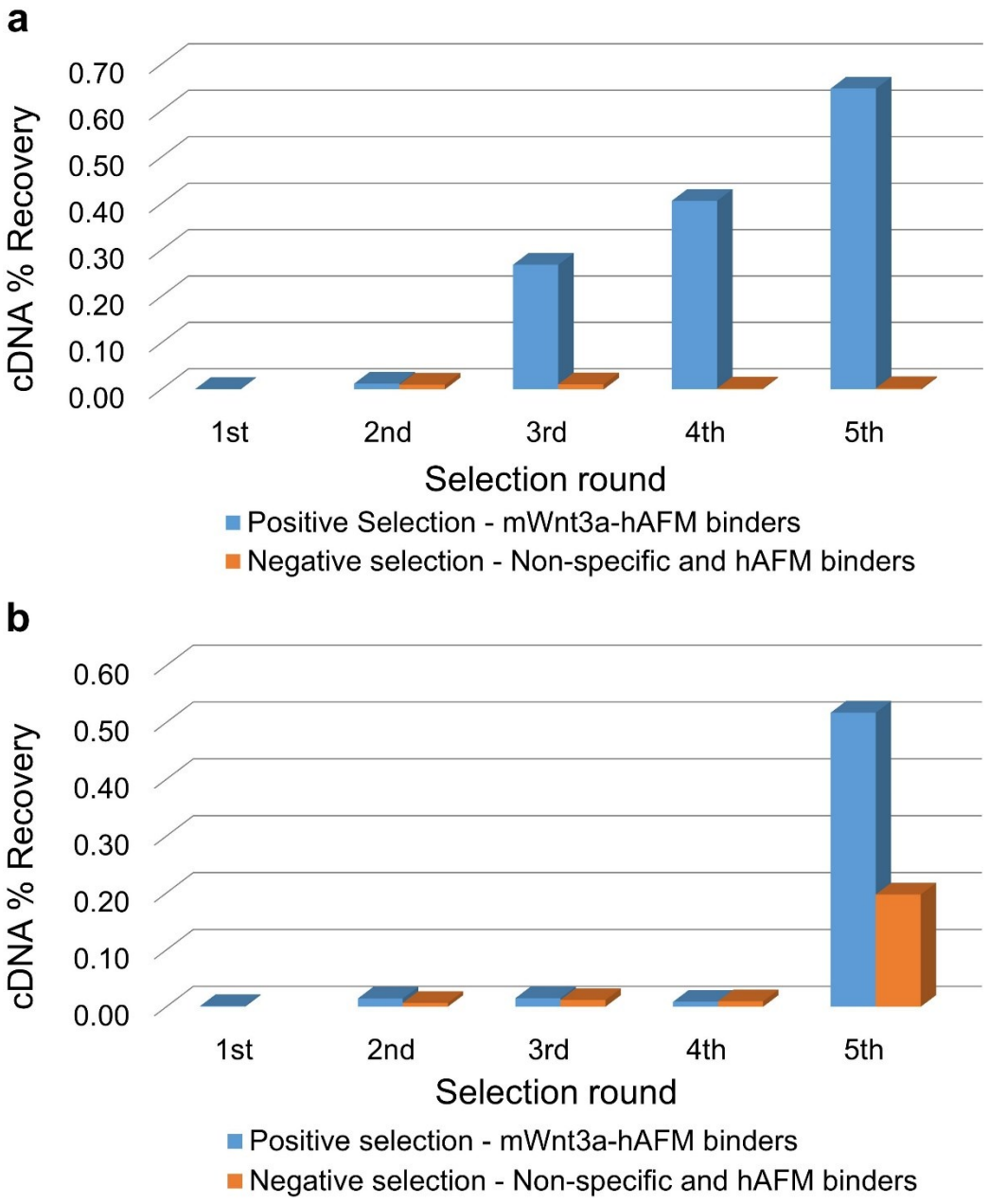

Figure 2.14 qPCR selection results of targeting the mWnt3a-hAFM complex with a WAp-D04-focused library through the RaPID system. (**a**) Graph shows recovered cDNA from the focused macrocyclic library per round of selection against mWnt3a-hAFM, obtained from the macrocyclic peptide library initiated by D-Tyr (**b**) Similar results corresponding to the library initiated by L-Tyr. Blue bars indicate the fraction corresponding to the cDNA of peptides bound to the complex, while orange bars indicate non-specific binders, including ones binding to only-hAFM-loaded magnetic beads.

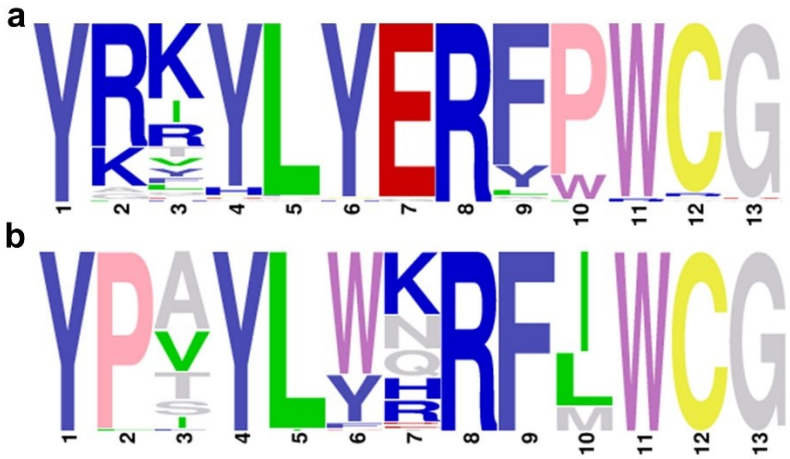

Figure 2.15 Sequence LOGO[76] graphs of the final round of selection of the WAp-D04-focused libraries against mWnt3a-hAFM. (**a**) LOGO represents the 80 most enriched sequences from the recovered peptide libraries initiated by D-Tyr. Note that the first Y residue of in the LOGO graph corresponds to D-Tyr (y) (**b**) Similar results for the libraries initiated by L-Tyr.

The selection campaign of the focused library yielded six mutant peptides of the wild-type parental peptide (WAp-D04-WT). All newly identified peptides contained a highly conserved Trp to Pro substitution at position 10, as represented by the single mutant WAp-D04-W10P, and exhibited higher frequency following isolation with mWnt3a-hAFM as compared to hAFM in 2D analysis (Figures 2.15 and 2.16). Double mutation occurred either at positions 2 or 3 along with the W10P mutation, with conservative mutations at R2 or K3 to a basic sidechain alternative (R2K or K3R) or hydrophobic sidechain alternative (K3I, K3T, or K3V) (Table 2.3). Thus, the result of this focused library selection indicated that WAp-D04-WT itself is well optimized, but that the subtle W10P mutation possibly enhanced the inherent binding ability of WAp-D04-WT. The library initiated by L-Tyr, in contrast, showed a larger degree of variability, particularly in positions 6, 7 and 10 and a fixed change from Arg to Pro in position 2, though an overall similarity to the original peptide sequence could still be observed. Based on these findings, we synthesized all six WAp-D04 mutants from the y-library, while considering the lower conservation observed in the L-library, three mutants from it were also prepared (Figures 2.17 and 2.18). All of these peptides were then tested for their binding and inhibitory activity as in the previous reporter assay.

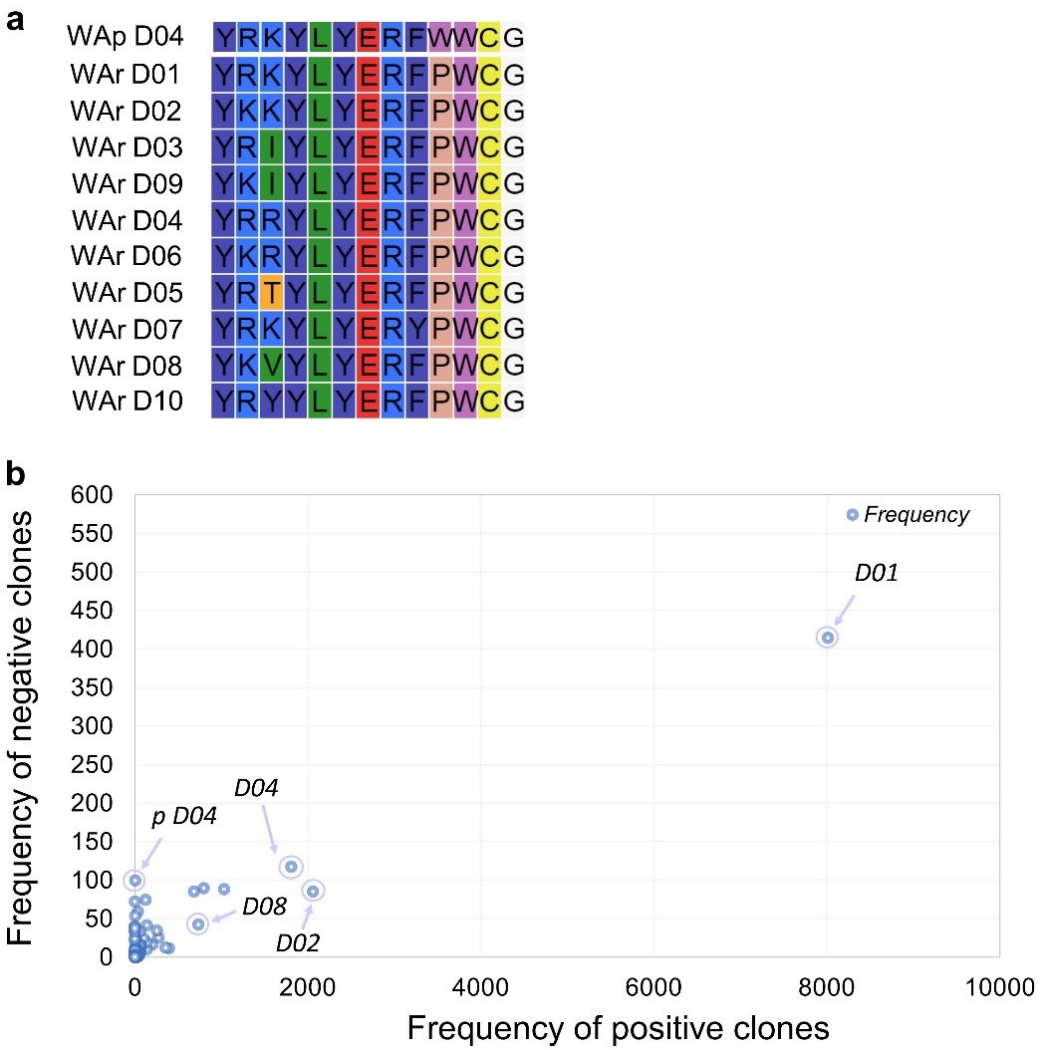

Figure 2.15 Alignment and 2D analysis of sequences of the enriched WAp-D04-focused, y-library. (**a**) Alignment of a few of the most enriched (frequent) sequences (shown here as WAr D) found within the library corresponding to the final round of selection against mWnt3a-hAFM (**b**) 2D analysis of a set of the 80 most frequent sequences from the library, found to bind to hAFM (negative clones) or mWnt3a-hAFM (positive clones). Individual sequences are marked as blue spots, with some highlighted for comparison. Additionally, original peptide WAp-D04 (p D04 in graph) is also shown, displaying the presence of the parental sequence in the recovered focused library.

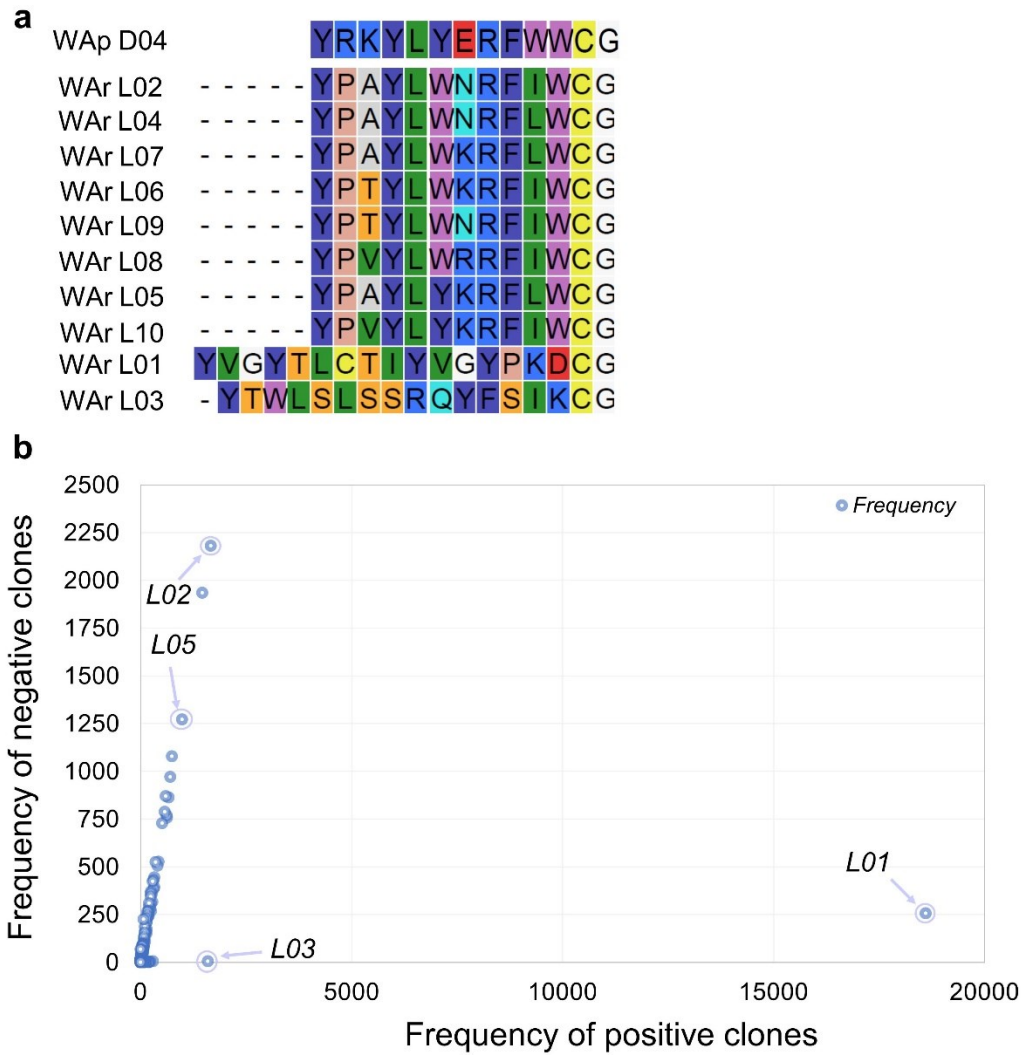

Figure 2.16 Alignment and 2D analysis of sequences of the enriched WAp-D04-focused, Y-library. (**a**) Alignment of a few of the most enriched (frequent) sequences (shown here as WAr L) found within the library corresponding to the final round of selection against mWnt3a-hAFM (**b**) 2D analysis of a set of the 80 most frequent sequences from the library, found to bind to hAFM (negative clones) or mWnt3a-hAFM (positive clones). Individual sequences are marked as blue spots, with some highlighted for comparison.

Peptide	Sequence	Number of reads	K_D (nM)	IC_{50} (nM)
WAp-D04-WT	^{Ac}yRKYLYERFWWCG	125	319	290
WAp-D04-W10P	^{Ac}yRKYLYERFPWCG	8014	39.5	56
WAp-D04-W10P/R2K	^{Ac}yKKYLYERFPWCG	2059	-	-
WAp-D04-W10P/K3I	^{Ac}yRIYLYERFPWCG	1808	-	-
WAp-D04-W10P/K3R	^{Ac}yRRYLYERFPWCG	1034	-	-
WAp-D04-W10P/K3T	^{Ac}yRTYLYERFPWCG	796	-	-
WAp-D04-W10P/R2K/K3Y	^{Ac}yKVYLYERFPWCG	395	-	-
WAfp-L02-WT	^{Ac}YPAYLWNRFIWCG	1669	-	-
WAfp-L02-W6Y/N7K/I10L	^{Ac}YPAYLYKRFLWCG	983	-	-
WAfp-L02-A3T/N7K	^{Ac}YPTYLWKRFIWCG	746	-	-

Table 2.3 Alignment, binding and inhibition properties of selected sequences from Wap-D04-focused, D-Tyr- and L-Tyr-initiated libraries found to bind the mWnt3a-hAFM complex. Sequences are numbered in increasing order of frequency (number of reads) within the final round of each recovered library. Steady-state K_D and IC_{50} values are shown for the parental and W10P single-mutant peptides of the y-library. The parental (WT) WAp-D04 sequence, which appeared in the final enriched y-library as well, is also shown above for comparison.

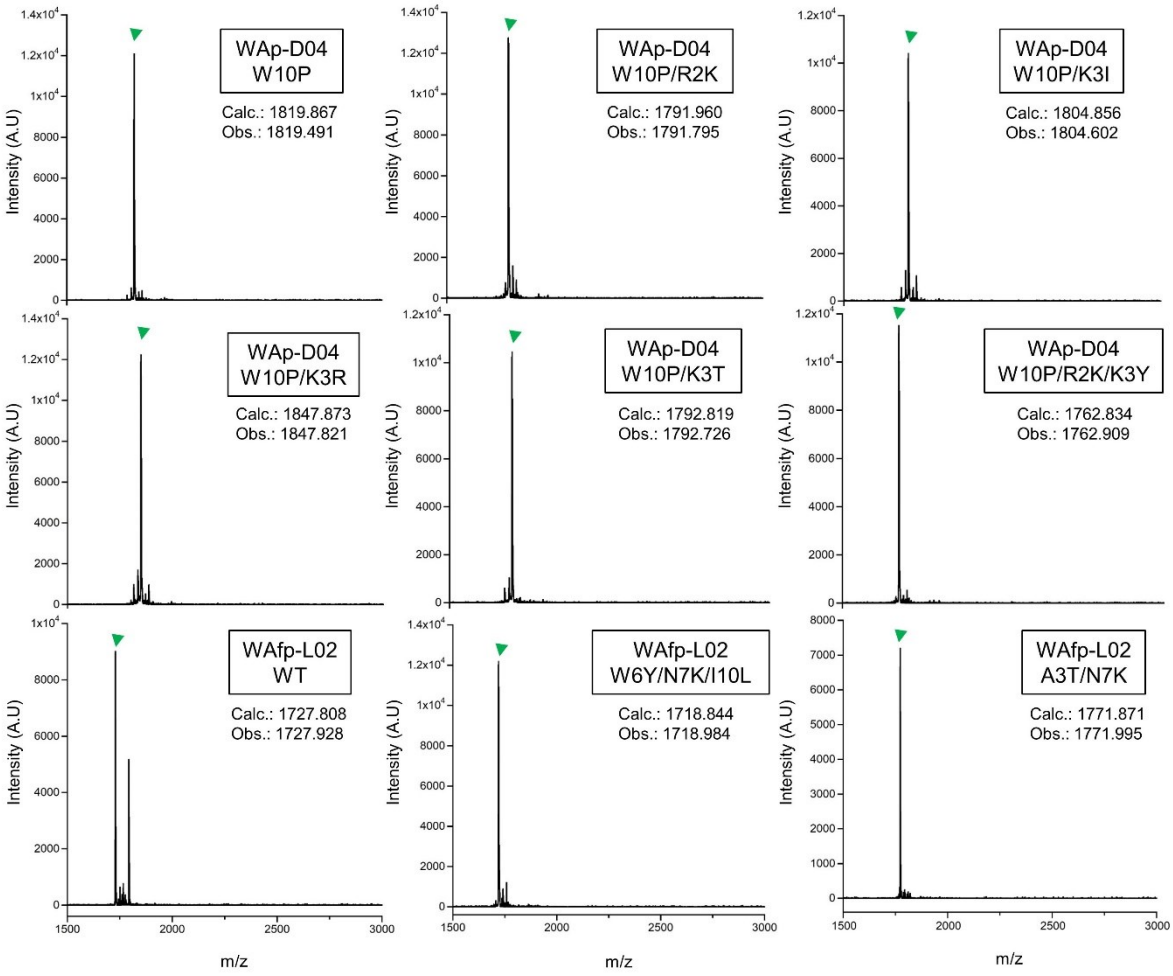

Figure 2.17 MALDI-TOF-MS spectra of selected and synthesized peptides from the WAp-D04-focused libraries. Shown as MS spectra of peptides shown in Table 2.3, each with its indicated mutation from the parental peptide. Green triangles indicate the $[M+H]^+$ molecular ion of each peptide, of which calculated (Calc.) and observed (Obs.) masses are also shown.

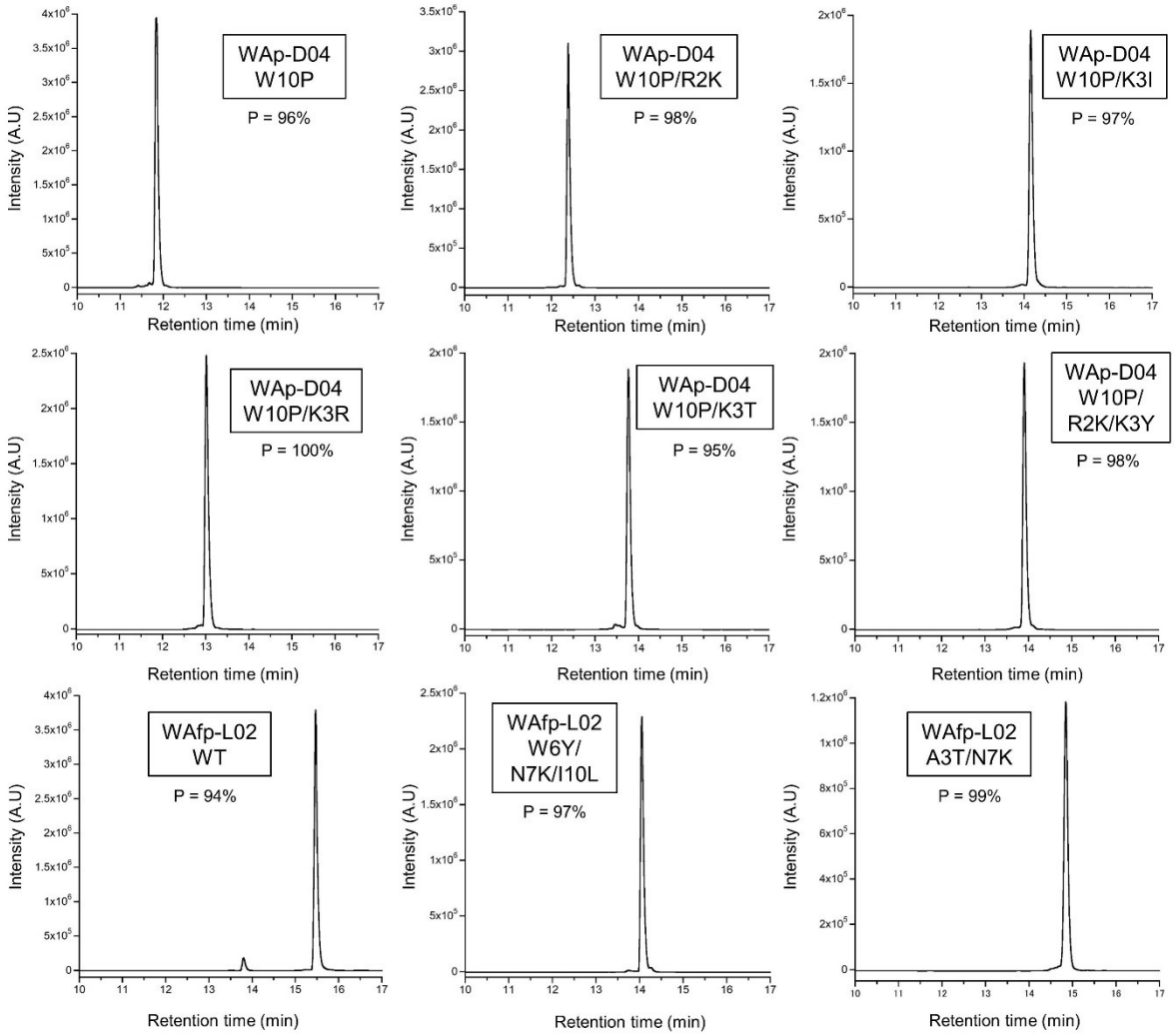

Figure 2.18 RP-UPLC chromatograms of selected and synthesized peptides from the WAp-D04-focused libraries. Shown are chromatograms of peptides shown in Table 2.3, each with its indicated mutation from the parental peptide and their calculated purity (P).

Inhibitory activity of WAp-D04-W10P mutants

The synthesized WAp-D04-W10P mutants were analyzed for Wnt3a signaling inhibitory activity at two concentrations values (0.16 and 1.6 μM) in the reporter assay for primary screening (Figure 2.19). Remarkably, all six peptides from the focused y-library exhibited stronger inhibition than the WT, particularly at 1.6 μM concentration, at which all peptides shut down Wnt signaling, *i.e.* they completely inhibited binding of mWnt3a to its cognate receptor. Even at 0.16 μM peptide concentration, appreciable inhibition occurred, where the single mutant WAp-D04-W10P (Figure 2.20) itself displayed slightly more potent inhibitory activity than the series of double mutants. This datum is consistent with the observation that it was the most abundant sequence in the next generation sequencing data (Table 2.3). In contrast, peptides from the Y-library, *i.e.* L02-WT and its mutants, were found to almost completely lose the original inhibitory activity seen in the parental peptide, even at high 1.6 μM peptide concentration in the case of the L02 mutants. These results however, seem to agree with the fact that the WAp-D04 wild type sequence was not observed in the original or focused Y-library, even if WAfp-L02 does share some structural similarity with the identified inhibitor, potentially hinting an effect of the stereochemistry of the initiating Tyr on binding to the mWnt3a ligand.

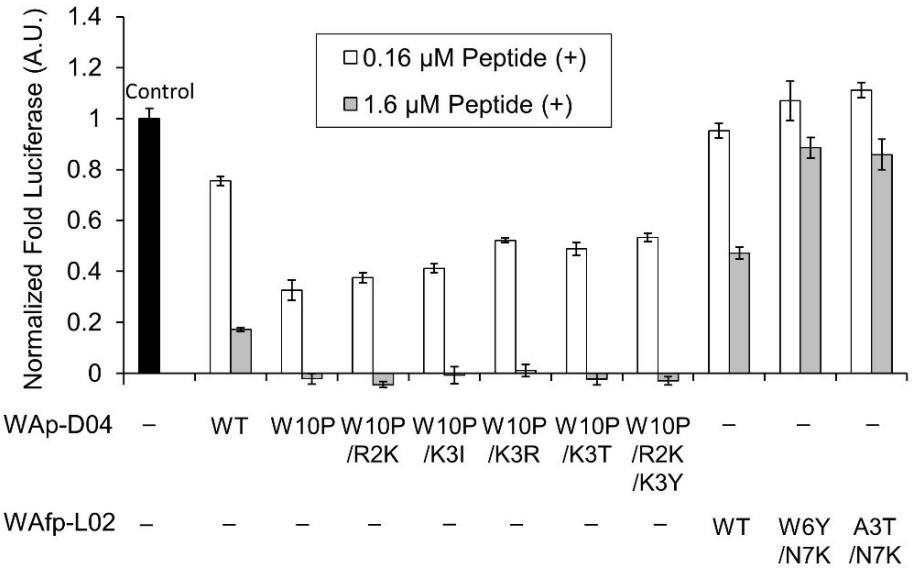

Figure 2.19 Focused library-selected peptides' activity showing luciferase reporter assay results for the peptides shown in Table 2.3. The effect of each peptide on activity was analyzed independently at 0.16 and 1.6 μM concentration in the presence of 10 nM Wnt3a-AFM complex. Shown are fold values relative to a basal Wnt signal reference (black bar) using 10 nM mWnt3a-hAFM in the absence of any peptide. All data was normalized to a blank signal generated in the presence of 10 nM AFM and in the absence of any peptide, subtracted from every value.

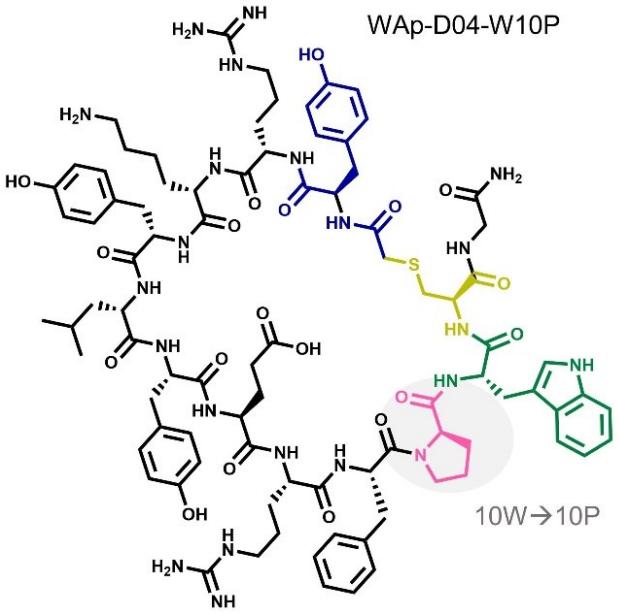

Figure 2.20 Structure of the strongest peptide inhibitors found in selection campaigns against mWnt3a-hAFM. The single W10P mutation (highlighted) was found to dramatically increase inhibitory activity of WAp-D04.

Further characterization through a titration of WAp-D04-W10P (7.8–4,000 nM) demonstrated that inhibition of Wnt3a signaling by this peptide was concentration dependent as with WAp-D04-WT, but approximately 5-fold more potent, *i.e.* IC_{50} of 56 nM as compared to 290 nM for WAp-D04 (Figure 2.21). This is a remarkable finding considering that these two compounds differ at only a single amino acid residue. Additionally, SPR studies using Fc-fusion isoforms of hAFM and mWnt3a-hAFM stabilized the steady state binding profiles of these peptides (Figure 2.22) and determined the steady state K_D value decreased from 319 nM of the WT to 39.5 nM of the W10P mutant, *i.e.* WAp-D04-W10P exhibited an 8-fold enhanced affinity from the parental peptide.

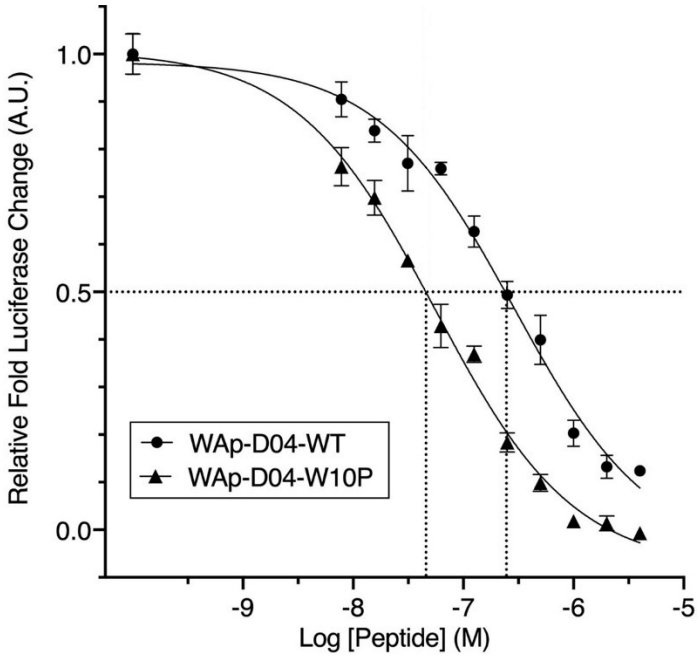

Figure 2.21 Overall inhibition rate properties of WAp-D04-WT and WAp-D04-W10P. Shown is a sigmoidal fit of independent luciferase reporter assay results for the two peptides under Wnt signaling stimulation with 10 nM mWnt3a-hAFM. Data points correspond to the mean of 4 measurements of the effects of each of the varying peptide concentrations on overall luciferase reporter activity. Values indicate changes in fold luciferase relative to a basal Wnt signal reference using 10 nM mWnt3a-hAFM in the absence of any peptide. Concentration values of each peptide and activity corresponding to IC_{50} are marked with dotted lines for comparison.

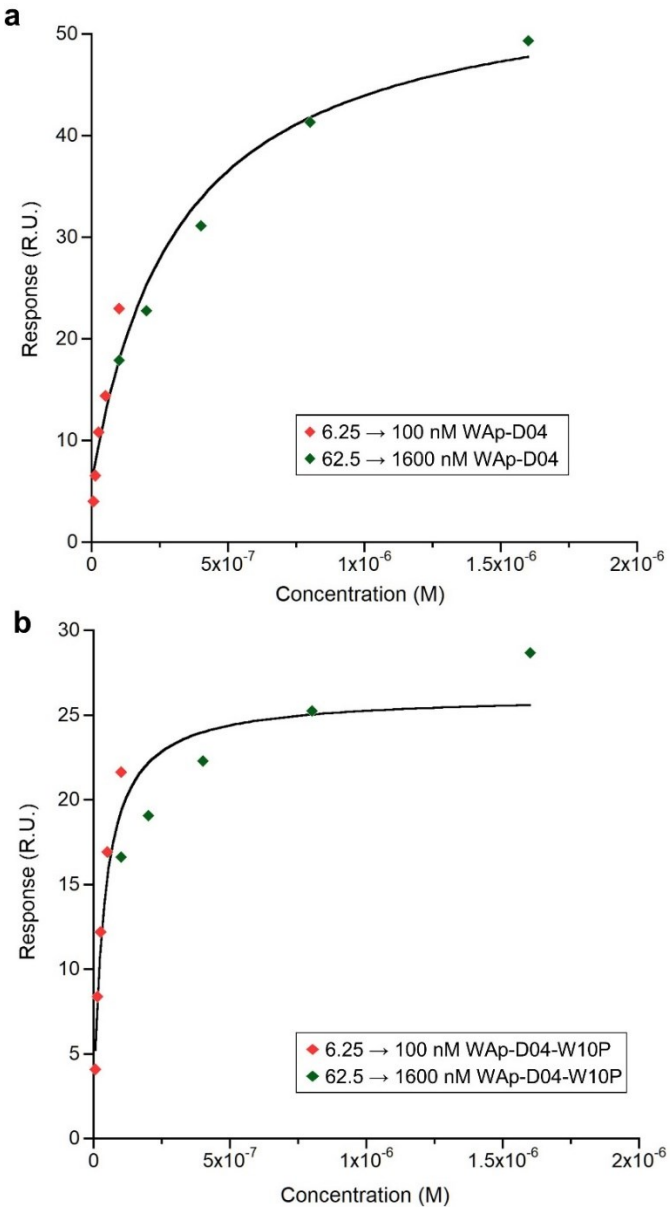

Figure 2.22 Steady state binding profiles of wild-type (WAp-D04) and optimized (WAp-D04-W10P) peptide inhibitors of Wnt signaling found in this work. (**a**) Sensorgram corresponding to concentration ranges of 6.25 to 100 nM (red diamonds) and 100 to 1600 nM (green diamonds) of wild-type peptide inhibitor WAp-D04 (**b**) Similar analysis for optimized peptide WAp-D04-w10p. Black curves indicate software fitting for K_D value determination.

Discussion

Wnt signaling is a critical component of embryonic development and post-development homeostasis, and its role in oncogenic processes such as colorectal cancer has led to the development of a number of different Wnt pathway inhibitors[59,77,78]. These inhibitors target diverse components of the Wnt signaling mechanism, including Fz receptors, components of the destruction complex and β-catenin. However, direct targeting of Wnt ligands themselves has remained challenging due to the relative instability of Wnt proteins and the consequent difficulty in developing agents against them and their analysis performed through varied methods, such as lipid-stabilization[58,79] and ultracentrifugation[80]. Even with such considerations, to the best of our knowledge, the present study described the first instance of a relatively small molecule actin as a direct Wnt protein inhibitor[58,59,77-80].

A key advantage of our approach is the use of a recently identified stabilized form of a Wnt ligand (mWnt3a-hAFM) allowing the direct selection of anti-mWnt3a macrocyclic peptides through the RaPID system. RaPID is remarkably versatile and reliable, allowing the screening of a vast sequence space of macrocyclic peptide libraries, potentially including both canonical and non-canonical amino acids[66,70,81,82]. However, RaPID screening and its cell-free character generally requires "soluble", *i.e.* pure and stable "bait" proteins, and it is therefore not well applicable to "insoluble" proteins with intrinsic structural fragility that results in self-aggregation. Furthermore, use of protein complexes present the additional difficulty of binding non-specific members of the libraries used, limiting the range of proteins able to target through the system. The unique strategy reported here (*i.e.* the use of a stabilizing protein partner during the selection process) solubilizes such fragile proteins by folding them adequately within a complex, preventing exposure of their insoluble hydrophobic domains and making selection against these targets an achievable task.

Notably, the ~70 kDa protein partner (hAFM) present in the complex used in our approach had not been deeply studied until recently, with studies showing that its Wnt-stabilizing role might be potentially due

in part to binding and covering of the palmitoleoylated Ser in Wnt's Fz binding site[50], while allowing varied Wnt proteins' solubility, biological activity and long-term storage seems to indicate the complex might be one of the ways secreted Wnt proteins are transported and available in body fluids[44,47].

It is also worth noting that, despite our best efforts of applying aggressive counter-selection to the "solubilizing" protein partner hAFM, the enriched pool of peptides yet contained background binders to this partner. This is a somewhat surprising finding, considering similar counter-selection strategies have proven to be effective in previous RaPID selection campaigns (*e.g.* when suppressing the recovery of Fc binding peptides during selection against Fc-tagged proteins[83]). Nonetheless, the application of a large number of cycles against Wnt3a's partner protein, as well as the use of the deep-sequencing data analysis technique we applied in this work (*i.e.* comparing sequences recovered from both Wnt3a/hAFM-coated beads and hAFM-coated beads) allowed us to qualitatively discriminate which peptides bound solely to the mWnt3a target. This way, we were able to distinguishably identify mWnt3a binders over hAFM binders, and together with the application of a functional assay using the Wnt-signaling reporter cell line, led us to the a rare hit molecule WAp-D04, an 11-member-ring macrocyclic peptide capable of binding mWnt3a specifically and inhibiting the mWnt3a-receptor interaction with a sub-μM level. These characteristics also come in contrast to currently available protein mimetics or small-molecules with non-specific effects, or that target membrane and/or intra-cellular pathway components[61,84-91].

As mentioned above, Wnt ligands are not commonly targeted for inhibition of the pathway, with available drugs commonly involving other components of the pathway. Such therapeutics include Foxy-5, a formylated hexapeptide Wnt5a mimetic targeting Fz2 and Fz5[61,84], Rosmantuzumab, a monoclonal antibody targeting r-spondin 3 (RSOP3)[85] or Imatinib, a small molecule which targets tyrosine kinases[86,87]. Additionally, approaches with more general and non-specific effects like inducing endocytosis and apoptosis using Celecoxib[88-90] and Niclosamide[91] are also known as potential antineoplastic therapeutics involving deregulation of the pathway. In contrast, our findings have determined the first case of a

medium-sized molecule able to strongly inhibit the pathway through the selective binding to a Wnt member, attaining potentially beneficial binding selectivity profiles.

Building on this finding, the subsequent selection campaign using a "pharmacophore-focused library" enabled us to identify several improved Wnt3a inhibitors. Notably, the selection itself showed a suppressed background recovery, confirming a biased binding of the original peptide and its variations towards mWnt3a, while the lack of stability and loss of conservation in the L-Tyr-initiated library seemed to indicate a possibility that stereochemistry of the first residue was involved in the binding mode to its mWnt3a target. This hypothesis was also supported partly when analyzing the activity of a set of peptides enriched in the L-Tyr-initiated library, which showed an almost complete loss of Wnt pathway inhibition properties when compared to the original WAp-D04. In contrast, all members of the group of peptides initiated by D-Tyr that maintained the W10P mutation with slight variations in positions 2 and 3 showed a considerable increase in their inhibition activity compared to the original structure, with almost no considerable change in the intensity of their effect. These results pointed towards a less critical of these positions (2 and 3) in binding, while proving the change in position 10 from an aromatic, hydrophobic amino acid to an aliphatic, more structurally constrained residue.

A deeper analysis comparing these apparent small changes in structure of only a single amino acid exhibited a surprisingly large effect on inhibition properties, leading us to discover the most potent member in our libraries, the single W10P mutant, a 5-fold enhanced inhibitors with 56 nM IC_{50} exclusively through this single substitution. Additionally, the peptide showed an 8-fold improvement in mWnt3a binding affinity relative to the parental WAp-D04 molecule. This makes the mutant W10P one of the most potent Wnt inhibitors yet described, a fact rather surprising considering that the improved activity and affinity arise from a single W10P substitution near the cyclizing Cys residue.

Identification of both WAp-D04 and its W10P in our selection campaigns remains a remarkable finding, particularly considering the lack of structurally (both in sequence and ring size) similar analogues within

any of the recovered final round peptide libraries. Additionally, the W10P mutant was not originally identified in the recovered libraries from the first selection campaign against mWnt3a-hAFM, pointing towards the translation limitations of our system. Although able to generate vast peptide libraries of more than 10^{12}-10^{13} members, the system is still not able to completely translate each theoretically possible member of the initial libraries of largest random codon length for the first selection round, in which even single copies of translated peptides are present. Consequently, the focused library campaign looked to improve the potential of this initial hit, and was successful not only in identifying an optimized version of the peptides, but also in confirming the structural traits mostly necessary for binding to the complex and inhibition of the Wnt signaling chain through its mostly conserved motifs.

Although at this stage we cannot concretely define exactly why or how the W10P mutation was able to enhance its activity, the mutation occurred near the cyclizing C12 and Pro is the unique secondary amino acid among other proteinogenic amino acids. Thus, the W10P mutation may increase the structural rigidity of the parental WAp-D04, giving an overall positive effect on the binding to mWnt3a. Next steps for such a confirmation should include performing further studies on this mutation as well as other silent mutations observed in WAp-D04 along with their three-dimensional analysis such as X-ray crystallography, to analyze the structure (for example, helical o sheet-like) of the peptide as well as its binding mode to the target, to provide an in-depth understanding of the molecular action of how the inhibition occurs and how it can be further improved. Furthermore, structure-activity relationships need to be analyzed deeper in order to bring forward key amino acids or their motifs that are critical for biological activity. Varying the library selection design can be beneficial for this effect. For example, increasing diversity in the WAp-D04-foused libraries or, more effectively, incubating the mWnt3a-hAFM complex with already identified strong-binding inert peptides such as WAp-D02, -D11 or -L05 before the positive selection step to make these inactive binding sites unavailable for binding of the large original libraries, can increase the possibilities of finding bioactive peptide members.

Moreover, the studies we have carried out so far have only used proteinogenic amino acids in the random region of the peptides, leaving potential for further improvement using more structurally varied non-proteinogenic residues. For improvement of the identified peptides, we would suggest applying a deep-mutational scanning[92] with separate canonical and non-canonical libraries against both hAFM and the mWnt3a-hAFM complex, in order to analyzed more detailed changes in binding efficiency towards each target and what amino acids in the chain are more susceptible to non-specific binding.

Although with room for further improvement, our approaches successfully targeted a "non-pure" form of the insoluble Wnt target, stabilized by a larger, highly glycosylated protein partner such as AFM, allowing the identification of highly selective and bioactive peptides. This particular accomplishment also calls attention to affinity-based approaches for screening libraries against commonly insoluble proteins, displaying an alternative method for targeting unstable proteins with unavailable detailed structural information.

Conclusions

In the present chapter, we have discovered *de novo* macrocyclic peptides that can strongly bind a normally insoluble mWnt3a protein, and thereby potently inhibit Wnt3a signaling. Targeting of structurally frail proteins for therapeutic screening has long been considered a challenging task, mainly due to the loss of integrity or activity of such proteins outside their native cell environment and throughout the process of pharmacophore selection schemes. In this work, we addressed the challenges by developing a unique RaPID selection strategy that made use of a protein partner-stabilized Wnt ligand, and performed 2D deep-sequencing analysis to discriminate specific binders of our main target, mWnt3a. Starting from a randomized library of macrocyclic peptides, we identified an initial hit inhibitor that served as the basis for a focused library, in turn allowing the identification of an analogue with improved binding kinetics and inhibitory activity. The discovery of such molecules constitutes a useful initial tool in the development of a novel class of modulators of the Wnt pathway, which in turn can lead to a deeper understanding of its associating structural and signaling interactions. Furthermore, our approach has made achievable the targeting of a highly hydrophobic and not commonly targeted protein, and although currently successful in this single scenario, could prove applicable to other Wnt proteins or similar unstable proteins, expanding the scope of display screening techniques such as RaPID and bringing forward a new class of potential pharmacophores for understudied proteins.

Materials and Methods

Protein Expression and Purification

Biotinylated and PA-tagged mWnt3a and hAFM, as well as Fc-fusion isoforms of both proteins were kindly provided in collaboration with Prof. Jun Takagi at the Laboratory of Protein Synthesis and Expression, Institute for Protein Research, The University of Osaka, Osaka, Japan. Briefly, biologically active mouse Wnt3a (mWnt3a) in complex with human afamin (hAFM) was prepared according to a method described previously[44]. N-terminally PA-tagged mWnt3a and N-terminally Target-tagged hAFM were co-transfected into Expi293F cells to establish a stable cell line secreting the Wnt3a-AFM complex, followed by the purification of the complex by using an anti-PA tag NZ-1 antibody column[93]. The purified complex dissolved in PBS (20 mM phosphate, 150 mM NaCl, pH 7.0) was biotinylated by EZ-Link NHS-Lc-Biotin (Thermo Fisher Scientific Inc.) to facilitate bead immobilization. Biotin incorporation was estimated to be 1-2 moles of biotin per mole Wnt3a. We also confirmed that the biotinylation did not diminish biological activity of mWnt3a by using a TOP flash reporter assay. Uncomplexed hAFM was expressed in a similar manner and purified by anti-Target tag P20.1 antibody column[94], biotinylated, and immobilized onto the beads for the negative selections. For certain SPR assays, hAFM fused with human IgG1 Fc was used in place of the Target-tagged hAFM described above.

mRNA Library Preparation

The initial randomized library was designed to contain a T7 Polymerase and ribosome binding site, a peptide encoding region constituted by an initiating AUG codon followed by 6 to 15 contiguous NNK codons (in independent libraries), a UGC Cys codon and a $(Gly\text{-}Ser)_3$ region, in turn followed by a stop codon and a small sequence region complementary to a DNA splint used for Puromycin ligation. Independent libraries were transcribed and purified through gel electrophoresis, resuspended in water to a 10 μM concentration, and then combined in equal volumes for a total 10 μM concentration. For the WAp-D04-focused library, the inhibitor's structure was varied as shown in Fig. 3a for a total of 50%

randomization (corresponding to 5 amino acids) in 5 different groups, each with increasing number of sequential randomized residues. A total of 31 independent libraries were purified separately as stated, and combined again in equal volumes to a total 10 μM concentration.

RaPID Selection

Peptide libraries were prepared from initial 10 μM RNA libraries using the FIT system in a similar manner as previously reported [72,83], aiming for a total 150 μL translation for the first round of selection. Briefly, mRNA libraries were ligated to Puromycin using a T4 RNA Ligase at 25 °C for 30 minutes, then extracted once with 1 volume of phenol-chloroform-isoamyl alcohol (PCI) solution and again with a chloroform-isoamyl alcohol (CI) solution, then precipitated by addition of 1/10 volume of 3 M NaCl and twice its volume of ethanol and finally washed with 70% ethanol, briefly air-dried and resuspended in water. The libraries were then translated using a Met-deficient FIT system in the presence of 50 μM ClAc-D-Tyr-tRNA$^{fMet}_{CAU}$ or ClAc-L-Tyr-tRNA$^{fMet}_{CAU}$ to give the corresponding initiating stereochemistry to the first amino acid in each library. Translation was then carried out at 37 °C for 30 minutes, and after an incubation period of 12 minutes at 25 °C one tenth of its volume of 100 mM EDTA was added to the reaction mix and left incubating again for an additional period of 30 minutes to finalize macrocyclization. mRNA-peptide product libraries were then reverse transcribed to its corresponding cDNA using an MLV (H-) Reverse Transcriptase (Promega) for 1 hour at 42 °C, mixed with acetylated BSA in TBS-T pH 7.5 buffer to a final 1 mg/mL concentration, neutralized with the same buffer and desalted using a Sephadex G-25 Fine (GE Healthcare) column previously swelled in the same buffer, to a total of 400 μL. At this point, 0.5 μL of the final library was diluted 1000 times in water to make an input sample reference to calculate recovered cDNA after the selection process. Prepared libraries were then exposed to the target mWnt3a-hAFM complex previously immobilized on M-280 Streptavidin Dynabeads (LifeTechnologies®) for a total of 80 pmol loaded target (200 nM target complex concentration when resuspended in the peptide pool). Peptide pools containing these loaded beads were then incubated at 4 °C for 30 minutes, washed 3 times with cold TBS-T pH 7.5 buffer to discard the unbound peptide fraction

and finally resuspended in cold PCR buffer. cDNA cognate to the target-binding peptide fraction was then recovered by heating the samples 95 °C for 5 minutes and separating the supernatant. A small amount of the input and recovered cDNA samples were then analyzed using real-time qPCR on a Roche LightCycler® system and the remainder was amplified by PCR. The amplified samples were then purified by one extraction each with PCI and CI solutions, precipitated with ethanol and resuspended in water. The resulting samples were then transcribed to mRNA, forming the initial library for the next round. Following rounds of selection were carried out using the same scheme, though performing translation at a total 5 µL scale and 10 pmol of target protein (still maintaining final 200 nM when exposed to libraries). Additionally, before incubating the library in the target complex, they were first exposed in 10 separate cycles to a mixture containing 25% free M-280 Streptavidin Dynabeads (LifeTechnologies®), 25% of the same beads saturated with biotin and 50% of the same beads loaded only with hAFM in twice the molar amount of the objective target concentration (for a total of 20 pmol). These "negative selection" cycles were performed in order to lower the possibility of recovering non-specific peptides or those with preferential binding to the protein partner instead of the original target mWnt3a. The cycles were carried out for at 4 °C for 30 minutes for the first and last cycles, and otherwise for 15 minutes at the same temperature. Moreover, an additional 20 times the molar amount of free (untagged) hAFM were added to the final samples before exposing them to the target mWnt3a-hAFM complex to further decrease the recovery of non-specific peptides. Samples were then incubated in beads containing 10 pmol of the target and corresponding cDNA was recovered and amplified as before.

Deep-sequencing analysis program

Raw FASTA data corresponding to the recovered peptide libraries during selection were obtained through high-throughput sequencing using a MiSeq system by Illumina®, and the data was processed with Python in an Enthought Canopy® environment according to the script below (kindly provided by Toby Passioura), where sequences were read based on a determined dictionary and sorted in a summary file in

terms on their identity and frequency within each round. 2D analysis was performed based on these results, taking the raw data from the last round from each “positive” and negative” selection.

Program script:

```
def OpenReadingFrame(DNASequence,minLen,maxLen):

translation = {
"TTT": "F", "TCT": "S", "TAT": "Y", "TGT": "C",
"TTC": "F", "TCC": "S", "TAC": "Y", "TGC": "C",
"TTA": "L", "TCA": "S", "TAA": "*", "TGA": "*",
"TTG": "L", "TCG": "S", "TAG": "*", "TGG": "W",

"CTT": "L", "CCT": "P", "CAT": "H", "CGT": "R",
"CTC": "L", "CCC": "P", "CAC": "H", "CGC": "R",
"CTA": "L", "CCA": "P", "CAA": "Q", "CGA": "R",
"CTG": "L", "CCG": "P", "CAG": "Q", "CGG": "R",

"ATT": "I", "ACT": "T", "AAT": "N", "AGT": "S",
"ATC": "I", "ACC": "T", "AAC": "N", "AGC": "S",
"ATA": "I", "ACA": "T", "AAA": "K", "AGA": "R",
"ATG": "M", "ACG": "T", "AAG": "K", "AGG": "R",

"GTT": "V", "GCT": "A", "GAT": "D", "GGT": "G",
"GTC": "V", "GCC": "A", "GAC": "D", "GGC": "G",
"GTA": "V", "GCA": "A", "GAA": "E", "GGA": "G",
"GTG": "V", "GCG": "A", "GAG": "E", "GGG": "G"}

StartCodon = 'ATG'
SubString = DNASequence

while StartCodon in SubString:
 StartIndex = SubString.find(StartCodon)
 SubString = SubString[SubString.find(StartCodon):]
 PeptideSequence = ''
 translationString = SubString
 while len(translationString) > 3:
  if 'N' in translationString[0:3]:
   PeptideSequence += 'X'
  else:
   PeptideSequence += translation[translationString[0:3]]
```

```
 translationString = translationString[3:]
 if (len(PeptideSequence)>maxLen):
  return SubString[0:(len(PeptideSequence)*3)],PeptideSequence
  break
 if 'CGS' in PeptideSequence:
  if len(PeptideSequence)>minLen:
   return SubString[0:(len(PeptideSequence)*3)],PeptideSequence
   break
  else:
   break
  elif '*' in PeptideSequence:
   if len(PeptideSequence)>minLen:
    return SubString[0:(len(PeptideSequence)*3)],PeptideSequence
    break
   else:
    break
SubString = SubString[3:]

#--------------------------------------------------------------------------

#--------------------------------------------------------------------------

def SortedPeptideSequencesList(fastqFileLocation,minLen,maxLen):
 RawDataFile = open(fastqFileLocation, 'r')
 Lines = RawDataFile.readlines()
 RawDataFile.close
 PeptideSequences = {}
 PeptideSequencesList = []

 SelectionRoundNumber = fastqFileLocation[fastqFileLocation.find('.')-1]

 for Line in Lines:
  if ('TAATACGACTCACTATA' in Line) and ('GGGGGGCGGAAA' in Line):
   Line = OpenReadingFrame(Line,minLen,maxLen)
   if Line != None:
    ORF = Line[0]
    Peptide = Line[1]
    if Peptide not in PeptideSequences:
     PeptideSequences[str(Peptide)] = 1
    else:
     PeptideSequences[str(Peptide)] = PeptideSequences[str(Peptide)] + 1
```

```
 for key, value in PeptideSequences.iteritems():
   PeptideSequencesList.append([str(SelectionRoundNumber), key, value])
 SortedPeptideSequences = sorted(PeptideSequencesList, key = lambda x: x[2], reverse = True)
 return SortedPeptideSequences

#--------------------------------------------------------------------------

#--------------------------------------------------------------------------

def SelectionResultsSummary(DataFolderLocation, BaseSelectionRoundNumber,
TopNPeptidesNumber, SummaryFileName):

 import os
 minLen = 5
 maxLen = 25
 ConcatenatedResultsList = {}
 for file in os.listdir(DataFolderLocation):
  CurrentFile = ''
  if file.endswith('.fastq'):
   CurrentFile = os.path.join(DataFolderLocation, file)
   SelectionRoundNumber = CurrentFile[CurrentFile.find('.')-1]
   SingleRoundResults = SortedPeptideSequencesList(CurrentFile,minLen,maxLen)
   ConcatenatedResultsList[SelectionRoundNumber] = SingleRoundResults
 RoundsList = sorted(ConcatenatedResultsList.keys())
 TotalNumberOfPeptidesList = []
 for Round in RoundsList:
  RoundData = ConcatenatedResultsList[Round]
  NumberOfPeptidesInARound = 0
  for PeptideInstance in range(len(RoundData)):
   NumberOfPeptidesInARound = NumberOfPeptidesInARound + RoundData[PeptideInstance][2]
  TotalNumberOfPeptidesList = TotalNumberOfPeptidesList + [NumberOfPeptidesInARound]
 TopNPeptidesList = []
 for Number in range(TopNPeptidesNumber):
  TopNPeptidesList = TopNPeptidesList +
[ConcatenatedResultsList[str(BaseSelectionRoundNumber)][Number][1]]

 ListOfPeptidesOccurancesByRound = []
 ListOfPeptidesFractionsByRound = []

 for SelectedPeptide in TopNPeptidesList:
  PeptideOccurancesByRound = []
  PeptideFractionsByRound = []
```

```
  for Round in RoundsList:
   AbundanceInARound = 0
   FractionInARound = 0
   RoundData = ConcatenatedResultsList[Round]
   for PeptideData in RoundData:
    PeptideSequence = PeptideData[1]
    if PeptideSequence == SelectedPeptide:
     AbundanceInARound = PeptideData[2]
     FractionInARound =
float(PeptideData[2])/float(TotalNumberOfPeptidesList[RoundsList.index(Round)])
   PeptideOccurancesByRound = PeptideOccurancesByRound + [AbundanceInARound]
   PeptideFractionsByRound = PeptideFractionsByRound + [FractionInARound]
  ListOfPeptidesOccurancesByRound = ListOfPeptidesOccurancesByRound +
[PeptideOccurancesByRound]
  ListOfPeptidesFractionsByRound = ListOfPeptidesFractionsByRound + [PeptideFractionsByRound]

#--------------------------------------------------------------------------------

#--------------------------------------------------------------------------------

 CSVFileName = SummaryFileName + '.csv'
 SelectioResultsSummaryFile = open(CSVFileName, 'w')
 SelectioResultsSummaryFile.write('peptide sequence' + ',')
 for Round in RoundsList:
  SelectioResultsSummaryFile.write('round # ' + Round + ' occurence (#)' + ',')
 SelectioResultsSummaryFile.write('\n')
 for PeptideIndex in range(len(TopNPeptidesList)):
  SelectioResultsSummaryFile.write(TopNPeptidesList[PeptideIndex] + ',')
  SummaryRoundsData = ListOfPeptidesOccurancesByRound[PeptideIndex]
  for RoundDatum in SummaryRoundsData:
   SelectioResultsSummaryFile.write(str(RoundDatum) + ',')
  SelectioResultsSummaryFile.write(TopNPeptidesList[PeptideIndex] + ',')
  SummaryRoundsData = ListOfPeptidesFractionsByRound[PeptideIndex]
  for RoundDatum in SummaryRoundsData:
   SelectioResultsSummaryFile.write('{:.3%}'.format(RoundDatum) + ',')
  SelectioResultsSummaryFile.write('\n')
  SelectioResultsSummaryFile.close()

#___DataFolderLocation, BaseSelectionRoundNumber, TopNPeptidesNumber,
SummaryFileName___
SelectionResultsSummary(r"C:\\, , 1000, r"C:\\")
```

Peptide Synthesis and Purification

Selected peptides were synthesized through standard solid-phase peptide synthesis with a Biotage Syro I® parallel synthesis system using a common Fmoc-protected amino acid chemistry on NovaPEG Rink amide resin at a 25 μmol scale. Deprotection of the final N-terminal was carried out as a last step, and the loaded resin was washed 5 times with dimethylformamide (DMF) and dichloromethane (DCM). Resin was then swelled in DCM for 10 minutes, resuspended in 0.2 M diisopropylethylamine (DIPEA) and then washed 6 times with DMF. Chloro-Acetylation of the free N-terminal amino acid was carried out by addition of a coupling mixture containing 6.3 equivalents each of Chloro-acetic acid (ClAcOH), HOBt and diisopropylcarbodiimide (DIC), reacting for 1 hour at room temperature. Resin was then washed 3 times with DMF, methanol (MeOH) and DCM before drying *in vacuo*. Deprotection and cleavage of the peptides from the resin was then performed by resuspending the resin in 2 mL of a TFA deprotection cocktail containing 2.5%$_{v/v}$ each of triisopropylsilane (TIS), 3,6-dioxa-1,8-octanedithiol (DODT) and water for 3 hours at room temperature under continuous mixing. Resin was then washed twice with 2 mL TFA, and the peptide solution was then concentrated by centrifugal evaporation, later precipitating the cleaved peptides with cold ether. Collected peptides were then washed with cold ether 5 times and dried *in vacuo* before dissolving in DMSO. Cyclization of peptides was finally carried out in the presence of trimethylamine (TEA). Peptides were then purified by reverse-phase HPLC in a Shimadzu LC-20AP system using a Merck Cromolith® Column with a gradient of 0.1% TFA/Acetonitonitrile containing 0.1% TFA, and collected fractions were then concentrated and freeze-dried. The resulting peptides were dissolved in low-concentration HCl for exchange to an HCl salt and freeze-dried again twice. Final peptides were dissolved in a small volume of DMSO and reserved at -20 °C. Structural identity of each peptide and their evolution through the synthesis scheme was confirmed through MALDI-TOF MS, while the final purity of the samples by UPLC.

Surface Plasmon Resonance

For the evaluation of the interaction between the mWnt3a and the peptides obtained in the initial selection series, purified mWnt3a–hAFM complex or hAFM alone were directly immobilized onto the Series S Sensor Chip CM5 (GE healthcare; 29104988) at a surface density of ~7,800 RU (for complex) or ~5,600 RU (for hAFM), respectively, using an amine coupling kit (GE healthcare; BR100050) according to the manufacturer's protocol. The binding was evaluated by injecting peptide solutions serially diluted using the running buffer (20 mM HEPES-NaOH (pH7.5), 150 mM NaCl, 0.05% Surfactant P20) maintaining the final concentration of DMSO as 0.1%. The runs were conducted in a single cycle kinetics mode employing the following parameters; flow rate of 30 μl/min, contact time of 120 s, and dissociation time of 300 s. After each run, the surface was regenerated by injecting 3M $MgCl_2$ until the response returned to the original baseline level. The binding curves of the measurement cell (mWnt3a–hAFM) were subtracted with that of reference cell (hAFM), and used to derive K_D values. Data were obtained using a BIAcoreT200 instrument (GE Healthcare) at 25°C, and the results were analysed by using BIAcoreT200 evaluation software version 4.1. For the evaluation of the mWnt3a-binding properties of the peptides obtained in the second round of selection from the focused library, hAFM fused with human IgG1 Fc was used in place of the Target-tagged hAFM described above. Thus mWnt3a–hAFM-Fc complex as well as hAFM-Fc were expressed in Expi293F cells and purified by either immobilized NZ-1 antibody resin or rProteinA Sepharose Fast Flow (GE healthcare, 17-1279-03) and immobilized on a series S Sensor Chip CM5 via Human Fc capture kit (GE healthcare; BR100839) at a density of ~10,000 RU. The binding of peptides was evaluated similarly to the method described above, except for the use of steady-state affinity analysis mode in the BIAevaluation 4.1.

TOP Flash Luciferase Assay

The effects of each peptide on the biological activity of mWnt3a were evaluated in a paracrine-type reporter cell assay as described previously[44]. Briefly, HEK293 cells stably transfected with a firefly luciferase gene under the control of a TCF/LEF response element (BPS Bioscience, #60531) were seeded

at 30,000 cells/50 μL/well in 96-well white-clear plates (Corning, #3610), followed by an overnight culture before the assay. 10 μL of PBS containing 100 nM purified mWnt3a–hAFM complex or hAFM alone and 40 μL of peptide solution in 10% serum-containing media were added to the reporter cells, maintaining the final concentration of DMSO at 0.1%. After culturing under 5% CO_2 at 37 °C for 6 h, cells were briefly washed with PBS and lysed by adding 20 μL/well of cell lysis buffer (Promega, E153A). Luciferase activities of the lysates were directly measured in the same plate using the luciferase assay reagent (Promega, E1500) and an SH-9000 microplate reader (Corona electric, Inc.).

Chapter 3: Screening of Peptide Ligands against a natural Frizzled receptor-bound Wnt3a complex

Bioactivity measurements shown in this chapter were performed in collaboration with Ms. Kyoko Matoba, Dr. Emiko Mihara and Prof. Jun Takagi at the Laboratory of Protein Synthesis and Expression at The University of Osaka, Osaka, Japan.

Introduction

In chapter 2 of this work, we showed how we were able to attain *de novo* strong binder and inhibitor mid-sized molecules to mWnt3a, part of the Wnt family of proteins involved Wnt signaling for cellular development and homeostasis. Application of the RaPID system to a stabilized form of mWnt3a by use of a previously bound protein partner (hAFM) inert to the signaling itself, which involved carrying out different independent screening cycles against its partner together with a comparative deep-sequencing 2D analysis, allowed us to initially isolate moderate binding cyclic peptides that showed binding bias toward the Wnt ligand within the mWnt3a-hAFM complex, while bioactivity reporter cell assays led us to identify a rare hit peptide with strong inhibition properties. Moreover, further optimization through block mutagenesis screening of the found molecule allowed us to greatly improve both binding and inhibition properties of the hit peptide, leading to an 8-fold enhanced binding and 5-fold enhanced inhibition for a single mutant species.

hAFM has been found to greatly stabilize Wnt3a, allowing both long-term storage and at the same time lacking any hindrance to Wnt signaling, potentially indicating this partner is either not binding strongly to any of the potential active (interacting) sites of the Wnt ligand or is outcompeted by any naturally interacting proteins. Consequently, however, the use of such a complex during our selection screening inherently limits the binding area of any potential inhibitors from our designed libraries. Accordingly,

initial results in Chapter 2 indicating a single inhibitor within a library of more than 10^{12} members could point towards a limiting factor of using such a stabilizing partner in our selection schemes, while the affinity character of the system is also put at disadvantage when having a non-natural partner protein that calls for non-specific interactions with peptides within the libraries.

With such considerations, we envisioned that screening a Wnt protein stabilized not by an inert protein partner, but by its natural Wnt signaling receptor, Fz, would allow new possibilities for identifying peptides with varying effects on the pathway. Yet, considering the remarkably strong binding kinetics to their natural binding receptors (*e.g.* K_D lower than 10 nM for Fz and LRP6[95]), finding peptide binders that are able to outcompete the area occupied by Fz during binding would prove to be largely challenging. Nonetheless, considering the limited surface occupied by the relatively small Fz receptor (Figure 3.1) and the lack of current structural information of Wnt-inhibitor complexes, we did surmise that the additional free binding area would allow the identification of peptides with an allosteric inhibition effect, or interfering with the protein-protein interaction of Wnt's with other receptor or protein binding partners in cell assays.

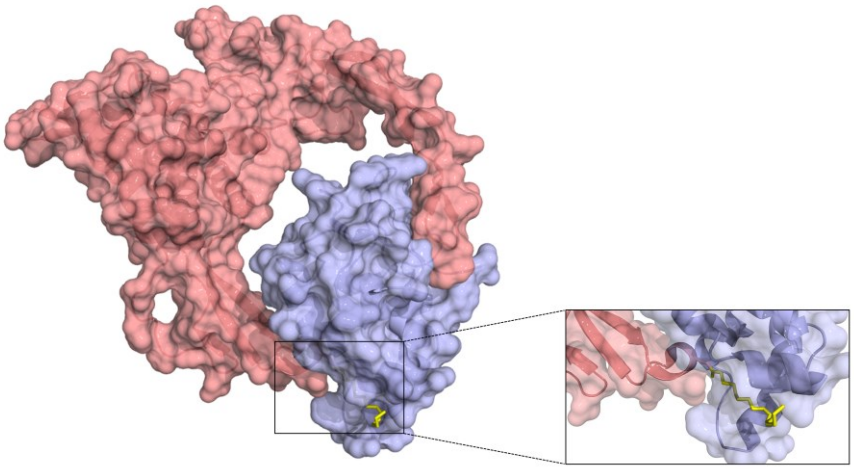

Figure 3.1 Crystal structure of hWnt3 (red) in complex with mFz8's CRD (blue) as reported by Hirai *et al.* (PDB 6AHY)[43]. Shown is an isolated single unit of the ligand and receptor complex, with an inset highlighting the palmitoleoyl residue (yellow) location within the receptor's groove.

Results

Library design and selection

As performed in chapter 2, we employed a RaPID screening approach in order to identify direct inhibitors of Wnt3a signaling, with slight modifications according to the different complex to be used (Figure 3.2), while the mWnt3a bait protein was stabilized by complexing it with mFz8 prior to the selection process. standard mRNA library consisting of AUG, $(NNK)_{6–15}$ (N = A, C, G or U and K = U or G), UGC, followed by $(GGCAGC)_3$-UAG codons to express two independent, thioether-cyclized macrocyclic peptide libraries under a reprogrammed genetic code assisted by flexizymes. The AUG initiator codon was assigned to L-*N*-chloroacetyl-Tyr (Y-library) or D-*N*-chloroacetyl-Tyr (y-library) in order to induce subsequent head-to-sidechain thioether cyclization with a downstream Cys residue, which could appear in the random region and/or the designated UGC codon after the random region. A triple repeat of a Gly-Ser peptide linker assigned by $(GGCAGC)_3$ allowed linking to a 3'-puromycin-CC-PEG-5' attached to the 3'-end of the mRNA library.

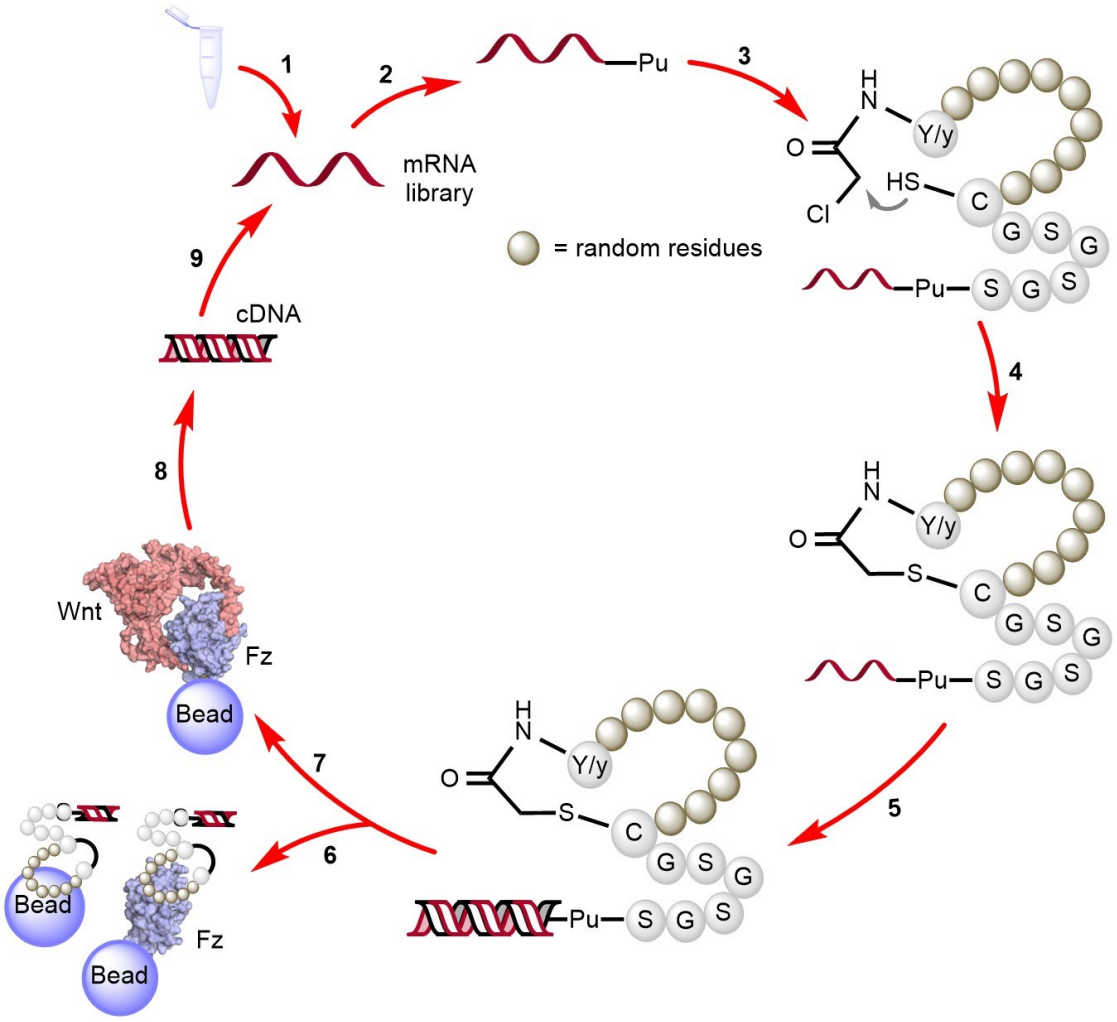

Figure 3.2 RaPID selection scheme for the identification of peptides selective to mWnt3a. On par with an standard scheme, (1) the designed mRNA library is prepared, (2) ligated with Puromycin (Pu) using a T4 RNA ligase (3) and translated into peptides using the FIT system to generate peptide-Pu-mRNA fusions, after which (4) macrocyclization would occur by reaction of L-Tyr (Y) or D-Tyr (y) with a downstream Cys at the end of the random region (brown spheres) or within the random region itself (5) This macrocyclic peptide library is ligated to each cognate RNA through a $(Gly\text{-}Ser)_3$ and Pu-linker region, and the RNA template is reverse transcribed into its cDNA (6) The library is then exposed several times to a combination of unloaded, biotin-saturated and biotinylated hAFM-loaded magnetic beads in order to lower the likelihood of recovering non-specific binders as much as possible (7) These fractions are discarded and the depleted library is then exposed in a single cycle to the biotinylated mWnt3a-hAFM complex-loaded magnetic beads (8) cDNA bound to the complex is then recovered and amplified by PCR followed by (9) transcription to generate the enriched mRNA library for the next round.

Prepared peptide-mRNA fusion libraries were "counter-selected" six times (*cf.* 10 counter-selection cycles to hAFM when working with mWnt3a-hAFM) against immobilized mFz8 in order to deplete peptides from the library with biased affinity for mFz8 or with non-specific binding to the Wnt ligand. Following counter-selection, the peptide library was then panned against immobilized mWnt3a-mFz8 complex (in the absence of any additional free mFz8). The cognate cDNAs of peptides that bound the complex were then recovered by PCR amplification and transcribed *in vitro* to generate the initial mRNA library for the subsequent round of selection.

Notably, after four sequential rounds of selection, qPCR results suggested the recovered peptide libraries (initiated by either D-Tyr or L-Tyr) were successfully and increasingly enriched, with a background (corresponding to any peptide binders non-specific to the target protein complex) almost completely suppressed throughout the whole selection process (Figure 3.3), a result that distinctly contrasts with the enriched background recovery seen during selection against the mWnt3a-hAFM complex. Such result, however, could point toward the enhanced specificity between mFz8 and its cognate mWnt3a, *i.e.* arising from the natural character of the Wnt ligand binding partner in this scenario.

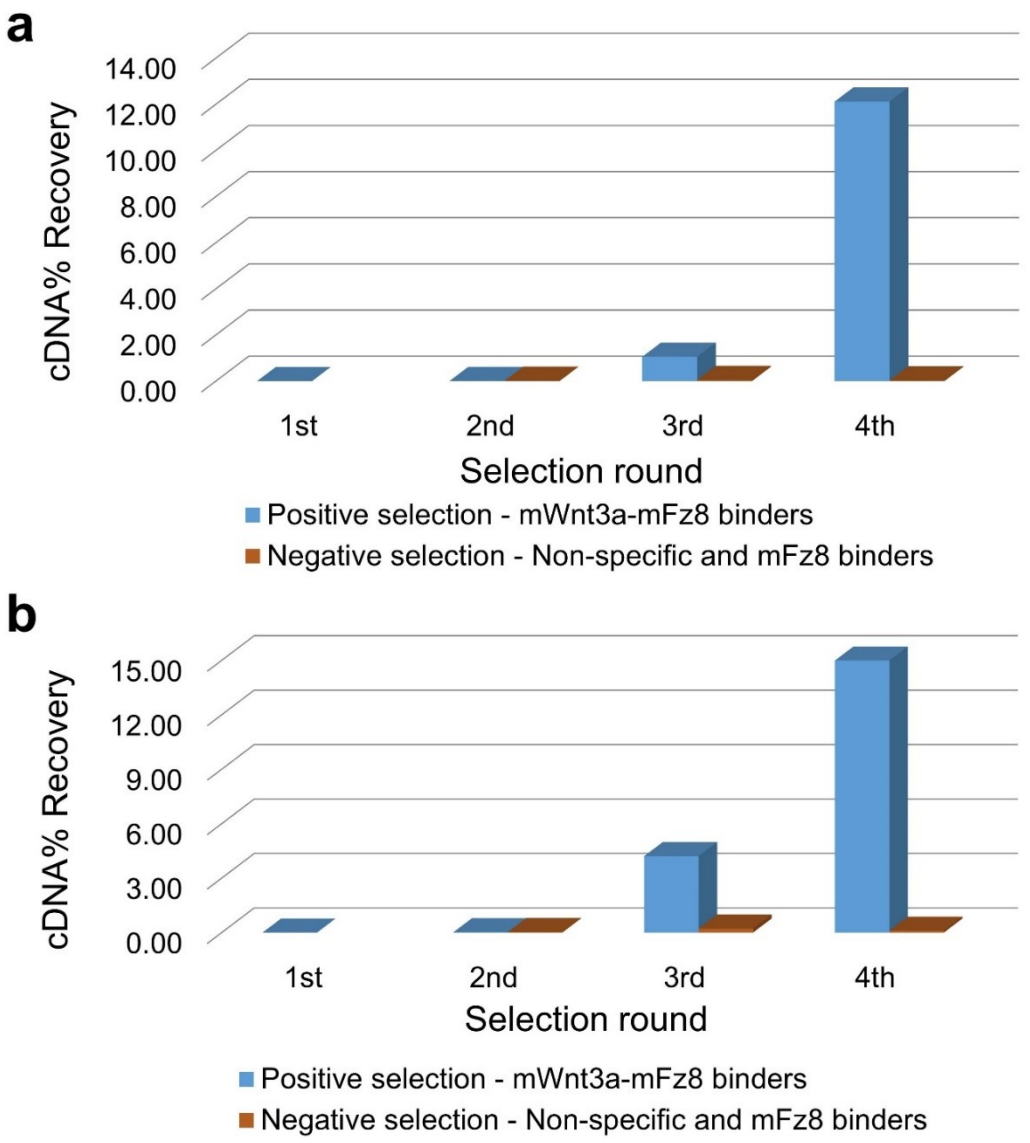

Figure 3.3 qPCR selection results of targeting the mWnt3a-mFz8 complex with the RaPID system. (**a**) Graph shows recovered cDNA per round of selection against mWnt3a-mFz8, obtained from the macrocyclic peptide library initiated by D-Tyr. (**b**) Similar results corresponding to the library initiated by L-Tyr. Blue bars indicate the fraction corresponding to the cDNA of peptides bound to the complex, while orange bars indicate non-specific binders, including ones binding to only-mFz8-loaded magnetic beads.

Initial sequencing of the recovered libraries binding the mWnt3a-Fz complex (Figure 3.4) showed a single dominating sequence in each of the y- and Y-libraries, while the peptides structures were unexpectedly found to be partially biased towards lariats, small cycles with a varying number of residues as non-cyclized tail. Such structures arise from the formation of the thioether cycle between the initial acetylated Tyr and a Cys within the random region instead of the set codon for Cys near the C-terminus of the peptide, a ligation preference we have observed to be the predominant in peptide species with multiple Cys, prepared ribosomally or synthetically[96]. This result contrasts with the macrocyclic structures cyclized to the C-terminal Cys more commonly found with our system, and the most common structure identified in both the original and WAp-D04-focused libraries against mWnt3a-hAFM shown in Chapter 2.

Considering the lowered background recovery and specificity of the mFz8-mWnt3a couple, we surmised that the binding peptides found would have a higher binding preference toward the Wnt ligand than the ones found in the original libraries against the mWnt3a-hAFM complex. Nonetheless, the strategy applied here, *i.e.* the use of a full protein partner as a stabilizing agent for a Wnt ligand, still requires a careful analysis in order to verify the approach and ensure such sequences are indeed binding solely in the presence of the Wnt target. Accordingly, in order to identify which sequences exhibited favored binding to Wnt3a within the mWnt3a-Fz complex, we again performed a two-dimensional deep-sequencing analysis comparing the most enriched sequences found to bind mFz8 and/or the mWnt3a-mFz8 complex. For this analysis, cDNA libraries recovered from each round targeting either mFz8 (from the final counter-selection cycle) and mWnt3a-mFz8 were sequenced separately, and the individual peptide sequences corresponding to each final 4th round of selection were compared with each other in terms of identity and frequency as well (Figures 3.5 and 3.6). This allowed assessing their enrichment within the recovered final libraries and the discrimination of cyclic peptides with specific affinity for Wnt3a out of the non-specific binding background.

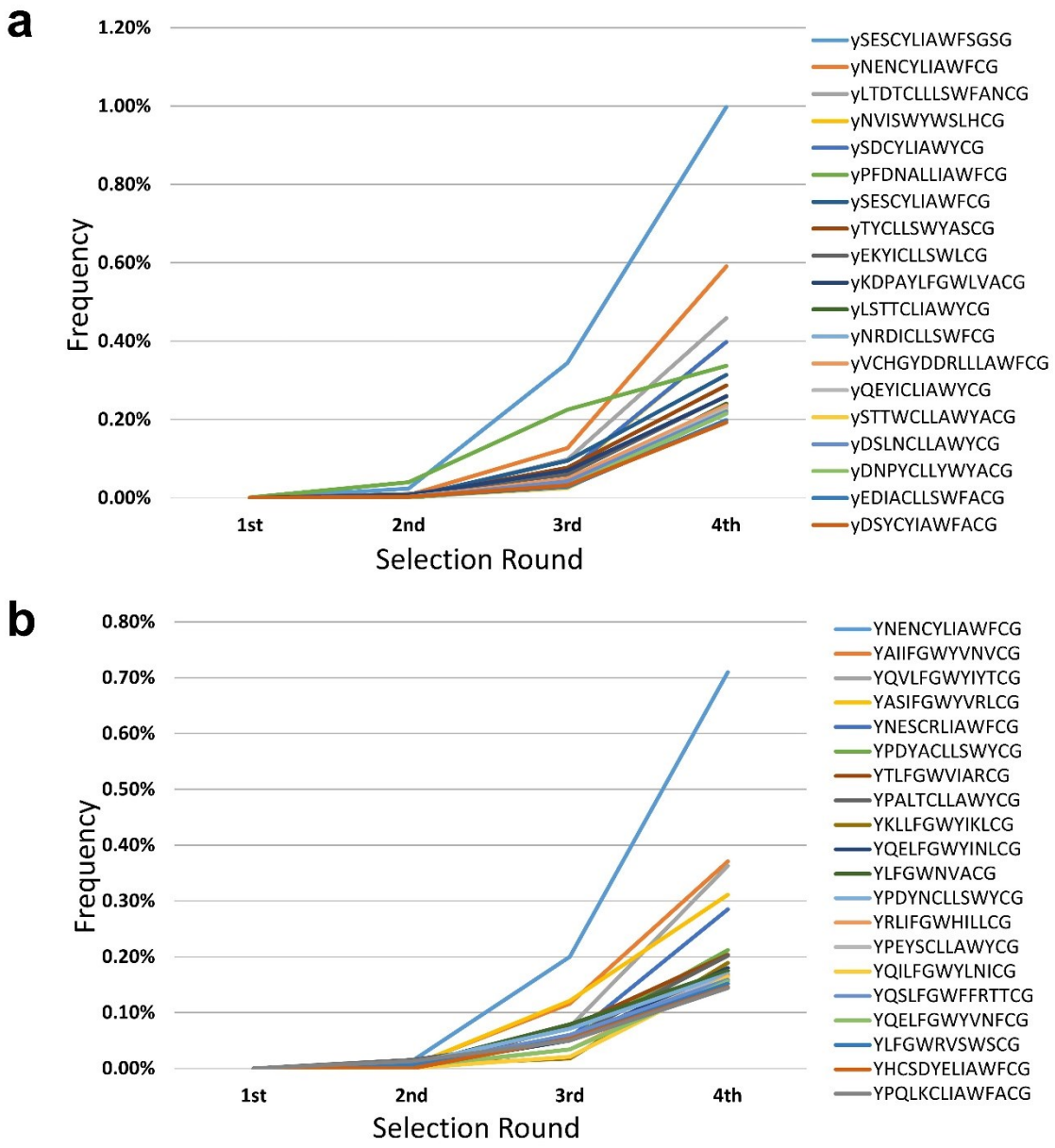

Figure 3.4 High-throughput sequencing of the selected peptide sequences against the mWnt3a-mFz8 complex. (**a**) Graph shows frequency (enrichment) per round of the 20 most abundant sequences throughout the selection process coming from the recovered libraries initiated by D-Tyr (**b**) Similar results for libraries initiated by L-Tyr. Individual sequences are shown in the right side, where y = D-Tyr and Y = L-Tyr.

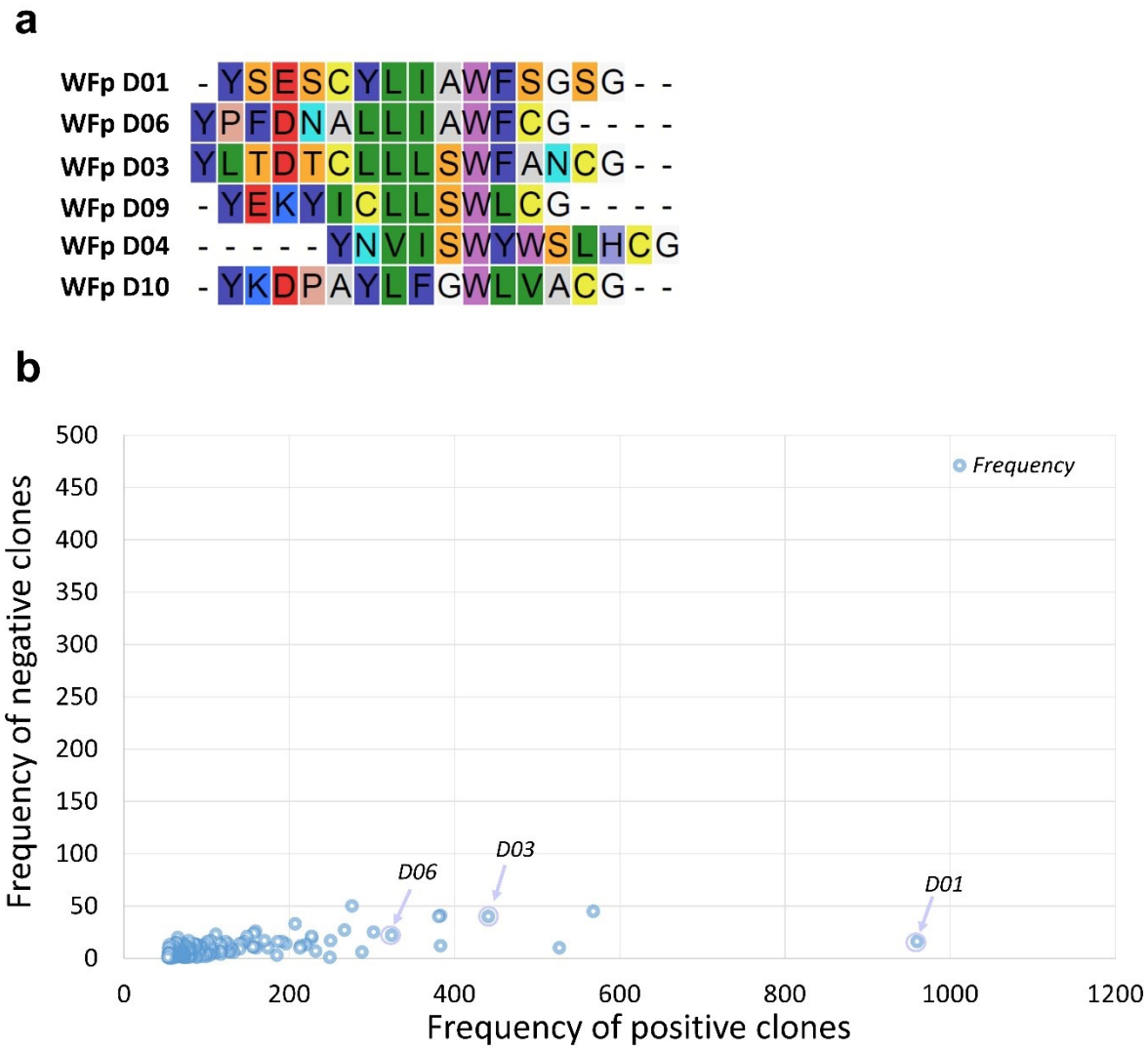

Figure 3.5 Alignment and 2D analysis of sequences in the enriched D-Tyr-initiated library. (**a**) Alignment of a few of the most enriched (frequent) sequences found within the library corresponding to the final round of selection against mWnt3a-mFz8 (**b**) 2D analysis of a set of the 80 most frequent sequences from the library, found to bind to mFz8 (negative clones) or mWnt3a-mFz8 (positive clones). Individual sequences are marked as blue spots, with some highlighted for comparison.

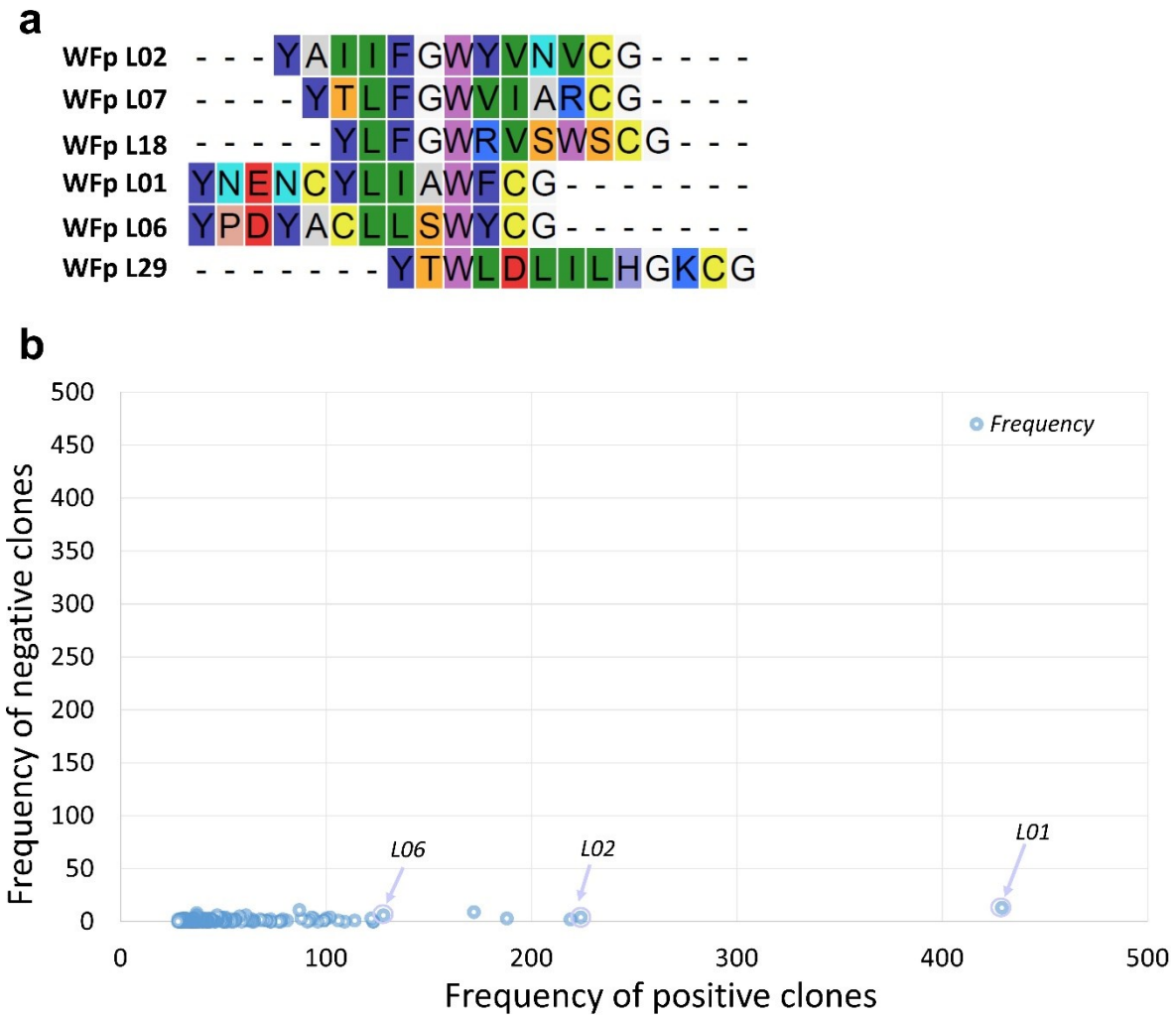

Figure 3.6 Alignment and 2D analysis of sequences in the enriched L-Tyr-initiated library. (**a**) Alignment of a few of the most enriched (frequent) sequences found within the library corresponding to the final round of selection against mWnt3a-mFz8 (**b**) 2D analysis of a set of the 80 most frequent sequences from the library, found to bind to mFz8 (negative clones) or mWnt3a-mFz8 (positive clones). Individual sequences are marked as blue spots, with some highlighted for comparison.

For the selection campaign against the mWnt3a-mFz8, and as can be observed in Figures 3.5 and 3.6, the majority of selected sequences appeared to exhibit a remarkable binding bias toward the complex, with low or almost non-appreciable binding to the mFz8 receptor, an event we had expected to some degree due to the aforementioned specificity between the receptor-Wnt couple. These results notably oppose those found against mWnt3a-mFz8, where most of the sequences (including those found within the mWnt3a-hAFM bound peptide libraries) bound the binding partner hAFM, while only a few were seen to show selectivity in presence of the Wnt ligand.

Even though such a scenario was observed, a few sequences were shown to be predominantly enriched, and considering their frequency within the library and structure conservation among the entire recovered libraries, a total eight peptides (Table 3.1), including both macrocyclic and lariat structures, were further analyzed for their binding by ribosomally expressing and panning them independently against mFz8 and mWnt3a-mFz8 in clone assays (Figure 3.7), determining that they all showed qualitative and specific binding against mWnt3a, without any binding to the immobilizing Protein A beads or the Fc-mFz8 fusion. From the group of sequences chosen, a total of six peptides were further selected for synthesis based on structural similarity, of which two included multiple Cys, for which Cys to Ser mutations were applied to generate cycles of different length. After confirming their binding to the mWnt3a-mFz8 target, the total eight peptides were synthesized independently by standard solid phase peptide synthesis and purified, confirming their structural integrity and purity through MALDI-TOF-MS (in both positive and negative modes due to their inconclusive ionization pattern in positive mode) and UPLC (Figures 3.8 to 3.10).

Peptide name	Sequence	Number of reads
WFp-D03-S1	^{Ac}yLTDTSLLLSWFANCG (S)	441
WFp-D03-S2	^{Ac}yLTDTCLLLSWFANSG (S)	441
WFp-D04	^{Ac}yNVISWYWSLHCG (S)	383
WFp-D10	^{Ac}yKDPAYLFGWLVACG (S)	249
WFp-L02	^{Ac}YAIIFGWYVNVCG (S)	224
WFp-L06-S1	^{Ac}YPDYASLLSWYCG (S)	128
WFp-L06-S2	^{Ac}YPDYACLLSWYSG (S)	128
WFp-L29	^{Ac}YTWLDLILHGKCG (S)	71

Table 3.1 Chosen sequences from libraries selected against mWnt3a-mFz8. Shown is an alignment of the eight peptides chosen for clone assays and synthesis, originating from D-Tyr (WFp-Dxx) and L-Tyr (WFp-Lxx)-initiated libraries found to bind the mWnt3a-mFz8 complex. Sequences are numbered in increasing order of frequency (number of reads) within each recovered library at round 4.

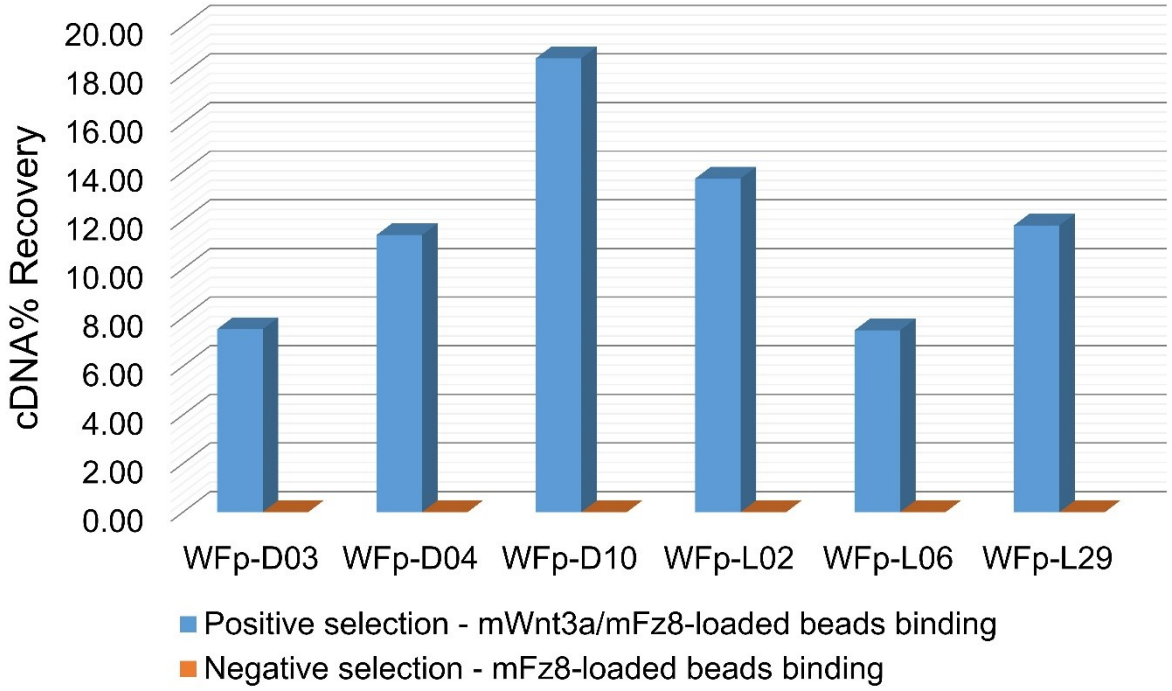

Figure 3.7 qPCR clone assay results of selected peptides against mWnt3a-mFz8. (a) Graph shows results obtained from single-clone, single-round selection assays (clone assays) targeting beads loaded with mWnt3a-mFz8 (blue bars) or unloaded and Fc-mFz8-loaded beads (orange bars) using individual sequences chosen from the selected libraries. Note that peptides WFp-D03 and WFp-L06 are shown as single peptides due to the simultaneous ribosomal expression of their S1 and S2 forms in the assay.

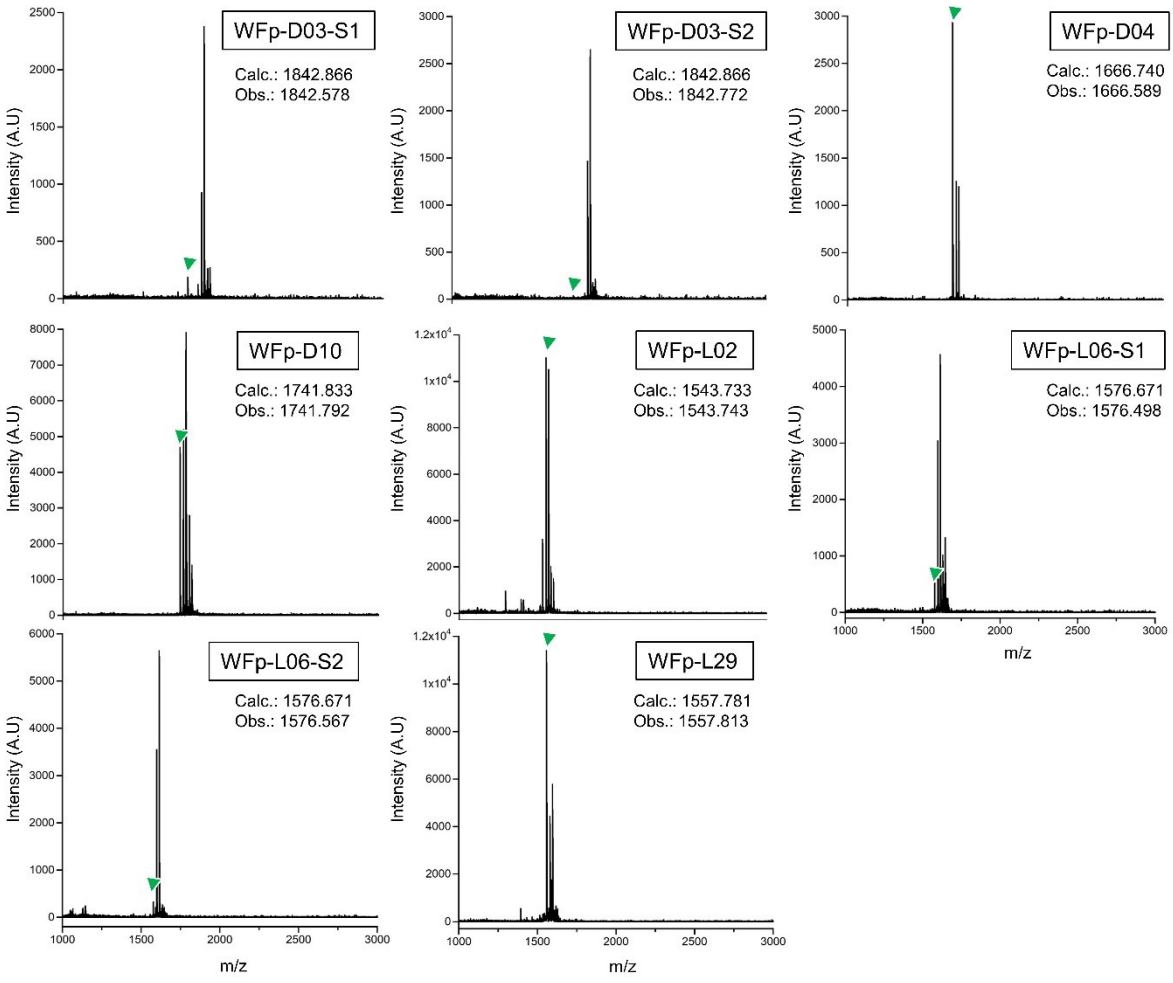

Figure 3.8 MALDI-TOF-MS spectra of selected and synthesized peptides selected from libraries against mWnt3a-mFz8. Shown are MS spectra of peptides shown in Table 3.1. All of the spectra were recorded in positive mode. Green triangles indicate the $[M+H]^+$ molecular ion of each peptide, of which calculated (Calc.) and observed (Obs.) masses are also shown.

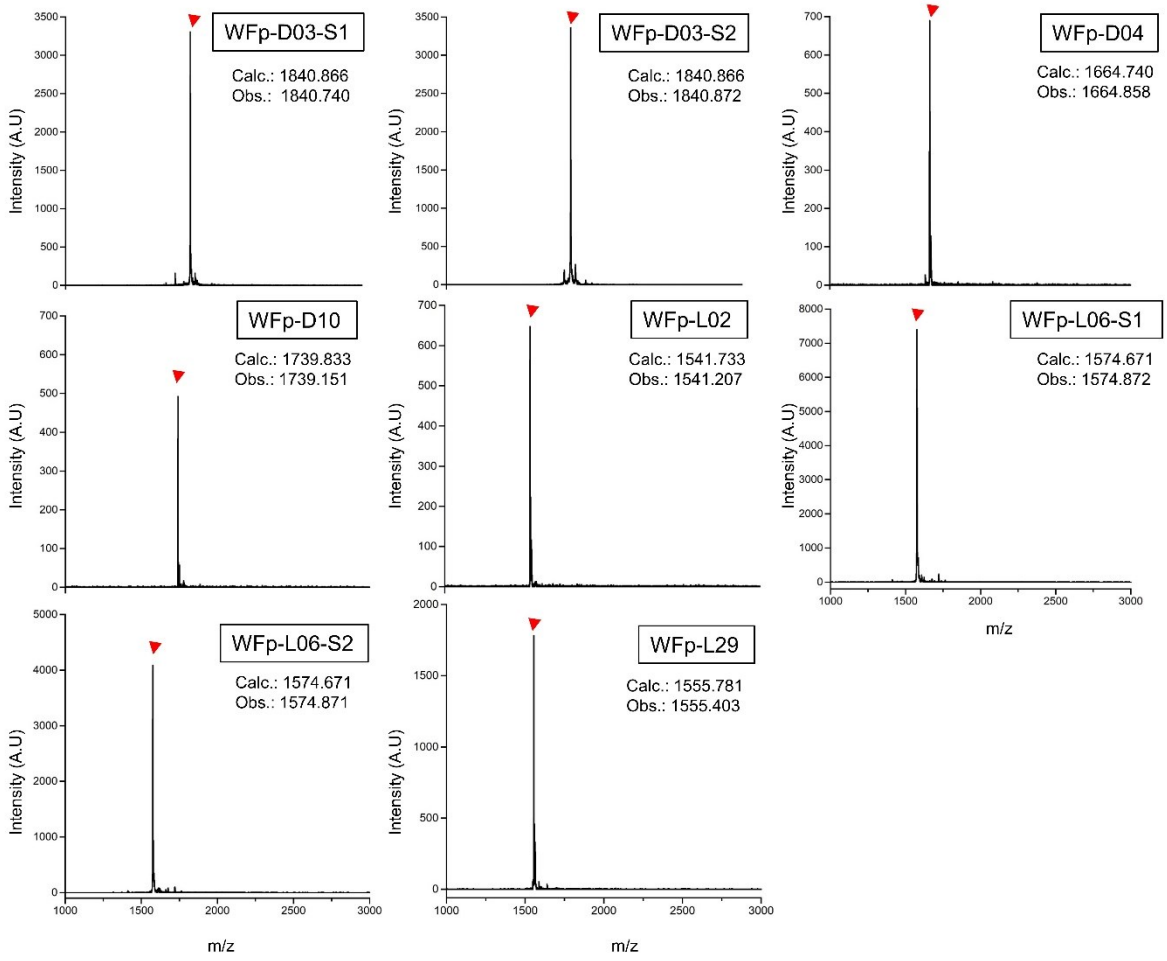

Figure 3.9 MALDI-TOF-MS spectra of selected and synthesized peptides selected from libraries against mWnt3a-mFz8. Shown are MS spectra of peptides shown in Table 3.1. All of the spectra were recorded in in negative mode. Red triangle indicates the $[M-H]^-$ molecular ion of each peptide, of which calculated (Calc.) and observed (Obs.) masses are also shown.

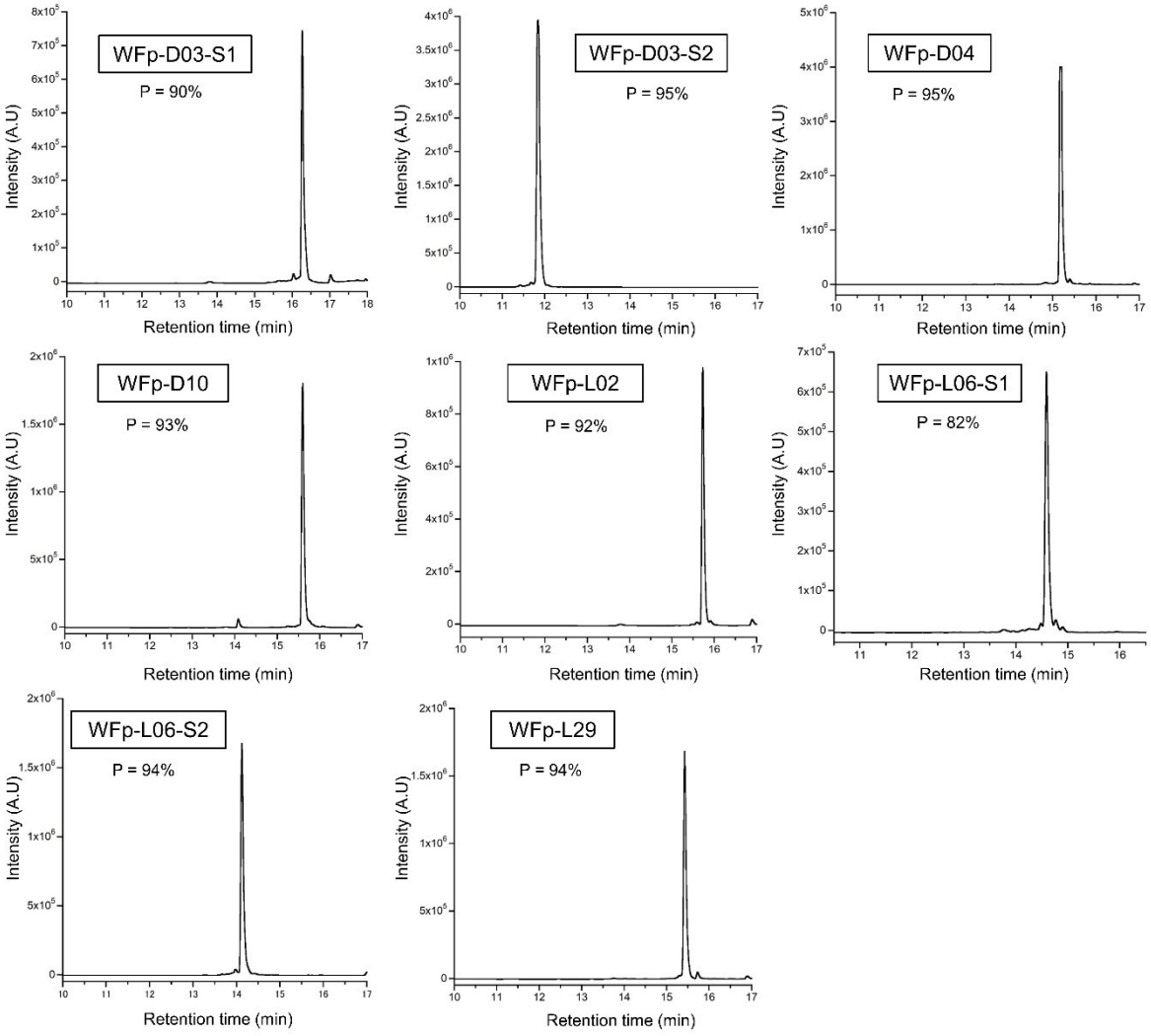

Figure 3.10 RP-UPLC chromatograms of selected and synthesized peptides from the libraries selected against mWnt3a-mFz8. Shown are chromatograms of peptides in Table 3.1, each with its calculated purity (P).

Binding profile and activity of selected peptides

Following this characterization, the binding profile of each of the synthesized peptides was also assessed using SPR against mFz8 and mWnt3a-mFz8 immobilized through amine coupling, using the former's signal as background subtraction for a more accurate assessment of the peptides' behavior. In a similar manner as with mWnt3a-mFz8, however, the obtained sensorgrams generally lacked stability and accuracy, indicating again the difficult assessment of these characteristics in a multi-component complex. Nonetheless, reliable binding affinities could be determined for four out of the eight with specific affinity for mWnt3a-mFz8 and dissociation constants (K_D) in the nanomolar range (Table 3.2).

Peptide name	Sequence	Number of reads	K_D (nM)
WFp-D04	Ac-yNVISWYWSLHCG (S–S)	383	55.0
WFp-L02	Ac-YAIIFGWYVNVCG (S–S)	224	4.9
WFp-L06-S2	Ac-YPDYACLLSWYSG (S–S)	128	3.9
WFp-L29	Ac-YTWLDLILHGKCG (S–S)	71	1.83

Table 3.2 Characterization of macrocyclic peptides selected against mWnt3a. Shown are sequence alignments and K_D values of peptides capable of binding to mWnt3a-hAFM. WFp-D04 peptide originating from y-library, while WAp-Lxx peptides from the Y-library. Sequences are numbered in increasing order of frequency (number of reads) within each recovered library at round 4.

Notably, these set of peptides with the most stable binding profiles showed very low K_D values, with three of them in the single-digit nanomolar range, including one with near the limit to pM range, indicating very strong binding toward the target Wnt complex. Additionally, the K_D values found through these experiments were in all of cases between one and two orders of magnitude stronger than the ones found

in the original library panned against mWnt3a-hAFM, with three of them one order lower than even the optimized WAr D01.

After finding these characteristics for mWnt3a-mFz8-binding peptides, we sought to assess Wnt3a signaling inhibition in a cell culture model as well. Making use again of the TCF/LEF element-dependent luciferase reporter assay, we measured reporter response following exposure to mFz8 (no signal stimulation) or mWnt3a-mFz8 (Wnt signaling stimulation) in combination with each of the selected peptides shown in Table 3.1 for inhibition (Figure 3.11).

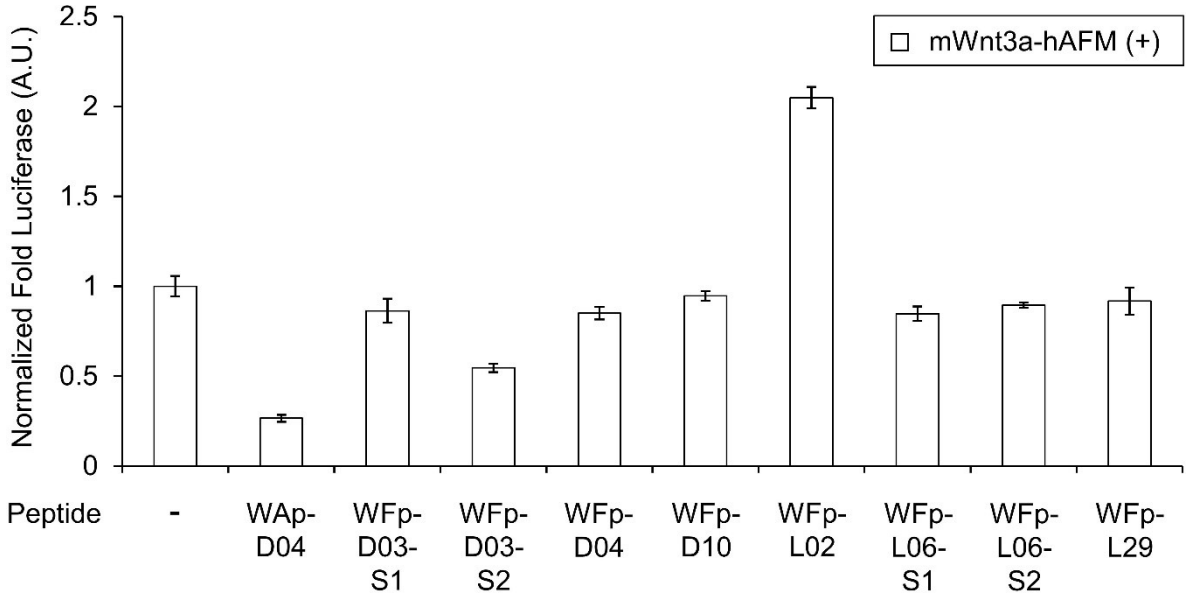

Figure 3.11 Inhibition of Wnt3a signaling by WAp-D04 and mWnt3a-mFz8-selected peptides. Luciferase reporter activity was assessed following cell treatment with 10 nM mWnt3a-hAFM in the presence or absence of 1 μM candidate peptide. Bars show mean values of a set of 4 data points, all relative to a reference signal stimulated by mWnt3a-hAFM in the absence of any peptide, while error bars indicate standard error. Data was normalized to a blank signal generated in the presence of 10 nM AFM and in the absence of any peptide, subtracted from every value.

Results from assays against this batch of peptides allowed us to identify a new peptide inhibitor of Wnt signaling, WFp D03-S2, the only one among this group capable of inhibiting signaling-dependent expression. However, comparing the activity of WFp-D03-S2 with that of WAp-D04, the first peptide

inhibitor identified in the selection against mWnt3a-hAFM, the new peptide's inhibiting properties were considerably weaker. It is however, remarkable that this new peptide possesses a structure completely different from those of WAp-D04 and WAp-D04-W10P, even exhibiting a lariat structure with a 6-membered cyclic structure pendant with a small 10 amino acid-long tail. Moreover, the analog of this peptide with a full macrocyclic structure, WFp-D03-S1, was not able to inhibit signaling in a similar manner, highlighting the importance of the lariat structure for inhibition and potentially binding to the target as well. Additionally, the inhibition properties of WFp-D03-S2 were confirmed to be concentration dependent as well in an independent reporter assay with a 25-1600 nM titration of the peptide, giving an apparent IC_{50} near 800 nM (Figure 3.12).

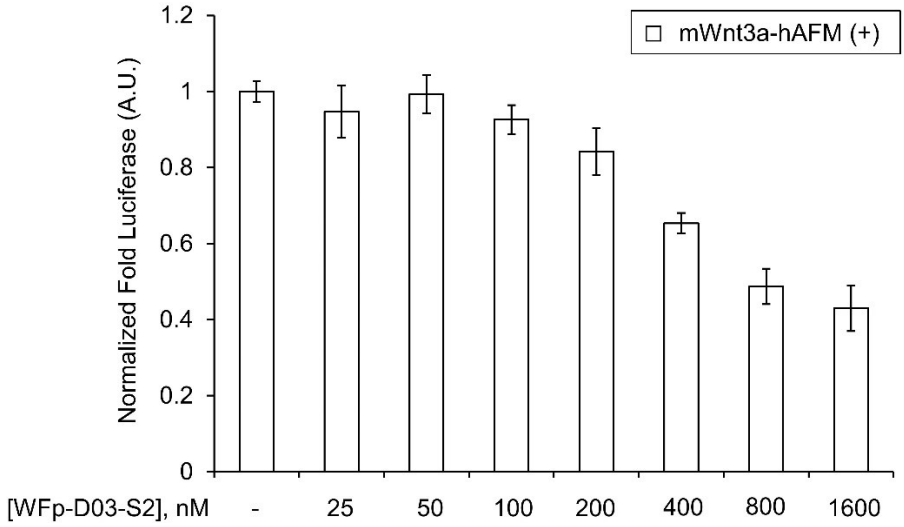

Figure 3.12 Inhibition of Wnt3a signaling by WFp-D03-S2. Luciferase reporter activity was assessed following cell treatment with 10 nM mWnt3a-hAFM in the presence or absence of the peptide. Bars show mean values of a set of four data points, all relative to a reference signal stimulated by mWnt3a-hAFM in the absence of any peptide, while error bars indicate standard error. Data was normalized to a blank signal generated in the presence of 10 nM AFM and in the absence of any peptide, subtracted from every value. Error bars indicated standard error.

Strikingly, however, among the peptides trialed in this assay, the peptide WFp-L02 was not found to inhibit Wnt signaling, while instead it seemed to promote Wnt signaling up to more than twice reference

levels generated with 10 nM mWnt3a-hAFM. Though an unexpected result while searching for allosteric inhibitors in this selection campaign against mWnt3a-mFz8, if the findings were to be confirmed it would represent the first case of a macrocyclic peptide able to promote Wnt signaling by direct binding to mWnt3a. In order to verify this hypothesis we also performed independent luciferase reporter assays with a 25-1600 nM titration against WFp-L02, and further analyzed the results under assay saturation conditions with a 15.63-4000 nM titration of the peptide after Wnt stimulation with 40 nM mWnt3a-hAFM, looking to confirm whether this effect was stable and concentration dependent (Figure 3.13).

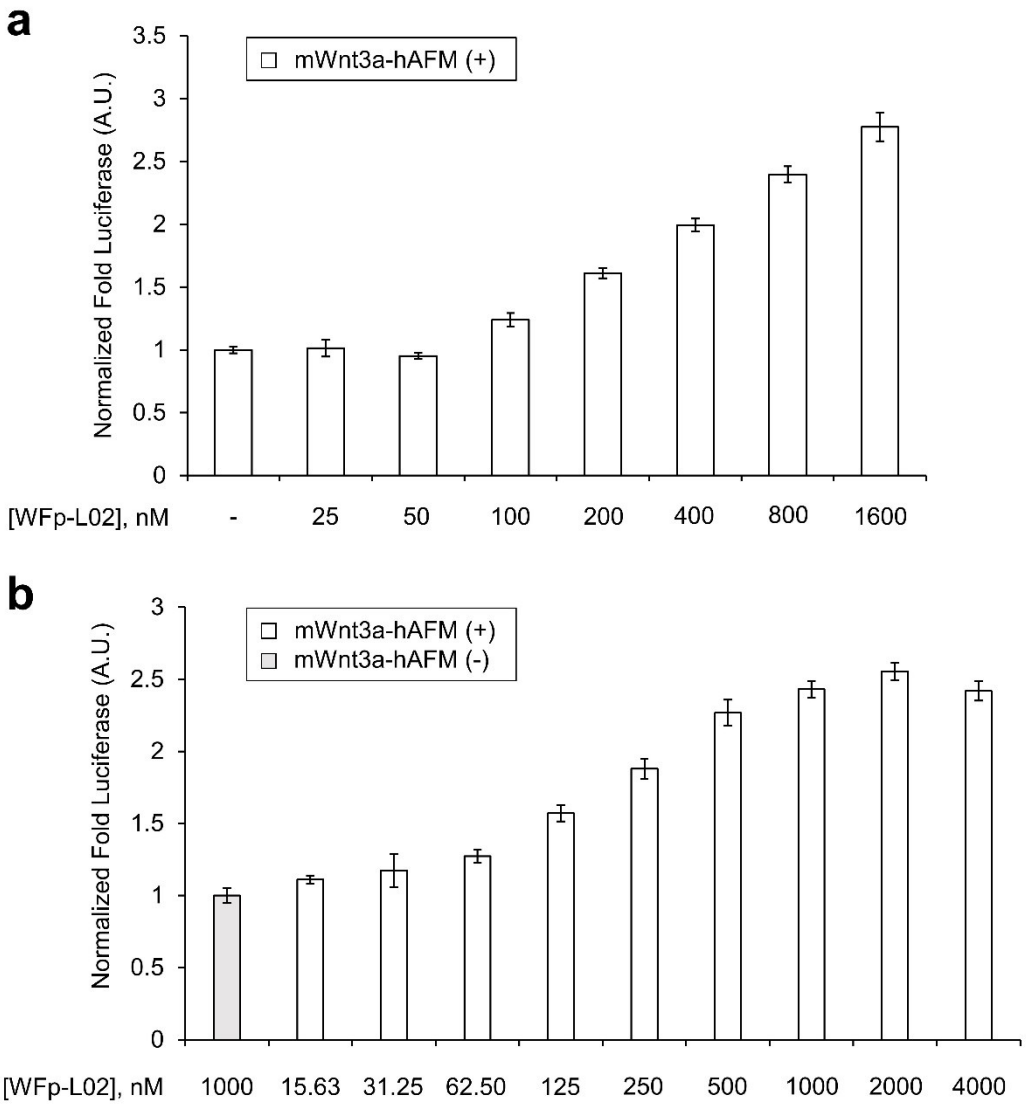

Figure 3.13 Stimulation of Wnt3a signaling by WFp-L02. (**a**) The effect of the peptide on reporter activity was analyzed in the presence of 10 nM mWnt3a-hAFM complex. Shown are fold values relative to a basal Wnt signal reference using the corresponding concentration of mWnt3a-hAFM in the absence of any peptide. All data was normalized to a blank signal generated in the presence of 10 nM AFM and in the absence of any peptide, subtracted from every value, while error bars indicate standard error. (**b**) Similar results for the peptide under assay saturation conditions with 40 nM mWnt3-hAFM stimulation of signaling, all relative to a basal reference with the presence of a high concentration of the peptide (in gray).

As can be observed, whether under regular or saturated conditions, we were able to confirm the signaling-promoting effect incurred by WFp-L02, which we consider to be the first of its kind to have such effect by direct binding to mWnt3a-Fz8. It is also remarkable that the peptide is structurally quite different from those of the inhibitors WAp-D04, WAp-W10P and WFp D03-S2, with a largely hydrophobic structure and only a few aromatic residues, contrary to the rest of inhibitors that were rich in them (Figure 3.14).

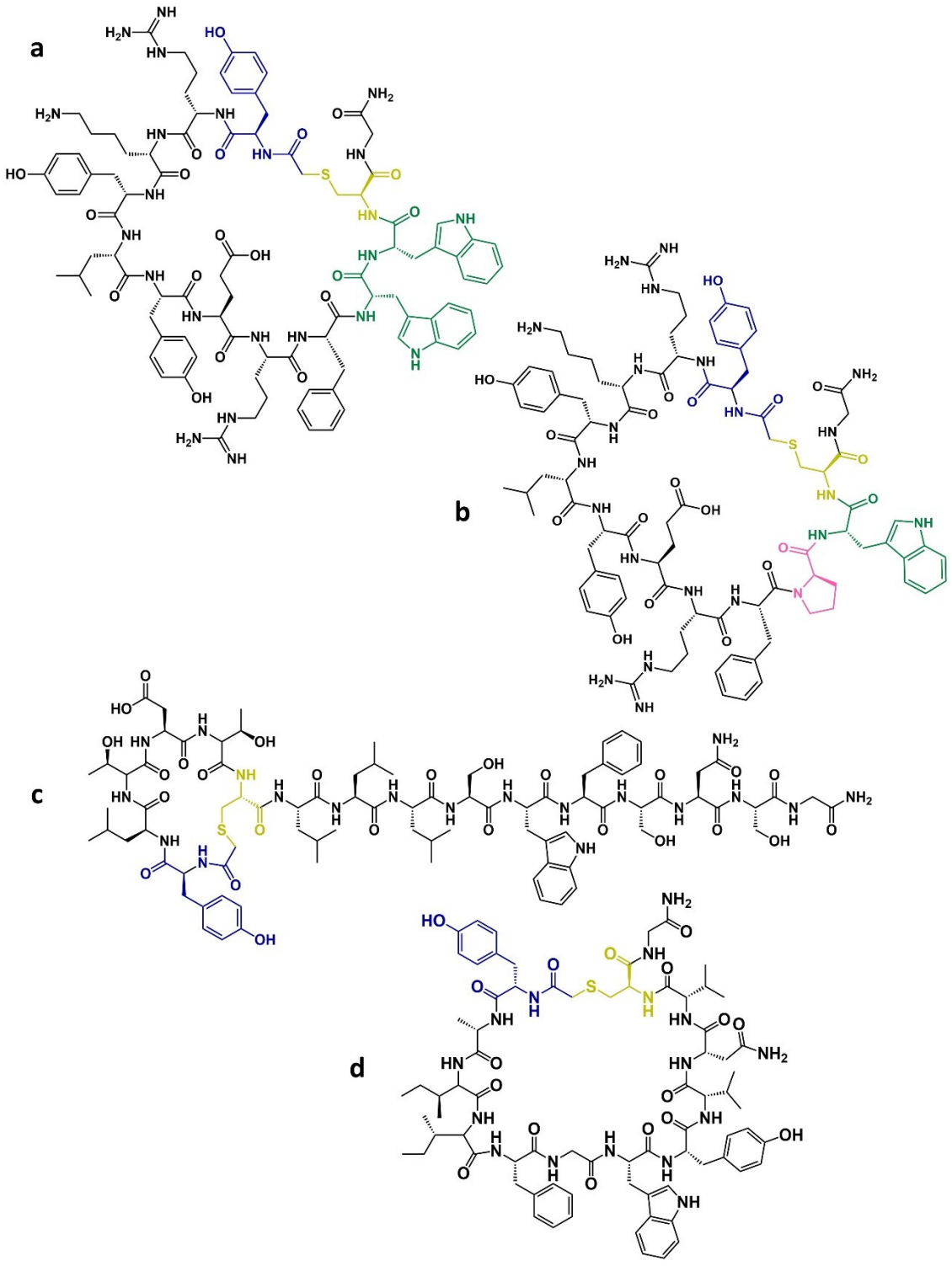

Figure 3.14 Structures of peptide modulators of Wnt signaling identified by targeting protein-stabilized complexes of mWnt3a in this work. (**a**) WAp-D04 (**b**) WAp-D04-W10P (**c**) WFp-D03-S2 and (**d**) WFp-L02.

Discussion

In the previous chapter of this work we were able to identify and optimize a rare hit inhibitor molecule of Wnt signaling, finally attaining a 12-member-ring macrocyclic peptide capable of strongly binding Wnt3a (K_D = 39.5 nM) and silence Wnt signaling with great intensity (IC_{50} = 56 nM). This accomplishment was brought by the application of the versatile RaPID platform to a complexed form of the commonly unstable protein mWnt3a partnered to hAFM, a large glycoprotein of the albumin family that stabilizes the Wnt ligand while still allowing its normal bioactivity for interaction with Fz receptor to turn on Wnt signaling. However, we remained skeptical of whether such an inert partner occupying a large binding area could hinder the discovery of additional inhibitors that could bind to areas other than the active site of mWnt3a (which allows interaction with its natural binding partners), potentially ruling out any allosteric effects of the peptides identified through such a campaign.

With these considerations, we performed an additional selection screening against mWnt3a-mFz8, a natural complex form of the protein containing the target Wnt ligand and its natural receptor partner. Nonetheless, the strong binding characteristics of this complex in turn lowered the possibilities of identifying direct inhibitors that could compete out the receptor and bind to the Wnt-Fz interface. Still, considering that we had already obtained an inhibitor potentially acting through this mechanism and with room for further optimization, we carried out a selection scheme similar to the one performed by panning libraries against mWnt3a-hAFM, expecting to recover allosteric peptide inhibitors of Wnt signaling binding to other surfaces of the complex.

Notably, the negative background (corresponding to recovered non-specific peptide fractions), which was consistently increased and maintained throughout the selection process against mWnt3a-hAFM, was almost completely suppressed during this campaign against mWnt3a-mFz8. These results could point to the high specificity of the natural Fz receptor partner toward Wnt3a, which localizes its interacting areas mostly to the arm domains of the Wnt ligand, yet is largely covered by its anterior, inter-arm domain,

which leaves fewer binding domains in the receptor for recovering peptide binders not specific to Wnt within the complex (Figure 3.1). Consequently, the large and free areas of the Wnt ligand in this complex leave more space available for peptide binders that, though most probably incapable of outcompeting Fz receptors for the arm domains, have large possibilities for hindering either Wnt or Fz interactions with other co-receptors. Even more so, the structural variability (*e.g.* different cycle length and the presence of lariat structures) not observed for the recovered peptide pools binding to mWnt3a-hAFM, seems to also point toward these factors. Nonetheless, lack of structural information regarding the mWnt3a-hAFM complex hinders further confirmation of these results.

2D analysis of the sequences identified through this approach also seems to illustrate the high-specificity of the Wnt3a-Fz interaction. As seen in Figure 3.5, very low binding bias towards the single receptor was observed for almost all of the recovered sequences in the analyzed pool. This trait was particularly noticeable in the L-Tyr-initiated recovered peptide fraction.

It is remarkable that our findings pointed toward peptides that showed much stronger K_D values when compared to the peptides identified while targeting mWnt3a-hAFM, potentially taking advantage of binding areas unavailable when mWnt3a is bound to the stabilizing hAFM. From the most stable SPR results obtained, one peptide presented binding almost one order of magnitude stronger, while three of them went as far as near two order stronger values and surpassed the binding capabilities observed for our previously optimized inhibitor, WAp-D04-W10P. Additionally, WFp-L29 exhibited a K_D value near the pM limit, one of the strongest observed even among inhibitors or activators targeting other components of Wnt signaling.

Our findings directed us to another inhibitor of Wnt signaling, WFp-D03-S2, a lariat-structured peptide which, as the previously optimized WAp-D04 and its W10P mutant, was able to inhibit Wnt signaling by directly binding mWnt3a. Nonetheless, its inhibiting properties were found to be weaker than either of its predecessors, with an IC_{50} near half as potent as the initial hit WAp-D04 (near 800 nM). However, it

remains remarkable that the binding to sites other than the main Wnt-Fz interacting surface could inhibit the signaling, depicting an additional key advantage of our approach to finding bioactive peptide binders through the use of different protein-stabilized complexes, *i.e.* utilizing target proteins stabilized differently through varying complexes.

Strikingly, however, though our initial objective while targeting the Wnt3a-Fz complex was to identify allosteric inhibitors of Wnt signaling, we were also able to obtain an actual overactivator of the signaling, which stimulated signaling-dependent reporter expression in our assays, a property we were able to confirm it occurs solely due to the presence of the peptide. This particular finding opens up a much wider range of possibilities towards the control of Wnt signaling. As aforementioned, the role of Wnt signaling in disease is quite complex, showing overexpression of Wnt signaling-promoting components of the pathway in some cases as well as a lack of them (thereby with a lowered signaling activity and gene expression) in others. With these considerations, several therapeutics targeting the pathway not just for inhibition, as in the case of Fz-blocking agents like Foxy-5 or PRCN inhibitors, but for its overactivation have been developed as well (Figure 3.15). A common target of some of them is the kinase GSK3, which intervenes in the pathway as part of the DC in the multiple phosphorylation of β-catenin during its targeting for degradation (*i.e.* Wnt signaling in an off state). For this kinase, several small molecule inhibitors have been developed that cause a decrease of the phosphorylation (and consequently, of the degradation of) β-catenin, which in a synergistic effect with Wnt ligand binding on Fz receptors causes a continued and increased activation of Wnt signaling. Among these inhibitors are the purine QS11, which promotes multiple development axis formation[97], LY20900314, a bisarylmaleimide highly cytotoxic to human melanoma cell lines[98], and BIO, a bromoindirubinoxime able to reversibly maintain pluripotency of embryonic stem cells[99].

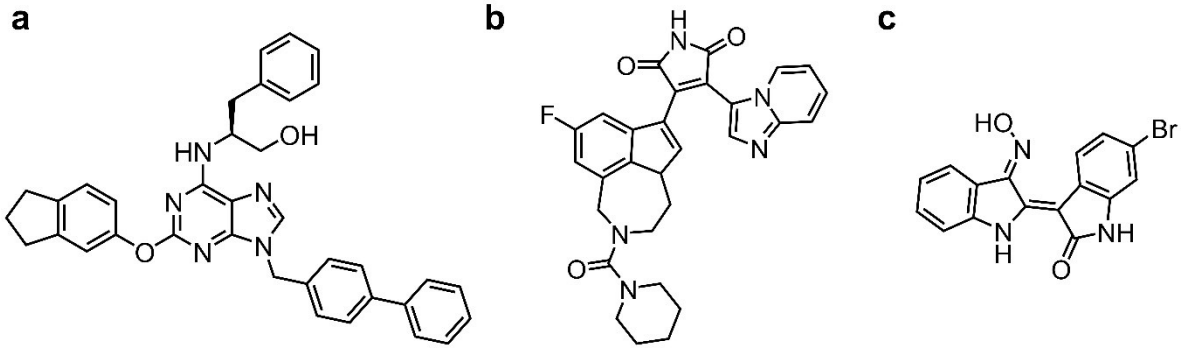

Figure 3.15 Chemical structures of small molecules developed as signaling-promoting agents of the Wnt pathway targeting GSK3. Shown are (**a**) QS11 (**b**) LY20900314 and (**c**) BIO.

As an activator of the Wnt pathway, WFp-L02 therefore brings forward novel possibilities and several advantages for the development of Wnt signaling-promoting therapeutics. As a starting point, its medium-sized molecular character targeting mWnt3a directly pins down its effect to the extracellular area. Furthermore, its particular specificity profile to the target Wnt ligand represents an advantageous property considering that other activator targets like GSK3 are involved in a variety of processes unrelated to Wnt signaling as well. Finally, the general lack of charged and polar amino acids may benefit its binding to the Wnt ligand, as well as any potential internalization through the cellular membrane.

As in the case with WAp-D04 and its W10P optimized mutant, we currently lack structural information regarding the binding mode and mechanism of action for the newly identified peptides WFp-D03-S2 and WFp-L02, but the occupation of Wnt's active binding site due to the presence of its Fz receptor already restricts its action to the outside of the Wnt-Fz surface, a possibility not present in the selection campaign against mWnt3a-hAFM. Consequently, the mechanism of action of WFp-D03-S2 for Wnt signaling should be, in terms of the Wnt-Fz interaction, of allosteric nature. Moreover, though the main starting point of the Wnt signaling pathway occurs through the aforementioned protein-protein interaction, it has been stablished that oligomerization of the Wnt-Fz couple (particularly with LRP5/6) is also pivotal for the signaling cascade, although the exact ratio of oligomerization or an stable and isolated form of the Wnt-Fz-LRP tetramer has been isolated and\or structurally characterized as of yet or is under continuous

discussion[95]. Supporting this interaction, LRP5/6 has also been found to prevent Fz-regulated tumor metastasis through direct interaction with the Fz receptor[100]. Considering this action and the allosteric character of the inhibition brought by the action of WFp-D03-S2, we hypothesize the binding mode of this peptide positions it in an area critical for the interaction of the Wnt-Fz and LRP, either blocking or weakening it as to reduce the overall signaling (regulated gene expression) output, although the bound area could be affecting the interaction with other receptors or restricting the mobility of the Wnt-Fz couple before binding to a co-receptor.

Besides the inhibiting peptide WFp-D02-S2 found in the selection campaign against mWnt3a-mFz8, the nature of the overstimulation caused by the peptide WFp-L02 should require a different focus to help elucidate how it occurs. As aforementioned, a small number of molecules have been found to have an overall similar effect by binding, for example, an intracellular component of the pathway as β-catenin. However, the peptide we identified interacts solely with the initiating component of the signaling cascade. Although the current lack of crystallographic information regarding the binding mode of our peptide and even the interacting components of the initiating phases of the signaling in a timely manner, the most well-known mechanism of regular activation of Wnt signaling occurs through sequestering of the DC and recruiting to the cellular membrane. Yet, the main interaction that causes this event has been found to be dependent on the presence of the small phosphoprotein Dvl, which is recruited to the inner domain of the Fz receptor, where it polymerizes, plays a role in the phosphorylation of LRP5/6 and acts as a full anchor the Axin skeleton of the DC, consequently sequestering it as well and promoting β-catenin accumulation[101-104]. In this regard, we consider the role of WFp-L02 to potentially be linked to the stabilization (restriction) of the Wnt-Fz or Wnt-Fz-LRP complex, favoring an increased level of Dvl recruitment and, consequently, to increased levels of β-catenin. We hypothesize this increase might explain the augmented signal observed in our assays for cells incubated with the peptide when compared to the basal signal from untreated cell cultures.

Nevertheless, we expect further experiments with mutations in each peptide's chain and deeper structural studies can favor the elucidation of the mechanism of action of such novel molecules with notable effect on "controlling" mWnt3a-dependent Wnt signaling for developing novel therapeutics. In particular, considering the larger bioactivity range of the peptides libraries, pursuing selection in more stringent conditions and deep-mutational scanning could bring forward variations in the structure that can benefit the binding and biological effect. Overall, we remark the potential of the molecules identified in this chapter for a more careful and complete therapeutic approach based on the modulation of Wnt signaling, rather than or in combination with an on/off state change that can be more appropriate for complex disease states.

Conclusions

In chapter 3 of this work we have identified *de novo* macrocyclic peptides able to either inhibit or overstimulate mWnt3a-dependent Wnt signaling responses, effectively attaining molecules able to control the activation state of the pathway. Based on results obtained in chapter 1, we performed a selection campaign against mWnt3a, a structurally frail protein understudied in therapeutic development due its lack of stability and quick aggregation in non-cellular environments. Considering our successful selection and identification of peptide inhibitors through a strategy taking advantage of a protein partner and stabilizing agent (hAFM), we applied a similar scheme with a form of the mWnt3a protein in complex with its natural receptor, mFz8. Though such a structure was not expected to favor finding of peptides hindering the Wnt-Fz interaction due to the strong binding characteristics of this complex, the strategy still allowed the discovery of novel peptide WFp-D03-S2, a lariat cyclic peptide able to inhibit the pathway albeit with lower efficiency than its WAp-D04-W10P predecessor (IC_{50} near 800 nM), though its action is expected to occur allosterically rather than directly. Strikingly, through this approach we were also able to discover another peptide, WFp-L02, a macrocycle which was able to promote Wnt signaling rather than inhibiting it. Although sequential studies on these two peptides, particularly their binding modes and the effects of secondary structural mutations on activity should be performed in order to gain insights into their mechanism of action, the identification of hit molecules with opposite activities by direct binding to a Wnt ligand already greatly expands the scope of potential therapeutics that exhibit specific target binding, and can control such a complex mechanism with varying effects, helping to develop therapies against disease states with different signaling states and phenotypic consequences.

Materials and Methods

Protein Expression and Purification

Fc-fusion and PA-tagged mWnt3a and mFz8 proteins were kindly provided in collaboration with Prof. Jun Takagi at the Laboratory of Protein Synthesis and Expression, Institute for Protein Research, The University of Osaka, Osaka, Japan.

mRNA Library Preparation

Initial randomized library was designed as in chapter 2, based on a random DNA region encoding NNK codons of 6 to 15 codon-length, a set UGC Cys codon and a $(Gly\text{-}Ser)_3$ region, transcribed purified and combined as before to a final 10 uM concentration.

RaPID Selection

Peptide libraries were prepared from initial 10 uM RNA libraries using the FIT system in a similar manner as in chapter 1, aiming for a total 150 uL translation for the first round of selection. Prepared libraries were exposed to the target mWnt3a-mFz8 complex previously immobilized on Protein A Dynabeads (LifeTechnologies®) for a total of 80 pmol loaded target (200 nM target complex concentration when resuspended in the peptide pool). Peptide pools containing these loaded beads were then incubated at 4 °C for 30 minutes, washed 3 times with cold TBS-T pH 7.5 buffer to discard the unbound peptide fraction and finally resuspended in cold PCR buffer. cDNA cognate to the target-binding peptide fraction was then recovered by heating the samples 95 °C for 5 minutes and separating the supernatant. A small amount of the input and recovered cDNA samples were then analyzed using real-time qPCR on a Roche LightCycler® system and the remainder was amplified by PCR. The amplified samples were then purified by one extraction each with PCI and CI solutions, precipitated with ethanol and resuspended in water. The resulting samples were then transcribed to mRNA, forming the initial library for the next round. Following rounds of selection were carried out using the same scheme, though

performing translation at a total 5 uL scale and 10 pmol of target protein (still maintaining final 200 nM when exposed to libraries). Additionally, before incubating the library in the target complex, they were first exposed in 6 separate cycles to a mixture containing 50% free Protein A Dynabeads (LifeTechnologies®) and 50% of the same beads loaded only with Fc-mFz8 in twice the molar amount of the objective target concentration (for a total of 20 pmol). These "negative selection" cycles were performed in order to lower the possibility of recovering non-specific peptides or those with preferential binding to the protein partner instead of the original target mWnt3a. The cycles were carried out for at 4 °C for 30 minutes each. Samples were then incubated in beads containing 10 pmol of the target mWnt3a-mFz8 and corresponding cDNA was recovered and amplified as before.

Deep-sequencing analysis program

Sequencing data corresponding to each recovered library and round during selection was obtained as in chapter 2 with a Miseq Illumina® system, and processed and 2D analyzed with the same described Python script in the same Enthought Canopy® environment.

Peptide Synthesis and Purification

Selected peptides were synthesized as before through standard solid-phase peptide synthesis with a Biotage Syro I® parallel synthesis system using a common Fmoc-protected amino acid chemistry on NovaPEG Rink amide resin at a 25 μmol scale as in chapter 2. Final peptides were dissolved in a small volume of DMSO and reserved at -20 °C. Structural identity of each peptide and their evolution through the synthesis scheme was confirmed through MALDI-TOF MS, while the final purity of the samples by UPLC.

General conclusions

The studies described in this thesis work have focused on varied efforts for identifying cyclic peptide binders to a mWnt3a ligand, member of a numerous family of proteins pivotal in one of the best-studied mechanisms for cellular development and adult homeostasis, the Wnt pathway. Although the general role of these proteins and its notable relationship with a large variety of disease states that include carcinogenic processes have been known for decades, their definite structural traits and the signaling chains they incur in have remained elusive even to this day. One of the main causes for this lack of essential information is due to the characteristically high hydrophobic character attained by the presence of a palmitoleoylated Ser that is critical for their binding to their coupling receptors (mainly Fz membrane receptors) and activity, but that in turn makes them largely insoluble in non-native cellular environments, precipitating readily or losing biological activity with temperature changes or large storage time. Although with large difficulties, pivotal discoveries on the binding mode of two of their isoforms during this decade have renewed the attention into the structural characteristics of Wnt ligands, while the identification of a bioactive stabilized complex of a Wnt ligand with an inert partner brought us to challenge identifying molecule candidates that could affect the Wnt pathway, and therefore potentially bring forward beneficial properties that could benefit the treatment for the different diseases the signaling chain is related to.

Considering the challenging traits of Wnt proteins and the disadvantages of using a non-covalent complex in therapeutics development, we envisioned that the use of the RaPID system, a versatile platform for identifying macrocyclic peptide binders to diverse proteins, together with a careful selection scheme and detailed sequencing analysis would make an adequate strategy for overcoming the difficulties in the assessment of Wnt ligand inhibitors. Throughout our experiments with an mWnt3a-hAFM complex, the inherent non-selective binding caused by the presence of an inert protein partner in complex with our Wnt target proved challenging, but optimization of selection schemes and a 2D dimensional analysis performed on the recovered peptides libraries allowed us to identify a unique, single peptide hit that was able to

strongly bind to the Wnt ligand (with an apparent selectivity over the partner hAFM) and inhibit mWnt3a-dependent signaling in a cellular model. Additionally, further mutagenesis and optimization of this molecule led us to a single mutant with largely improved binding profiles and inhibition properties, a changed interestingly brought upon by a W10P mutation that potentially restricted the peptide structure, and consequently its binding mode to the Wnt ligand.

Albeit with positive results from such a campaign against the mWnt3a-hAFM, taking into account its structural characteristics and the selection scheme challenges it poses, we performed an additional RaPID screening with another protein-stabilized form of the Wnt target, a complex with its natural Fz receptor. From this campaign, we were able to isolate peptides that could bind the target and affect Wnt signaling and that, considering the strong kinetics of the Wnt-Fz interaction, could act most probably through an allosteric mechanism. Accordingly, a single peptide hit with a lariat structure that exhibited inhibition characteristics in the sub-micromolar IC_{50} range, though with less intensity than its optimized predecessor. Strikingly, however, we were also able to identify a fully macrocyclic peptide that could overstimulate Wnt signaling, a property we confirmed through varied conditions in our cellular model.

Altogether, our selection strategy based on the use of protein-stabilized Wnt targets allowed us to identify cyclic peptides with both inhibition and overstimulation effects on Wnt signaling. These results represent the first mid-sized molecules of their kind that accomplish such a feat through the direct interaction with a secreted Wnt ligand, affecting the Wnt-Fz or Wnt-Fz-co-receptor interactions necessary for the signal transduction cascade to occur. Notably, all these structures are structurally varied, and could pose a novel molecule model for the development of therapeutics against complex diseases that involve changes in the activation states of Wnt signaling. Furthermore, our strategies call for attention toward new methods for affinity-based screening approaches that target insoluble and/or unstable proteins lacking structural information, bringing forward convenient tools for their application on understudied targets.

References

1. R. Nusse, *Cell Res*, 2005, **15**, 28-32.
2. R. P. Sharma and V. L. Chopra, *Dev Biol*, 1976, **48**, 461-465.
3. N. E. Baker, *EMBO J*, 1987, **6**, 1765-1773.
4. R. Nusse and H. E. Varmus, *Cell*, 1982, **31**, 99-109.
5. R. Nusse, A. van Ooyen, D. Cox, Y. K. Fung and H. Varmus, *Nature*, 1984, **307**, 131-136.
6. R. Nusse and H. Clevers, *Cell*, 2017, **169**, 985-999.
7. T. Zhan, N. Rindtorff and M. Boutros, *Oncogene*, 2017, **36**, 1461-1473.
8. J. L. Stamos and W. I. Weis, *Cold Spring Harb Perspect Biol*, 2013, **5**, a007898.
9. L. Azzolin, T. Panciera, S. Soligo, E. Enzo, S. Bicciato, S. Dupont, S. Bresolin, C. Frasson, G. Basso, V. Guzzardo, A. Fassina, M. Cordenonsi and S. Piccolo, *Cell*, 2014, **158**, 157-170.
10. E. C. van Kappel and M. M. Maurice, *Br J Pharmacol*, 2017, **174**, 4575-4588.
11. W. de Lau, W. C. Peng, P. Gros and H. Clevers, *Genes Dev*, 2014, **28**, 305-316.
12. O. Kazanskaya, A. Glinka, I. del Barco Barrantes, P. Stannek, C. Niehrs and W. Wu, *Dev Cell*, 2004, **7**, 525-534.
13. K. S. Carmon, X. Gong, Q. Lin, A. Thomas and Q. Liu, *Proc Natl Acad Sci U S A*, 2011, **108**, 11452-11457.
14. J. Sampietro, C. L. Dahlberg, U. S. Cho, T. R. Hinds, D. Kimelman and W. Xu, *Mol Cell*, 2006, **24**, 293-300.
15. K. M. Cadigan and M. L. Waterman, *Cold Spring Harb Perspect Biol*, 2012, **4**.
16. S. Angers and R. T. Moon, *Nat Rev Mol Cell Biol*, 2009, **10**, 468-477.
17. C. Metcalfe, C. Mendoza-Topaz, J. Mieszczanek and M. Bienz, *J Cell Sci*, 2010, **123**, 1588-1599.
18. H. Hikasa, J. Ezan, K. Itoh, X. Li, M. W. Klymkowsky and S. Y. Sokol, *Dev Cell*, 2010, **19**, 521-532.
19. W. H. Lien and E. Fuchs, *Genes Dev*, 2014, **28**, 1517-1532.
20. A. M. Daulat and J. P. Borg, *Trends Cancer*, 2017, **3**, 113-125.
21. G. Corda and A. Sala, *Oncogenesis*, 2017, **6**, e364.
22. B. Gao, *Curr Top Dev Biol*, 2012, **101**, 263-295.
23. J. Navajas Acedo, M. G. Voas, R. Alexander, T. Woolley, J. R. Unruh, H. Li, C. Moens and T. Piotrowski, *Nat Commun*, 2019, **10**, 3993.

24. J. Wu and M. Mlodzik, *Dev Cell*, 2008, **15**, 462-469.
25. D. Devenport, *J Cell Biol*, 2014, **207**, 171-179.
26. A. Jenny, J. Reynolds-Kenneally, G. Das, M. Burnett and M. Mlodzik, *Nat Cell Biol*, 2005, **7**, 691-697.
27. G. Das, A. Jenny, T. J. Klein, S. Eaton and M. Mlodzik, *Development*, 2004, **131**, 4467-4476.
28. K. Schlessinger, A. Hall and N. Tolwinski, *Genes Dev*, 2009, **23**, 265-277.
29. T. Nikolova, M. Wu, K. Brumbarov, R. Alt, H. Opitz, K. R. Boheler, M. Cross and A. M. Wobus, *Differentiation*, 2007, **75**, 100-111.
30. K. Willert, J. D. Brown, E. Danenberg, A. W. Duncan, I. L. Weissman, T. Reya, J. R. Yates, 3rd and R. Nusse, *Nature*, 2003, **423**, 448-452.
31. A. H. Nile and R. N. Hannoush, *J Biol Chem*, 2019, **294**, 726-736.
32. R. Takada, Y. Satomi, T. Kurata, N. Ueno, S. Norioka, H. Kondoh, T. Takao and S. Takada, *Dev Cell*, 2006, **11**, 791-801.
33. X. Gao and R. N. Hannoush, *Nat Chem Biol*, 2014, **10**, 61-68.
34. J. Rios-Esteves and M. D. Resh, *Cell Rep*, 2013, **4**, 1072-1081.
35. J. Rios-Esteves, B. Haugen and M. D. Resh, *J Biol Chem*, 2014, **289**, 17009-17019.
36. R. Tuladhar and L. Lum, *Biochem Soc Trans*, 2015, **43**, 235-239.
37. S. Kakugawa, P. F. Langton, M. Zebisch, S. Howell, T. H. Chang, Y. Liu, T. Feizi, G. Bineva, N. O'Reilly, A. P. Snijders, E. Y. Jones and J. P. Vincent, *Nature*, 2015, **519**, 187-192.
38. C. Banziger, D. Soldini, C. Schutt, P. Zipperlen, G. Hausmann and K. Basler, *Cell*, 2006, **125**, 509-522.
39. T. Buechling, V. Chaudhary, K. Spirohn, M. Weiss and M. Boutros, *EMBO Rep*, 2011, **12**, 1265-1272.
40. K. A. Mulligan, C. Fuerer, W. Ching, M. Fish, K. Willert and R. Nusse, *Proc Natl Acad Sci U S A*, 2012, **109**, 370-377.
41. K. Menck, F. Klemm, J. C. Gross, T. Pukrop, D. Wenzel and C. Binder, *Oncotarget*, 2013, **4**, 2057-2066.
42. C. Y. Janda, D. Waghray, A. M. Levin, C. Thomas and K. C. Garcia, *Science*, 2012, **337**, 59-64.
43. H. Hirai, K. Matoba, E. Mihara, T. Arimori and J. Takagi, *Nat Struct Mol Biol*, 2019, **26**, 372-379.
44. E. Mihara, H. Hirai, H. Yamamoto, K. Tamura-Kawakami, M. Matano, A. Kikuchi, T. Sato and J. Takagi, *Elife*, 2016, **5**.

45. L. Jerkovic, A. F. Voegele, S. Chwatal, F. Kronenberg, C. M. Radcliffe, M. R. Wormald, E. M. Lobentanz, B. Ezeh, P. Eller, N. Dejori, B. Dieplinger, F. Lottspeich, W. Sattler, M. Uhr, K. Mechtler, R. A. Dwek, P. M. Rudd, G. Baier and H. Dieplinger, *J Proteome Res*, 2005, **4**, 889-899.
46. H. S. Lichenstein, D. E. Lyons, M. M. Wurfel, D. A. Johnson, M. D. McGinley, J. C. Leidli, D. B. Trollinger, J. P. Mayer, S. D. Wright and M. M. Zukowski, *J Biol Chem*, 1994, **269**, 18149-18154.
47. H. Dieplinger and B. Dieplinger, *Clin Chim Acta*, 2015, **446**, 105-110.
48. B. Kollerits, C. Lamina, C. Huth, P. Marques-Vidal, S. Kiechl, I. Seppala, J. Cooper, S. C. Hunt, C. Meisinger, C. Herder, L. Kedenko, J. Willeit, B. Thorand, D. Dahnhardt, D. Stockl, K. Willeit, M. Roden, W. Rathmann, B. Paulweber, A. Peters, M. Kahonen, T. Lehtimaki, O. T. Raitakari, S. E. Humphries, P. Vollenweider, H. Dieplinger and F. Kronenberg, *Diabetes Care*, 2017, **40**, 1386-1393.
49. A. Altamirano, A. Naschberger, B. G. Furnrohr, R. Saldova, W. B. Struwe, P. M. Jennings, S. Millan Martin, S. Malic, I. Plangger, S. Lechner, R. Pisano, N. Peretti, B. Linke, M. M. Aguiar, F. Fresser, A. Ritsch, T. Lenac Rovis, C. Goode, P. M. Rudd, K. Scheffzek, B. Rupp and H. Dieplinger, *J Proteome Res*, 2018, **17**, 1269-1277.
50. A. Naschberger, A. Orry, S. Lechner, M. W. Bowler, D. Nurizzo, M. Novokmet, M. A. Keller, G. Oemer, D. Seppi, M. Haslbeck, K. Pansi, H. Dieplinger and B. Rupp, *Structure*, 2017, **25**, 1907-1915 e1905.
51. A. Naschberger, P. Juyoux, J. von Velsen, B. Rupp and M. W. Bowler, *Acta Crystallogr D Struct Biol*, 2019, **75**, 1071-1083.
52. T. Zhan, G. Ambrosi, A. M. Wandmacher, B. Rauscher, J. Betge, N. Rindtorff, R. S. Haussler, I. Hinsenkamp, L. Bamberg, B. Hessling, K. Muller-Decker, G. Erdmann, E. Burgermeister, M. P. Ebert and M. Boutros, *Nat Commun*, 2019, **10**, 2197.
53. L. Novellasdemunt, P. Antas and V. S. Li, *Am J Physiol Cell Physiol*, 2015, **309**, C511-521.
54. R. Haraguchi, R. Kitazawa, K. Mori, R. Tachibana, H. Kiyonari, Y. Imai, T. Abe and S. Kitazawa, *Sci Rep*, 2016, **6**, 25198.
55. H. Clevers, *Cell*, 2009, **139**, 227-229.
56. B. Chen, M. E. Dodge, W. Tang, J. Lu, Z. Ma, C. W. Fan, S. Wei, W. Hao, J. Kilgore, N. S. Williams, M. G. Roth, J. F. Amatruda, C. Chen and L. Lum, *Nat Chem Biol*, 2009, **5**, 100-107.

57. M. M. Fischer, B. Cancilla, V. P. Yeung, F. Cattaruzza, C. Chartier, C. L. Murriel, J. Cain, R. Tam, C. Y. Cheng, J. W. Evans, G. O'Young, X. Song, J. Lewicki, A. M. Kapoun, A. Gurney, W. C. Yen and T. Hoey, *Sci Adv*, 2017, **3**, e1700090.
58. N. Tuysuz, L. van Bloois, S. van den Brink, H. Begthel, M. M. Verstegen, L. J. Cruz, L. Hui, L. J. van der Laan, J. de Jonge, R. Vries, E. Braakman, E. Mastrobattista, J. J. Cornelissen, H. Clevers and D. Ten Berge, *Nat Commun*, 2017, **8**, 14578.
59. C. Y. Janda, L. T. Dang, C. You, J. Chang, W. de Lau, Z. A. Zhong, K. S. Yan, O. Marecic, D. Siepe, X. Li, J. D. Moody, B. O. Williams, H. Clevers, J. Piehler, D. Baker, C. J. Kuo and K. C. Garcia, *Nature*, 2017, **545**, 234-237.
60. X. Wang, J. Moon, M. E. Dodge, X. Pan, L. Zhang, J. M. Hanson, R. Tuladhar, Z. Ma, H. Shi, N. S. Williams, J. F. Amatruda, T. J. Carroll, L. Lum and C. Chen, *J Med Chem*, 2013, **56**, 2700-2704.
61. A. Safholm, K. Leandersson, J. Dejmek, C. K. Nielsen, B. O. Villoutreix and T. Andersson, *J Biol Chem*, 2006, **281**, 2740-2749.
62. T. N. Grossmann, J. T. Yeh, B. R. Bowman, Q. Chu, R. E. Moellering and G. L. Verdine, *Proc Natl Acad Sci U S A*, 2012, **109**, 17942-17947.
63. T. Passioura, K. Watashi, K. Fukano, S. Shimura, W. Saso, R. Morishita, Y. Ogasawara, Y. Tanaka, M. Mizokami, C. Sureau, H. Suga and T. Wakita, *Cell Chem Biol*, 2018, **25**, 906-915 e905.
64. K. Sakai, T. Passioura, H. Sato, K. Ito, H. Furuhashi, M. Umitsu, J. Takagi, Y. Kato, H. Mukai, S. Warashina, M. Zouda, Y. Watanabe, S. Yano, M. Shibata, H. Suga and K. Matsumoto, *Nat Chem Biol*, 2019, **15**, 598-606.
65. Y. Yamagishi, I. Shoji, S. Miyagawa, T. Kawakami, T. Katoh, Y. Goto and H. Suga, *Chem Biol*, 2011, **18**, 1562-1570.
66. J. Morimoto, Y. Hayashi and H. Suga, *Angew Chem Int Ed Engl*, 2012, **51**, 3423-3427.
67. Y. V. Schlippe, M. C. Hartman, K. Josephson and J. W. Szostak, *J Am Chem Soc*, 2012, **134**, 10469-10477.
68. A. Angelini, L. Cendron, S. Chen, J. Touati, G. Winter, G. Zanotti and C. Heinis, *ACS Chem Biol*, 2012, **7**, 817-821.
69. N. Terasaka, Y. Iwane, A. S. Geiermann, Y. Goto and H. Suga, *Int J Mol Sci*, 2015, **16**, 6513-6531.

70. Y. Kato, T. Kuroda, Y. Huang, R. Ohta, Y. Goto and H. Suga, *Angew Chem Int Ed Engl*, 2019, DOI: 10.1002/anie.201910894.
71. H. Murakami, A. Ohta, H. Ashigai and H. Suga, *Nat Methods*, 2006, **3**, 357-359.
72. Y. Goto, T. Katoh and H. Suga, *Nat Protoc*, 2011, **6**, 779-790.
73. H. Xiao, H. Murakami, H. Suga and A. R. Ferre-D'Amare, *Nature*, 2008, **454**, 358-361.
74. Y. Goto, A. Ohta, Y. Sako, Y. Yamagishi, H. Murakami and H. Suga, *ACS Chem Biol*, 2008, **3**, 120-129.
75. M. Molenaar, M. van de Wetering, M. Oosterwegel, J. Peterson-Maduro, S. Godsave, V. Korinek, J. Roose, O. Destree and H. Clevers, *Cell*, 1996, **86**, 391-399.
76. G. E. Crooks, G. Hon, J. M. Chandonia and S. E. Brenner, *Genome Res*, 2004, **14**, 1188-1190.
77. J. Hu, A. Dong, V. Fernandez-Ruiz, J. Shan, M. Kawa, E. Martinez-Anso, J. Prieto and C. Qian, *Cancer Res*, 2009, **69**, 6951-6959.
78. A. Gurney, F. Axelrod, C. J. Bond, J. Cain, C. Chartier, L. Donigan, M. Fischer, A. Chaudhari, M. Ji, A. M. Kapoun, A. Lam, S. Lazetic, S. Ma, S. Mitra, I. K. Park, K. Pickell, A. Sato, S. Satyal, M. Stroud, H. Tran, W. C. Yen, J. Lewicki and T. Hoey, *Proc Natl Acad Sci U S A*, 2012, **109**, 11717-11722.
79. N. T. Morrell, P. Leucht, L. Zhao, J. B. Kim, D. ten Berge, K. Ponnusamy, A. L. Carre, H. Dudek, M. Zachlederova, M. McElhaney, S. Brunton, J. Gunzner, M. Callow, P. Polakis, M. Costa, X. M. Zhang, J. A. Helms and R. Nusse, *PLoS One*, 2008, **3**, e2930.
80. R. Takada, Y. Mii, E. Krayukhina, Y. Maruyama, K. Mio, Y. Sasaki, T. Shinkawa, C. G. Pack, Y. Sako, C. Sato, S. Uchiyama and S. Takada, *Commun Biol*, 2018, **1**, 165.
81. H. Hirose, C. Tsiamantas, T. Katoh and H. Suga, *Curr Opin Biotechnol*, 2019, **58**, 28-36.
82. T. Katoh and H. Suga, *J Am Chem Soc*, 2018, **140**, 12159-12167.
83. K. Ito, K. Sakai, Y. Suzuki, N. Ozawa, T. Hatta, T. Natsume, K. Matsumoto and H. Suga, *Nat Commun*, 2015, **6**, 6373.
84. A. Safholm, J. Tuomela, J. Rosenkvist, J. Dejmek, P. Harkonen and T. Andersson, *Clin Cancer Res*, 2008, **14**, 6556-6563.
85. C. Chartier, J. Raval, F. Axelrod, C. Bond, J. Cain, C. Dee-Hoskins, S. Ma, M. M. Fischer, J. Shah, J. Wei, M. Ji, A. Lam, M. Stroud, W. C. Yen, P. Yeung, B. Cancilla, G. O'Young, M. Wang, A. M. Kapoun, J. Lewicki, T. Hoey and A. Gurney, *Cancer Res*, 2016, **76**, 713-723.
86. M. W. Deininger and B. J. Druker, *Pharmacol Rev*, 2003, **55**, 401-423.

87. P. M. Reeves, B. Bommarius, S. Lebeis, S. McNulty, J. Christensen, A. Swimm, A. Chahroudi, R. Chavan, M. B. Feinberg, D. Veach, W. Bornmann, M. Sherman and D. Kalman, *Nat Med*, 2005, **11**, 731-739.
88. I. Egashira, F. Takahashi-Yanaga, R. Nishida, M. Arioka, K. Igawa, K. Tomooka, Y. Nakatsu, T. Tsuzuki, Y. Nakabeppu, T. Kitazono and T. Sasaguri, *Cancer Sci*, 2017, **108**, 108-115.
89. A. Fujita, F. Takahashi-Yanaga, S. Morimoto, T. Yoshihara, M. Arioka, K. Igawa, K. Tomooka, S. Hoka and T. Sasaguri, *Hypertens Res*, 2017, **40**, 130-139.
90. C. Huang, Y. Chen, H. Liu, J. Yang, X. Song, J. Zhao, N. He, C. J. Zhou, Y. Wang, C. Huang and Q. Dong, *Oncotarget*, 2017, **8**, 115254-115269.
91. L. H. Wang, M. Xu, L. Q. Fu, X. Y. Chen and F. Yang, *Sci Rep*, 2018, **8**, 12776.
92. J. M. Rogers, T. Passioura and H. Suga, *Proc Natl Acad Sci U S A*, 2018, **115**, 10959-10964.
93. Y. Fujii, M. Kaneko, M. Neyazaki, T. Nogi, Y. Kato and J. Takagi, *Protein Expr Purif*, 2014, **95**, 240-247.
94. T. Nogi, T. Sangawa, S. Tabata, M. Nagae, K. Tamura-Kawakami, A. Beppu, M. Hattori, N. Yasui and J. Takagi, *Protein Sci*, 2008, **17**, 2120-2126.
95. E. Bourhis, C. Tam, Y. Franke, J. F. Bazan, J. Ernst, J. Hwang, M. Costa, A. G. Cochran and R. N. Hannoush, *J Biol Chem*, 2010, **285**, 9172-9179.
96. K. Iwasaki, Y. Goto, T. Katoh and H. Suga, *Org Biomol Chem*, 2012, **10**, 5783-5786.
97. Q. Zhang, M. B. Major, S. Takanashi, N. D. Camp, N. Nishiya, E. C. Peters, M. H. Ginsberg, X. Jian, P. A. Randazzo, P. G. Schultz, R. T. Moon and S. Ding, *Proc Natl Acad Sci U S A*, 2007, **104**, 7444-7448.
98. J. M. Atkinson, K. B. Rank, Y. Zeng, A. Capen, V. Yadav, J. R. Manro, T. A. Engler and M. Chedid, *PLoS One*, 2015, **10**, e0125028.
99. N. Sato, L. Meijer, L. Skaltsounis, P. Greengard and A. H. Brivanlou, *Nat Med*, 2004, **10**, 55-63.
100. D. N. Ren, J. Chen, Z. Li, H. Yan, Y. Yin, D. Wo, J. Zhang, L. Ao, B. Chen, T. K. Ito, Y. Chen, Z. Liu, Y. Li, J. Yang, X. Lu, Y. Peng, L. Pan, Y. Zhao, S. Liu and W. Zhu, *Nat Commun*, 2015, **6**, 6906.
101. K. N. Schaefer, M. Pronobis, C. E. Williams, S. Zhang, L. Bauer, D. Goldfarb, F. Yan, M. B. Major and M. Peifer, *Mol Biol Cell*, 2020, DOI: 10.1091/mbc.E19-11-0647, mbcE19110647.
102. H. C. Wong, A. Bourdelas, A. Krauss, H. J. Lee, Y. Shao, D. Wu, M. Mlodzik, D. L. Shi and J. Zheng, *Mol Cell*, 2003, **12**, 1251-1260.

103. S. Kishida, H. Yamamoto, S. Hino, S. Ikeda, M. Kishida and A. Kikuchi, *Mol Cell Biol*, 1999, **19**, 4414-4422.
104. A. Cliffe, F. Hamada and M. Bienz, *Curr Biol*, 2003, **13**, 960-966.

List of Accomplishments

Articles and Reviews

- Otero-Ramirez, M.E; Matoba, K.; Mihara, E.; Passioura, T.; Takagi, J. and Suga, H. "Macrocyclic Peptides that Inhibit Wnt Signaling via interaction with Wnt3a". *RSC Chem. Biol.* **2020**, 1-9 (Online Version March 2020).
- Tsiamantas, C.; Otero-Ramirez, M. E. And Suga, H. "Discovery of Functional Macrocyclic Peptides by Means of the RaPID System" in Goetz, G. (eds), "Cyclic Peptide Design". *Methods Mol. Biol.* **2019**, 2001, 299-315.
- Otero-Ramirez, M. E.; Passioura, T. and Suga, H. "Structural Features and Binding Modes of Thioether-Cyclized Peptide Ligands". *Biomedicines*. **2018**, 6, 116-128.

Symposiums and Awards

- "RaPID Selection of Macrocyclic Peptide Inhibitors of MT1-MMP-Induced Neoplastic Cell Migration". JPS Excellent Poster Presentation Award. *10th International Peptide Symposium*, ROHM Theater-Miyako Messe, Kyoto, Japan, December 2018.
- "RaPID ways for the discovery of novel cancer therapy approaches". *The 24th ZESTY Network Seminar*, The University of Tokyo, Tokyo, Japan, March 2018.

Acknowledgements

Quiero agradecer, ante todo, a Dios y a mi familia entera. Padres, desde el primer momento que me propuse salir de mi tierra a buscar nuevas oportunidades me brindaron el más sincero apoyo, y a lo largo de todos estos años han sido mi más grande soporte para sobreponerme a todas las dificultades que tal decisión trajo consigo. Nada sería sin todos los consejos y regaños que me han brindado a lo largo de mi vida entera. Me faltan las palabras para agradecerles.

A Javier Nakamatsu, el laboratorio π/4 y toda la comunidad y amigos PUCP que me han mantenido en el recuerdo y dado su amistad y consejo en momentos clave para poder sobrevivir al PhD.¡Muchas gracias!

I'd like to express my deepest gratitude to Prof. Hiroaki Suga, for giving me a chance among the hundreds of candidates and even when coming from so far away, as well as for supporting me in every way with both opportunities and hard lecturing when the time required it. Also, I'd like to thank Prof. Jun Takagi and Drs. Kyoko Matoba and Emiko Mihara for their collaboration, guidance and help all throughout the work on the Wnt projects. It's been a great experience (as well as a learning one) working with you, and it's also thanks to you I could get this far.

To Toby Passioura, Alex, Orly-chan and Max-kun, I'd like to thank you for giving me a sense of family and friendship even in the most difficult times of my program, and for the support all the way to the very end of it. Also, I'd like to specially thank Saya and her family, for the amazing memories I was able to make with you guys every year.

To Katoh-san, Goto-san, Risa-san, Hirose-aniki, thank you so much for lending me a shoulder to lean on from the senpais of life in order to keep moving, stop complaining, and work on improving myself to be a better professional and person. Similarly, to Seino, Nasir, Joe, Iwane-san, Hoji-san and all the sempais and friend that helped me so much to adjust to the new culture and science, thank you so much for all the good times.

To Kazuto, Eriko-san, Chakra, Tajima, Saho, Natori-san, Sakurai-sempai, Takuto, Sano, Kazune-chan, Takashi, Hirooka-sensei, Kantaro-sensei and everyone at Failte and all the friends who I've had the pleasure of playing together with, thank you so much for your support, friendship and amazing memories and music. If it weren't for you I would've probably given up along the way. This feat is also on you guys!

Finally, thanks to Saya, Kuroda, Takashi, Yoshikane, Kimura, Sakaguchi, Tajima, Tsutsumi, Takeue and everyone in the Suga lab, who made these five long and difficult years to get a PhD, with all its fun, sad, frustrating and rewarding times, the most memorable.

I wouldn't have been able to get here without everyone's support and kind words. I'll be forever in your debt. Thank you so much!!

¡¡Muchísimas gracias a todos!!